UMIST

The University of Manchester
Institute of Science and Technology
Department of Mechanical Engineering

6th Biennial Colloquium on Computational Fluid Dynamics

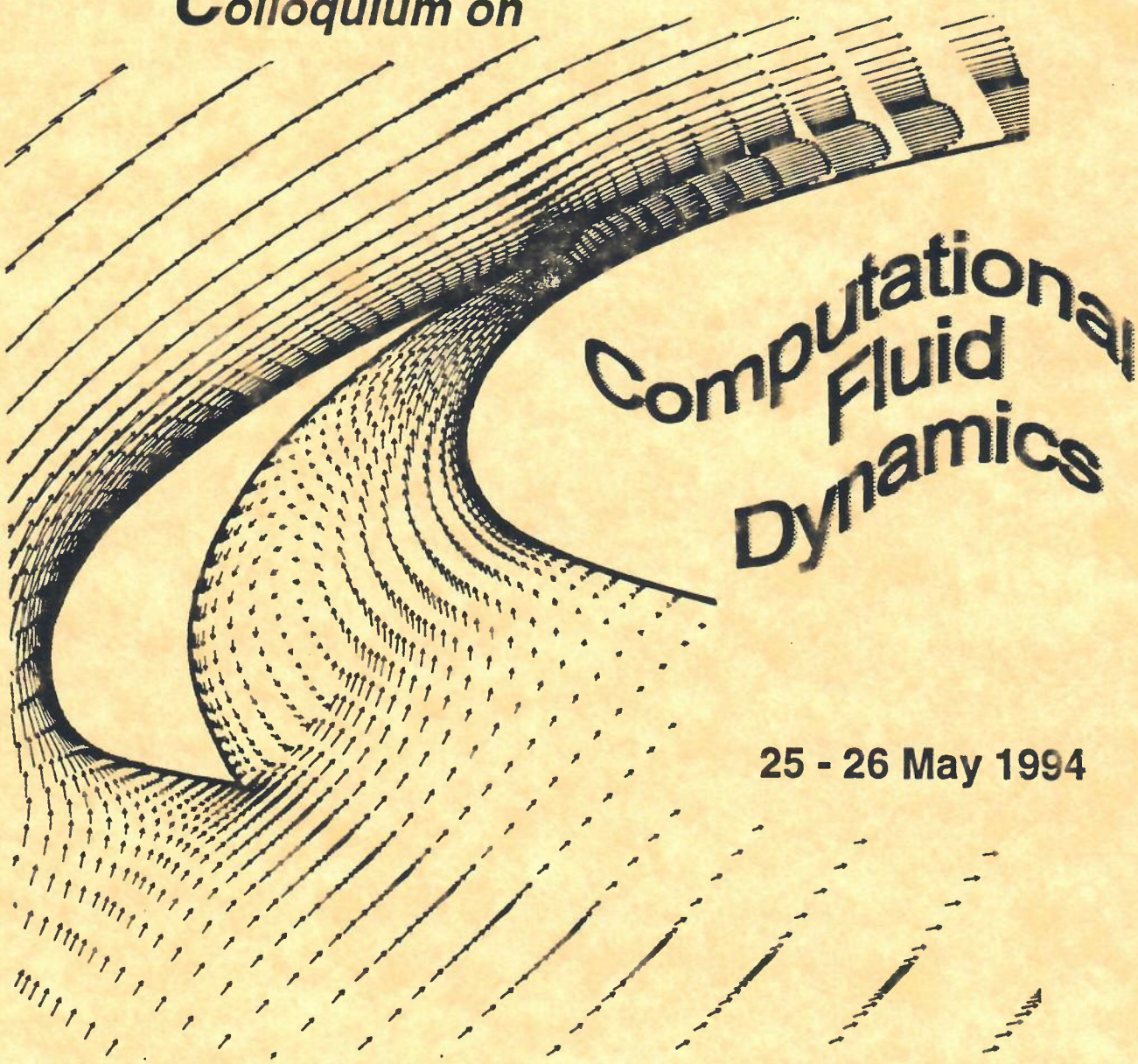

25 - 26 May 1994

PREFACE

The booklet contains the summaries of research projects presented at the 6th Biennial CFD Colloquium held at UMIST on 25-26 May 1994. The main aim of the Colloquium is to provide a broad view of ongoing research in Computational Fluid Dynamics undertaken in the Thermofluids Division of the Mechanical Engineering Department. The Colloquium also provides an opportunity for our research team, often for the first time, to present the outcome of their research themselves to an external audience.

It is in the very nature of the Colloquium that many - indeed, the majority - of the projects are incomplete, and so firm conclusions have often not yet emerged. Nevertheless, it is our hope that listeners and readers will find that every presentation contains some useful or interesting facts.

In our desire to produce a coherent yet concise, body of information for (relatively) easy consumption, the material reported in each summary has often been pruned to a small fraction of the total project. Since a *colloquium* should primarily serve as a platform for discussion, the researchers and supervisors associated with the projects presented will gladly give further details, both during and after the Colloquium. Likewise, readers of this booklet not attending the Colloquium should feel free to contact the contributors of summaries and request information in writing or in the form of referenced publications.

The large majority of projects summarised in the booklet are externally funded. It is thus appropriate that we should express our gratitude to our sponsors for their support and interest without which much of the work presented at the Colloquium could not have been undertaken.

PROCEEDINGS OF 5TH UMIST CFD COLLOQUIUM

Turbulence Modelling - A preview
Numerical Methods - A preview

« Session 1 »

Turbulence Modelling - *Fundamentals*

Paper

1.1 Sensitizing linear eddy-viscosity models to strain invariants

1.2 Development and application of a non-linear k-ϵ model

1.3 Further development of k-ω treatment including non-linear terms

1.4 An improved (basic) 2nd-moment closure for predicting transition

1.5 Generalised low-Re 2nd-moment closure without wall corrections

1.6 Adapting a '2D-limit' Reynolds-stress model for curved flows

1.7 Modelling of transition via 2nd-moment closure

1.8 Directions in 2nd moment closure

1.9 Direct numerical simulation of premixed turbulent combustion

« Session 2 »

Numerical Methods

2.1 Multiblock algorithm for general turbulent flows

2.2 Aspects of local mesh refinement

2.3 An unstructured-grid algorithm for incompressible flow

2.4 Unstructured-grid flow adaption for computation of transonic aerodynamic flows

2.5 Upstream monotonic approximations for turbulent flows

2.6 Numerical aspects of a Large Eddy Simulation algorithm

2.7 Parallel computing on distributed-memory machines

2.8 A special near-wall element for finite element computations of dense-gas dispersion over ground of variable elevation

« Session 3 »

Turbulence Modelling: Assessment & Validation

3.1 Sensitivity of 2D separation characteristics to turbulence modelling

3.2 Modelling non-equilibrium boundary layers with a modified k-ω model

3.3 Reynolds-stress and PDF transport modelling for non-premixed turbulent combustion

3.4 Second-moment modelling of buoyant flows in cavities

3.5 Second-moment modelling of flow in fluted tubes

3.6 Turbulence modelling for highly-loaded cascade blade

3.7 Differential stress transport modelling of swirling i.c. engine flows

« Session 4 »

Aerodynamic Flows

4.1 Modelling flows around high-lift subsonic aerofoil

4.2 Reynolds-stress modelling using an unstructured transonic NS solver

4.3 An embedded Cartesian Grid Approach to the computation of aerodynamic flows

4.4 Computation of aero-engine thrust-reverser flows

4.5 Second-moment-closure modelling of open separation from prolate spheroid at high incidence4.6

4.6 Computation of compressible and incompressible impinging multiple jets

4.7 CFD analysis of unconventional transonic aerofoil sections

« Session 5 »

Combustion, Two-phase Interaction, Radiation

5.1 Computer modelling of fuel sprays containing electrostatic charge

5.2 Radiation absorption in dense gas clouds by the discrete transfer method

5.3 Transport and reaction rate modelling for pre-mixed turbulent combustion

5.4 Premixed combustion modelling for IC engine applications

5.5 Particle dispersion in a plane horizontal jet

5.6 Development of a 3D non-orthogonal-grid computer code for d.i. diesel engine applications

5.7 Computer modelling of metered dose inhalers

« Session 6 »

Internal Flows

6.1 Computation of flow and heat transfer through stationary and rotating U-bends

6.2 Computation of flow and heat transfer through ribbed passages

6.3 Modelling of flow in rotor-stator cavities

6.4 Modelling the flow in a transition duct

6.5 Computation of 3D flow in linear turbine cascade

AN INTRODUCTION TO TURBULENCE MODELLING AT UMIST - 1994

As in previous colloquia in the series, nearly all the research projects reported at this 6th Colloquium are concerned with turbulent flow. Papers in Sessions 1 and 3 involve devising or assessing new or newish models of turbulence while those in later sessions provide an assessment of more established proposals in flows very different from those for which they were devised. The long sequence of steps in a model's development and assessment implied above is an inevitable consequence of turbulence modelling being an inexact science.

The aim of turbulence modelling research is to devise a general framework for computing turbulent flows. This requires, besides generality, flexibility and accuracy of the numerical algorithm, a mathematical representation of the turbulent motion that is also widely applicable, as regards geometry, boundary conditions and phenomena. It is this desire for generality that in the past, has driven us towards implementing second-moment closures into our software - not just for thin shear flows but recirculating and three-dimensional flows too.

However, geometric inadequacies in the modelling of flow through or around topographically complex surfaces, has demanded that we search for new and better approaches to closure. At second-moment level there is considerable effort at removing (or, at the least, greatly reducing the importance of) wall-reflection terms. Moreover, in modelling at all levels, we have been trying to remove 'wall-reflection' effects (that explicitly makes reference to wall distance) in the scale-determining equation. As will be reported, there seem some advantages to replacing the energy dissipation rate, ε, by (ε/k) or possibly by some other variable.

While the great superiority of second-moment closures over linear eddy-viscosity schemes is now widely acknowledged, there is, inevitably, a computational penalty. Work, both at UMIST and the University of Manchester has therefore been recently directed towards developing an approach that captured much of the strain-sensitivity power of second-moment closures while retaining the economy of eddy viscosity schemes. The result is the non-linear eddy-viscosity modelling presented in the opening three talks of Session 1. A novel feature of that work is the evaluation, by solving transport equations, of a dimensionless parameter characterizing the state of turbulence.

Research on second-moment closure occupies most of the remainder of Session 1. Transition from laminar to turbulent flow in the presence of a weak external turbulence field is a problem addressed both with a variant of the Basic Model and also with a version of the New Model that contains no wall-reflection agency. The New Model also achieves success in predicting turbulent flow parallel to the wall, including the near-wall sublayer, and in particular, flow in non-circular ducts. An area where success (at removing wall reflection) has eluded us so far is in impinging flows and the penultimate presentation reports on prospects and problems in this particularly difficult class of flows.

The final contribution in Session 1 involves a large change in strategy to the direct numerical simulation of turbulent combusting flows. Research of this type can be expected to play an increasingly important role in turbulence research not just at UMIST but nationally over the remainder of the century.

Session 3 provides greater variety partly because, in several cases, a range of models - both those generated locally and those devised elsewhere - are tested for particular cases. Models range from eddy-viscosity schemes to second-moment closures involving cubic pressure-strain approximations. Non-linear EVM's have only just begun to appear in these application-orientated studies. As remarked above, the elimination of wall-reflection terms from second-moment closure becomes more difficult in impinging and separated flows but even here progress is being made. A novelty is the use, with second moment closure, of two transport equations for, essentially, different turbulent time scales. The approach adds little to the cost (of a second moment calculation) and can be expected to be taken up more extensively in our modelling work in the future.

As in previous proceedings in this series, there follows a tabulation of what we term 'standard turbulence models': schemes that are repeatedly employed in the presentations or, at least, used as the point of departure for modelling innovations. By so doing we are enabled to keep presentations to the two-page format yet still have space to discuss results. It is hoped that the inconvenience of having to refer elsewhere for the equations is outweighed by the benefits of having a compact yet informative volume.

Table 1a The Standard k~ε Eddy Viscosity Model (EVM)

$$\rho\left[\frac{2}{3}\,\delta_{ij}k - \overline{u_i u_j}\right] = \mu_t\left[\frac{\partial U_i}{\partial x_j} + \frac{\partial U_j}{\partial x_i}\right]$$

$$-\rho\overline{u_i\theta} = \frac{\mu_t}{\sigma_\Theta}\frac{\partial \Theta}{\partial x_i}$$

$$\mu_t = c_\mu \rho \frac{k^2}{\epsilon}$$

$$\frac{Dk}{Dt} = \frac{\partial}{\partial x_j}\left[\left[\nu + \frac{\nu_t}{\sigma_k}\frac{\partial k}{\partial x_j}\right]\right] + P + G - \epsilon$$

$$\frac{D\epsilon}{Dt} = \frac{\partial}{\partial x_j}\left[\left[\nu + \frac{\nu_t}{\sigma_\epsilon}\frac{\partial \epsilon}{\partial x_j}\right]\right] + c_{\epsilon 1}\frac{\epsilon}{k}\left[P + G\right] - c_{\epsilon 2}\frac{\epsilon^2}{k} + [YC]$$

$P \equiv -\overline{u_i u_j}\,\partial U_i/\partial x_j$; $\quad G \equiv -\beta_i \overline{u_i \theta}$

$YC \equiv$ Yap Correction $= \mathrm{Max}\left(0.83\left[\frac{\ell}{\ell_e} - 1\right]\left[\frac{\ell}{\ell_e}\right]^2 \frac{\epsilon^2}{k},\ 0\right]$

c_μ	$c_{\epsilon 1}$	$c_{\epsilon 2}$	σ_Θ	σ_k	σ_ϵ
0.09	1.45	1.92	0.9	1.0	1.3

Table 1b The Standard low Reynolds no. form of k~ε EVM

As Table 1a except:

$$c_\mu = 0.09 \exp\left[-3.4/(1 + R_t/50)^2)\right];\quad c_{\epsilon 2} = 1.92\ (1 - 0.3 \exp - R_t^2)$$

where $R_t \equiv k^2/\nu\tilde{\epsilon}$

and, in place of the equation for ϵ,

$$\frac{D\tilde{\epsilon}}{Dt} = \frac{\partial}{\partial x_j}\left[\left[\nu + \frac{\nu_t}{\sigma_\epsilon}\right]\frac{\partial \tilde{\epsilon}}{\partial x_j}\right] + c_{\epsilon 1}\frac{\epsilon}{k}\left[P + G\right] - c_{\epsilon 2}\frac{\epsilon^2}{k} + 2\nu\nu_t\left[\frac{\partial^2 U_i}{\partial x_k \partial x_\ell}\right]^2 + YC$$

where $\epsilon \equiv \tilde{\epsilon} - 2\,\nu\,(\partial k^{\frac{1}{2}}/\partial x_j)^2$; $\quad \mu_t = c_\mu\,\rho k^2/\tilde{\epsilon}$

The quantity $\tilde{\epsilon}$, which differs negligibly from ϵ beyond the near-wall sublayer, takes the value zero at the wall. In YC $\tilde{\epsilon}$ replaces ϵ.

Table 2: The Basic Differential Second-Moment Closure

A: Computing the Reynolds stresses

$$\frac{\partial \overline{u_i u_j}}{\partial t} + \underbrace{U_k \frac{\partial \overline{u_i u_j}}{\partial x_k}}_{C_{ij}} = d_{ij} + P_{ij} + F_{ij} + G_{ij} + \Phi_{ij} - \epsilon_{ij}$$

$$\frac{\partial \epsilon}{\partial t} + U_k \frac{\partial \epsilon}{\partial x_k} = d_\epsilon + \tfrac{1}{2} c_{\epsilon 1} (P_{kk} + G_{kk}) \frac{\epsilon}{k} - c_{\epsilon 2} \frac{\epsilon^2}{k} + YC$$

$$P_{ij} \equiv - \left\{ \overline{u_i u_k} \frac{\partial U_j}{\partial x_k} + \overline{u_j u_k} \frac{\partial U_i}{\partial x_k} \right\} \; ; \; F_{ij} \equiv - 2\Omega_k \left\{ \overline{u_j u_m} \, \epsilon_{ikm} + \overline{u_i u_m} \, \epsilon_{jkm} \right\} \; ;$$

$$G_{ij} \equiv - \left(\overline{u_j \theta} \beta_i + \overline{u_i \theta} \beta_j \right)$$

$$\Phi_{ij} = \Phi_{ij_1} + \Phi_{ij_2} + \Phi_{ij_3} + (\Phi_{ijw})$$

where $$\Phi_{ij_1} = - c_1 \frac{\epsilon}{k} \left[\overline{u_i u_j} - \frac{1}{3} \delta_{ij} \overline{u_k u_k} \right]$$

$$\Phi_{ij_2} = - c_2 \left[P_{ij} - C_{ij} + F_{ij} - \frac{1}{3} \delta_{ij} (P_{kk} - C_{kk}) \right]$$

$$\Phi_{ij_3} = - c_3 \left[G_{ij} - \frac{1}{3} \delta_{ij} G_{kk} \right]$$

$$\epsilon_{ij} = \frac{2}{3} \delta_{ij} \epsilon \; ; \; d_{ij} = \frac{\partial}{\partial x_k} \left[c_s \frac{k}{\epsilon} \overline{u_k u_\ell} \frac{\partial \overline{u_i u_j}}{\partial x_\ell} \right]$$

$$d_\epsilon = \frac{\partial}{\partial x_k} \left[c_\epsilon \frac{k}{\epsilon} \overline{u_k u_\ell} \frac{\partial \epsilon}{\partial x_\ell} \right]$$

YC ≡ Yap correction, see Table 2

Wall Flows Only

$$\Phi_{ijw} = \left[c_1' \frac{\epsilon}{k} \left[\overline{u_k u_m} \, n_k n_m \, \delta_{ij} - \frac{3}{2} \overline{u_i u_k} \, n_k n_j - \frac{3}{2} \overline{u_k u_j} \, n_k n_i \right] \right.$$

$$+ c_2' \left[\Phi_{km_2} \, n_k n_m \, \delta_{ij} - \frac{3}{2} \Phi_{ik_2} \, n_k n_j - \frac{3}{2} \Phi_{kj_2} \, n_k n_i \right]$$

$$\left. + c_3' \left[\Phi_{km_3} \, n_k n_m \, \delta_{ij} - \frac{3}{2} \Phi_{ik_3} \, n_k n_j - \frac{3}{2} \Phi_{kj_3} \, n_k n_i \right] \right] \frac{k^{3/2}}{c_\ell \epsilon x_n}$$

c_1	c_2	c_3	c_s	c_ϵ	$c_{\epsilon 1}$	$c_{\epsilon 2}$	c_1'	c_2'	c_3'	c_ℓ
1.8	0.6	0.5	0.22	0.18	1.44	1.92	0.5	0.3	0	2.5

Table 2 (cont'd)

B: Computing the Scalar Flux and Variance (Free Shear Flow Form)

$$\frac{\partial \overline{u_i\theta}}{\partial t} + \underbrace{U_k \frac{\partial \overline{u_i\theta}}{\partial x_k}}_{c_{i\theta}} = d_{i\theta} + P_{i\theta} + F_{i\theta} + G_{i\theta} + \Phi_{i\theta} - \epsilon_{i\theta}$$

$$\frac{\partial \frac{1}{2}\overline{\theta^2}}{\partial t} + U_k \frac{\partial \frac{1}{2}\overline{\theta^2}}{\partial x_k} = d_\theta + P_\theta - \epsilon_\theta$$

$$P_{i\theta} \equiv \underbrace{- \overline{u_i u_k} \frac{\partial \Theta}{\partial x_k} - \overline{u_k\theta} \frac{\partial U_i}{\partial x_k}}_{P_{i\theta 2}} \; ; \; F_{i\theta} \equiv - 2\Omega_k \, \overline{\theta u_m} \, \epsilon_{ikm}$$

$$G_{i\theta} \equiv - \beta_i \frac{\overline{\theta^2}}{\Theta}$$

$$d_{i\theta} = c_\theta \frac{\partial}{\partial x_k} \left[\overline{u_\ell u_k} \frac{\partial \overline{u_i\theta}}{\partial x_k} \right]$$

$$d_\theta = c_\theta \frac{\partial}{\partial x_k} \left[\overline{u_\ell u_k} \frac{\partial \overline{\theta^2}}{\partial x_k} \right]$$

$$\Phi_{i\theta} = \Phi_{i\theta 1} + \Phi_{i\theta 2} + \Phi_{i\theta 3} + (\Phi_{i\theta w})$$

$$\Phi_{i\theta 1} = - c_{1\theta} \frac{\epsilon}{k} \overline{u_i\theta} \; ; \; \Phi_{i\theta 2} = - c_{2\theta} \left(P_{i\theta 2} - C_{i\theta} + F_{i\theta} \right)$$

$$\Phi_{i\theta 3} = - c_{3\theta} \, G_{i\theta} \; ; \; \epsilon_{i\theta} = 0$$

$$P_\theta \equiv - \overline{u_k\theta} \, \partial\Theta/\partial x_k \; ; \; \epsilon_\theta = \frac{1}{2} \frac{\overline{\theta^2}\epsilon}{k} R \; ; \; R^{-1} = 1.5 \, (1 + A_{2\theta}) \; ;$$

$$A_{2\theta} \equiv \frac{\overline{u_i\theta} \; \overline{u_i\theta}}{\overline{\theta^2} k}$$

$c_{1\theta}$	$c_{2\theta}$	$c_{3\theta}$	c_θ
3.0	0.5	0.5	0.18

Table 3: The New DSM Model

(For free flows only at present)

A: Computing the Reynolds stresses

As Basic Model except:

$$\Phi_{ij_1} = - c_1 \epsilon \left(a_{ij} + c_1' \left(a_{ik} a_{kj} - \frac{1}{3} \delta_{ij} A_2\right)\right) - \epsilon a_{ij}$$

$$\Phi_{ij_2} = - 0.6 \left[P_{ij} - \frac{1}{3} \delta_{ij} P_{kk}\right] + 0.3 \epsilon a_{ij} (P_{kk}/\epsilon)$$

$$- 0.2 \left\{\frac{\overline{u_k u_j}}{k} \overline{u_\ell u_i} \left[\frac{\partial U_k}{\partial x_\ell} + \frac{\partial U_\ell}{\partial x_k}\right] - \frac{\overline{u_\ell u_k}}{k} \left[\overline{u_i u_k} \frac{\partial U_j}{\partial x_\ell} + \overline{u_j u_k} \frac{\partial U_i}{\partial x_\ell}\right]\right\}$$

$$- c_2 \left[A_2 (P_{ij} - D_{ij}) + 3 a_{mi} a_{nj} (P_{mn} - D_{mn})\right]$$

$$+ t \left\{\left[\frac{7}{15} - \frac{A_2}{4}\right] \left[P_{ij} - \frac{1}{3} \delta_{ij} P_{kk}\right]\right.$$

$$+ 0.2 \epsilon \left[a_{ij} - \frac{1}{2} \left[a_{ik} a_{kj} - \frac{1}{3} \delta_{ij} A_2\right]\right] \frac{P}{\epsilon} - 0.05 a_{ij} a_{\ell k} P_{k\ell}$$

$$+ 0.1 \left[\left[\frac{\overline{u_i u_m}}{k} P_{mj} + \frac{\overline{u_j u_m}}{k} P_{mi}\right] - \frac{2}{3} \delta_{ij} \frac{\overline{u_\ell u_m}}{k} P_{m\ell}\right]$$

$$+ 0.1 \left[\frac{\overline{u_\ell u_i}}{k^2} \frac{\overline{u_k u_j}}{k^2} - \frac{1}{3} \delta_{ij} \frac{\overline{u_\ell u_m}}{k^2} \frac{\overline{u_k u_m}}{k^2}\right] \left[6 D_{\ell k} + 13 k \left[\frac{\partial U_\ell}{\partial x_k} + \frac{\partial U_k}{\partial x_\ell}\right]\right]$$

$$\left. + 0.2 \frac{\overline{u_\ell u_i}}{k^2} \frac{\overline{u_k u_j}}{k^2} (D_{\ell k} - P_{\ell k})\right\}$$

where $a_{ij} \equiv \left(\frac{\overline{u_i u_j}}{k} - \frac{1}{3} \delta_{ij} \frac{\overline{u_k u_k}}{k}\right)$; $A_2 \equiv a_{ij} a_{ij}$; $A_3 \equiv a_{ij} a_{jk} a_{ki}$;

$$A \equiv 1 - \frac{9}{8} (A_2 - A_3)$$

and $D_{ij} \equiv - \left\{\overline{u_i u_k} \frac{\partial U_k}{\partial x_j} + \overline{u_j u_k} \frac{\partial U_k}{\partial x_i}\right\}$

$$\frac{D\epsilon}{Dt} = d_\epsilon + c_{\epsilon 1} \frac{\epsilon}{k} (P_{kk} + G_{kk}) - c_{\epsilon 2} \frac{\epsilon^2}{k}$$

c_1	c_1'	c_2	c_2'	$c_{\epsilon 1}$	$c_{\epsilon 2}$
$3.1\ (A_2 A)^{\frac{1}{2}}$	1.2	0.60	0.0	1.0	$1.92/(1+0.7 A_2^{\frac{1}{2}} A)$
		0.55	0.6		

Table 3 (cont'd)

B: Computing the Scalar Fluxes and Variances

As Basic Model except:

$$\Phi_{i\theta 1} = - c_{1\theta} \frac{\epsilon}{k} \left[\overline{u_i\theta} \ (1+0.6A_2) + c'_{1\theta} \ a_{ik} \ \overline{u_k\theta} + c''_{1\theta} \ a_{ik}a_{kj} \ \overline{u_j\theta} \right] - c'''_{1\theta} \ Rka_{ij} \frac{\partial \Theta}{\partial x_j}$$

$$\Phi_{i\theta 2} = 0.8 \ \overline{\theta u_k} \frac{\partial U_i}{\partial x_k} - 0.2 \ \overline{\theta u_k} \frac{\partial U_k}{\partial x_i} + \frac{1}{6} \frac{\epsilon}{k} \overline{\theta u_i} \frac{P_{kk}}{\epsilon} - 0.4 \ \overline{\theta u_k} \ a_{i\ell} \left[\frac{\partial U_k}{\partial x_\ell} + \frac{\partial U_\ell}{\partial x_k} \right]$$

$$+ 0.1 \ \overline{\theta u_k} \ a_{ik}a_{m\ell} \left[\frac{\partial U_m}{\partial x_\ell} + \frac{\partial U_\ell}{\partial x_m} \right] - 0.1 \ \overline{\theta u_k} \ (a_{im} \ P_{mk} + 2a_{mk} \ P_{im})/k$$

$$+ 0.15 \ a_{m\ell} \left[\frac{\partial U_k}{\partial x_\ell} + \frac{\partial U_\ell}{\partial x_k} \right] (a_{mk} \ \overline{\theta u_i} - a_{mi} \ \overline{\theta u_k})$$

$$- 0.05 \ a_{m\ell} \left[7a_{mk} \left[\overline{\theta u_i} \frac{\partial U_k}{\partial x_\ell} + \overline{\theta u_k} \frac{\partial U_i}{\partial x_\ell} \right] - \overline{\theta u_k} \left[a_{m\ell} \frac{\partial U_i}{\partial x_k} + a_{mk} \frac{\partial U_i}{\partial x_\ell} \right] \right]$$

$$\frac{D\epsilon_\theta}{Dt} = \left\{ c_{\epsilon\theta 1} \frac{P_\theta}{\epsilon_\theta} + c'_{\epsilon\theta 1} \frac{\nu_t}{\epsilon} \left[\frac{\partial U_i}{\partial x_j} \right]^2 + \frac{c_{\epsilon\theta 3} G_{kk}}{2} \right\} \frac{\epsilon_\theta \epsilon}{Rk} - \left[c_{\epsilon\theta 2} \frac{\epsilon\epsilon_\theta}{k} + c'_{\epsilon\theta 2} \frac{\epsilon^2\theta}{k} \right]$$

$$+ c_{\epsilon\theta} \frac{\partial}{\partial x_k} \left[\frac{\overline{u_k u_\ell}}{\epsilon} \frac{k}{\epsilon} \frac{\partial \epsilon_\theta}{\partial x_\ell} \right]$$

$c_{1\theta}$	$c'_{1\theta}$	$c''_{1\theta}$	$c'''_{1\theta}$	$c_{\epsilon\theta 1}$	$c'_{\epsilon\theta 1}$
$1.7 \ (1 + 1.2 \ (A_2A)^{\frac{1}{2}})R^{\frac{1}{2}}$	$- 0.8$	1.1	$0.2A^{\frac{1}{2}}$	1.6	2.6

$c_{\epsilon\theta 2}$	$c'_{\epsilon\theta 2}$	$c_{\epsilon\theta 3}$	$c_{\epsilon\theta}$
$\frac{0.9}{1+1.1A_2A^{\frac{1}{2}}}$	$\frac{2.0}{1+1.1A_2A^{\frac{1}{2}}}$	2.6	0.18

Table 4: ASM Truncation

- Stress transport is eliminated by the approximations:

$$\frac{D\,\overline{u_i u_j}}{Dt} = \frac{\overline{u_i u_j}}{k}\,\frac{Dk}{Dt}$$

$$d_{ij} = \frac{\overline{u_i u_j}}{k}\,d_k$$

- Heat transfer studies employing an ASM approximation for the stress field have adopted the GGDH form for $\overline{u_i u_j}$:

$$\overline{u_i \theta} = 0.35\,\frac{k}{\epsilon}\,\overline{u_i u_k}\,\frac{\partial \Theta}{\partial x_k}$$

$$\frac{\overline{u_i u_j}}{k} = \frac{2}{3}\delta_{ij} - \frac{\nu_t}{k}S_{ij} + c_1\frac{\nu_t}{\tilde{\varepsilon}}\left(S_{ik}S_{kj} - \frac{1}{3}S_{kl}S_{kl}\delta_{ij}\right) + c_2\frac{\nu_t}{\tilde{\varepsilon}}\left(\Omega_{ik}S_{kj} + \Omega_{jk}S_{ki}\right) + c_3\frac{\nu_t}{\tilde{\varepsilon}}\left(\Omega_{ik}\Omega_{jk} - \frac{1}{3}\Omega_{lk}\Omega_{lk}\delta_{ij}\right) + c_4\frac{\nu_t k}{\tilde{\varepsilon}^2}\left(S_{ki}\Omega_{lj} + S_{kj}\Omega_{li} - \frac{2}{3}S_{km}\Omega_{lm}\delta_{ij}\right)S_{kl} + c_5\frac{\nu_t k}{\tilde{\varepsilon}^2}S_{ij}S_{kl}S_{kl} + c_6\frac{\nu_t k}{\tilde{\varepsilon}^2}S_{ij}\Omega_{kl}\Omega_{kl}$$

$$S_{ij} \equiv \frac{\partial U_i}{\partial x_j} + \frac{\partial U_j}{\partial x_i}, \qquad \Omega_{ij} \equiv \frac{\partial U_i}{\partial x_j} - \frac{\partial U_j}{\partial x_i}$$

$$\nu_t = c\, f\, \frac{k^2}{\tilde{\varepsilon}}$$

c_1	c_2	c_3	c_4	c_5	c_6
- 0.1	0.1	0.26	- 1.0	- 0.1	0.1

Table 5 UMIST's Standard Cubic Eddy-Viscosity Stress-Strain Correction

NUMERICAL PRACTICES - A Preview

Although turbulence, in all its varied manifestations, is rightly regarded as the principal challenge to CFD evolving towards a truly predictive aid to engineering design, no amount of creative turbulence modelling is productive without the availability of an accurate and efficient numerical framework into which newly formulated or improved models can be incorporated and which allows these models to be applied to geometrically and physically complex flows. A numerical procedure is often regarded as little more than a *vehicle* 'conveying' or 'driven by' mathematical closures of turbulence and other physical processes. While this perception is not invalid, in principle, the *vehicle* must satisfy a range of stringent and taxing specifications.

A numerical procedure must be based on accurate discretisation practices, for otherwise it is apt to return the wrong message about the predictive abilities of the turbulence models it incorporates; and a wrong or inaccurate message is, arguably, worse than no message at all. It must be geometrically flexible, allowing complex geometries to be accommodated without undue mesh depletion and distortion, both of which can be seriously detrimental to accuracy. It must be economical, for if it is not, the size and difficulty of the application will be constrained. Finally, and perhaps most importantly, the numerical procedure must retain its stability and boundedness when combined with the ever-more elaborate and increasingly non-linear turbulence closures being formulated.

Much of the work undertaken at UMIST over the past twelve years on numerical issues has been directed towards the implementation, validation and application of complex turbulence models in increasingly challenging geometries and flow conditions; the majority of summaries contained in **Sections 3 to 6** are devoted to exposing the ground covered in the past two years. Of particular interest has been the validation and improvement of Reynolds-stress and low-Re-number models in an ever widening spectrum of external and internal two- and three-dimensional flows involving, *inter alia*, strong curvature, separation, swirl, rotation, density gradients, compressibility and, increasingly, combustion. In this context, numerical accuracy, solution economy and the retention of iterative stability in the face of increasing model non-linearity and coupling have been of principal concern. The wish (and the need) to extend the validation range to complex geometries has motivated the development of a variety of general-mesh schemes able to accommodate curved surfaces.

At the time of the previous Colloquium, considerable geometric flexibility was already offered by single-block curved-orthogonal and non-orthogonal, structured-mesh procedures for two- and three-dimensional flows, as well as unstructured-mesh schemes for two-dimensional geometries. Over the past two years, these capabilities have been enhanced in several directions, principally through the development of general multiblock schemes for two- and three-dimensional geometries. A summary in **Section 2** highlights recent progress in this area, and **Fig. 1** conveys an impression of current capabilities in the context of flows around aerofoils, blades and in complex ducts. Further efforts have focused on flow- and geometry-dependent grid adaptation involving grid-movement, enrichment and embedding within structured- and unstructured-mesh schemes, particularly for external aerodynamics, and on the formulation of an iterative, pressure-based unstructured-mesh procedure for incompressible flow. Four summaries, three in **Section 2** and the third in **Section 4,** deal with related issues, while **Fig. 2** gives an indication of the methodologies pursued.

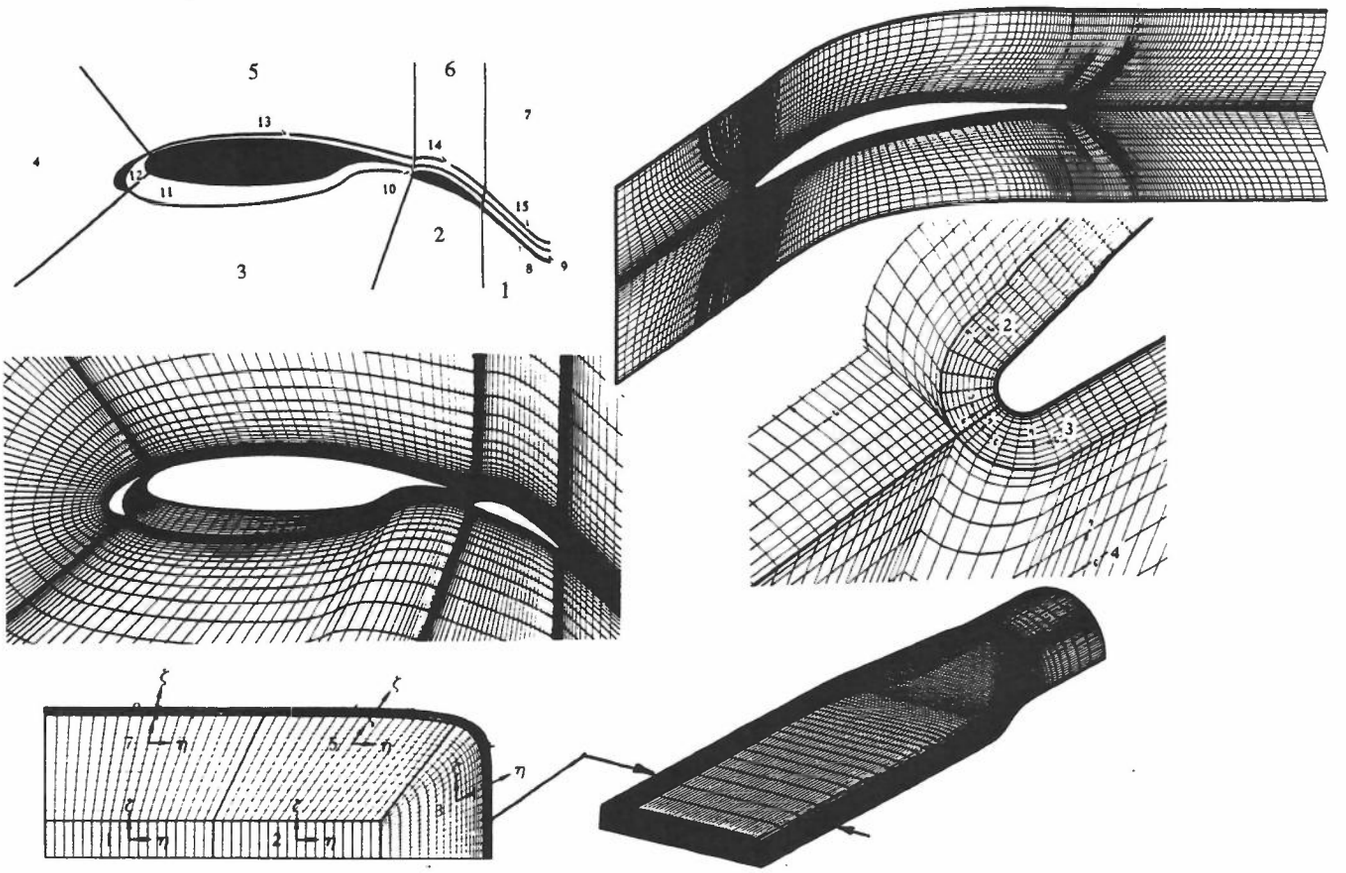

Fig. 1: Use of multiblock schemes for complex turbulent flows

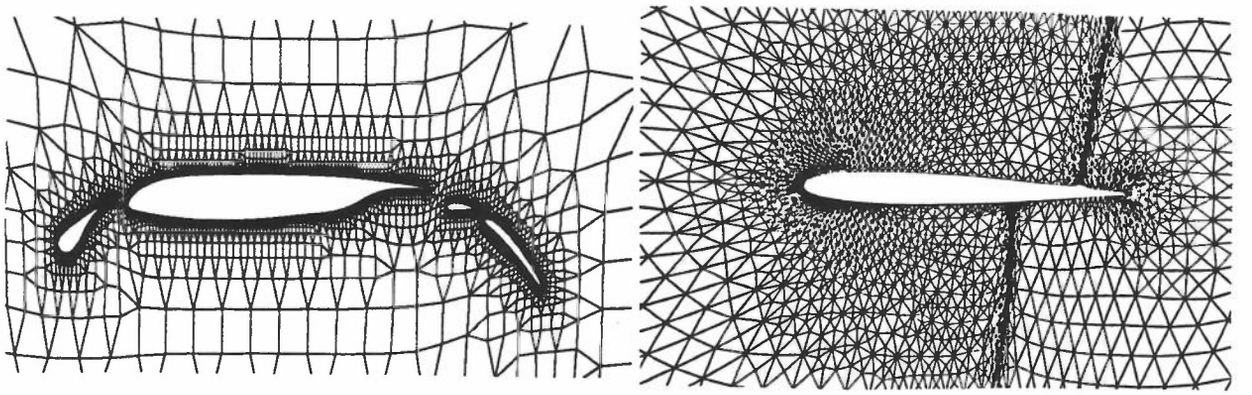

Fig. 2: Local grid refinement and adaptation for unstructured-grid schemes

In the area of numerical approximation techniques, the introduction of boundedness into second-order accurate discretisation of convection, especially of turbulence, has received particular attention over the past two years. A new, highly economical boundedness-preserving scheme, based on the QUICK approximation and termed **UMIST** (Upstream Monotonic Interpolation for Scalar Transport), has been devised and applied to a wide variety of conditions to approximate both mean-flow and turbulence convection, including that of the Reynolds stresses. Specifically in relation to LES - a new area of research at UMIST - a general non-orthogonal co-located finite volume scheme, involving second-order approximation in time and space and using Bi-conjugate Gradient and GMRES solvers, has been developed and is undergoing testing. Summaries relating to the "UMIST" scheme and LES are contained in **Section 2.**

Improvements in computational efficiency have in the past been pursued principally with the through multigrid acceleration, and several summaries dealing with MG efficiency in the computation of compressible and incompressible turbulent flows have been included in the proceedings of the **5th Colloquium**. In the past two years, increasing efforts have gone into parallel computing on a Transputer-based MIMD machine, particularly for turbulent transonic flows. This work is set to expand in the direction of multi-block implementations on powerful MPP machines, including the Intel Hypercube at the Daresbury Laboratory and the Cray T3D at the Edinburgh Parallel Computing Centre.

Looking ahead, we anticipate that the evolving adaptive multiblock and unstructured-grid schemes, coupled with increasing exploitation of MPP machines, will permit numerically reliable assessments to be made of established and improved forms of second-moment and non-linear eddy-viscosity closures to be undertaken in increasingly complex geometries - for example, multi-element high-lift aerofoils and car bodies. In parallel, work on LES and DNS is set gain an increasingly prominent profile in the spectrum of UMIST's CFD activities, principally as a consequence of the installation, in July/August 1994, of the Cray T3D in Edinburgh University. We expect this work to feed into as well derive benefits from both fundamental and applied research based of Reynolds-averaged modelling.

« Session 1 »

Turbulence Modelling - *Fundamentals*

SENSITIZING LINEAR EDDY VISCOSITY MODELS TO STRAIN INVARIANTS

Researcher : J.O. Ismael
Supervisor : M.A. Cotton
Department of Engineering, University of Manchester
Sponsor : SERC/DRA Farnborough

1. INTRODUCTION

The 'parent' or 'high Reynolds number' constitutive equation of k-ϵ models applied to flows in simple shear may be written $-\overline{uv} = C_\mu (k^2/\epsilon)dU/dy$. In the widely-used Launder and Sharma (LS) model [1] this relation is modified by the introduction of a viscous damping term, $f_\mu(Re_t)$. Dimensional analysis and the DNS studies of Lee et al. [2] indicate, however, that the parent relation should be generalized to read $-\overline{uv} = C_\mu f_s (S)(k^2/\epsilon)dU/dy$ where, in the present work, S is (initially) defined as $S = [(k/\epsilon)dU/dy]^2$. Viscosity-dependent damping is to be confined to regions of very low Re_t.

2. MODEL DEVELOPMENT

S is first cast in invariant form for application to general strain fields. Test cases examined to date at the University of Manchester have, however, been restricted to parallel or near-parallel flows and the basic linear stress-strain eddy viscosity formulation is retained at present (cf. Craft et al. [3]):

$$S = \frac{1}{2}\left[\frac{k}{\epsilon}\left(\frac{\partial U_i}{\partial x_j} + \frac{\partial U_j}{\partial x_i}\right)\right]^2 \quad ; \quad -\overline{u_i u_j} = \nu_t \left(\frac{\partial U_i}{\partial x_j} + \frac{\partial U_j}{\partial x_i}\right) - \frac{2}{3}\delta_{ij}k \tag{1}$$

$$\text{where } \nu_t = C_\mu f_s(S) f_\mu(Re_t) \frac{k^2}{\epsilon} \tag{2}$$

In earlier work [4] it was found that the above formulation combined with k- and ϵ-equations required the introduction of $f_\mu(Re_t)$ comparable in effect to $f_s(S)$. In the present study S is therefore made the subject of a third transport equation :

$$\frac{DS}{Dt} = \frac{1}{2}\frac{k}{\epsilon}\left(\frac{\partial U_i}{\partial x_j} + \frac{\partial U_j}{\partial x_i}\right)^2 + \frac{\partial}{\partial x_j}\left(\frac{\nu_t}{\sigma_s}\frac{\partial S}{\partial x_j}\right) - \frac{S}{k/\epsilon} \tag{3}$$

Following Maxey [5], S determined from equation (3) may be interpreted as a measure of effective total strain. In this manner historical influences (or 'memory') are brought to bear in the argument of the damping function.

3. RESULTS

Fig. 1 shows the combined damping function $f = f_s f_\mu$ compared with data derived by Patel et al. [6] and the LS model. The composition of the damping function is shown in Fig. 2 which serves to demonstrate that $f_s(S)$ is the principal agency of damping in the present model. In Figs. 3 and 4 profiles of U^+ and k^+ are compared with the DNS data of Kim et al. [7].

Full details of the model discussed here (which is not yet fully optimized) together with results for buoyancy-influenced flows are given in [8]. The present work proceeds in collaboration with Professor Launder, Dr. Craft and Mr. Suga.

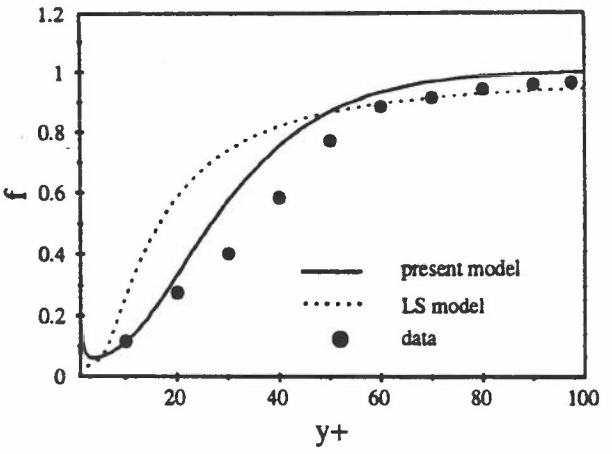

Fig.1 Present and LS damping functions (pipe flow, Re=50,000)

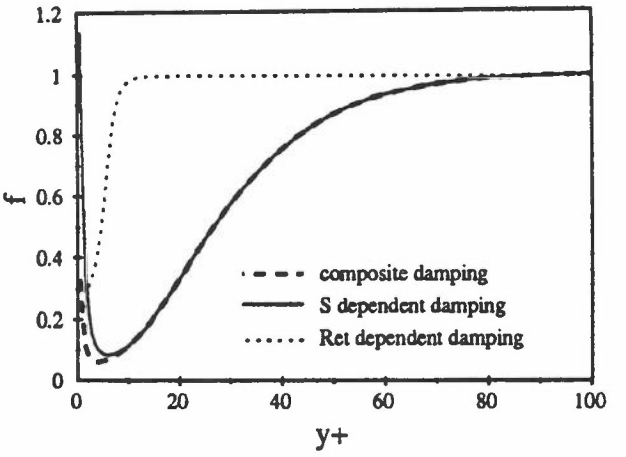

Fig.2 Composition of the present damping function (pipe flow, Re=50,000)

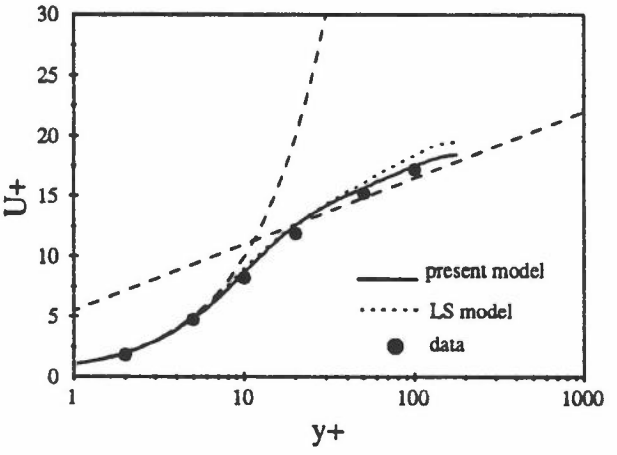

Fig.3 Velocity profile (channel flow, Re_τ=180)

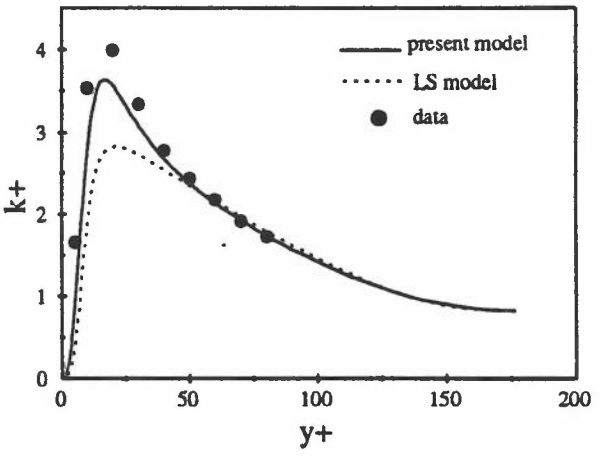

Fig.4 Turbulent kinetic energy profile (channel flow, Re_τ=180)

REFERENCES

1. Launder, B.E. and Sharma, B.I., Lett. Heat Mass Transfer, 1, 131-138 (1974).
2. Lee, M.J., Kim, J. and Moin, P., J. Fluid Mech., 216, 561-583 (1990).
3. Craft, T.J., Launder, B.E. and Suga, K., Proc. 6th UMIST CFD Colloquium, 1994.
4. Cotton, M.A. and Ismael, J.O., Proc. 5th Int. Symp. on Refined Flow Modelling and Turbulence Measurements, Paris, 1993.
5. Maxey, M.R., J. Fluid Mech., 124, 261-282 (1982).
6. Patel, V.C., Rodi, W. and Scheuerer, G., AIAA J., 23, 1308-1319 (1985).
7. Kim, J., Moin, P. and Moser, R., J. Fluid Mech., 177, 133-166 (1987).
8. Cotton, M.A. and Ismael, J.O., Abstract submitted to Int. Symp. on Turbulence, Heat and Mass Transfer, Lisbon, 1994.

DEVELOPMENT AND APPLICATION OF A NON-LINEAR k-ε MODEL

Researchers: K. Suga and T.J. Craft
Supervisor: Prof. B.E. Launder
Sponsors: Toyota Central R&D, Rolls Royce plc, SERC

1. INTRODUCTION

It is well known that conventional EVM's give unrealistic predictions for certain flow fields such as impinging flows, swirling flows and flows near curved surfaces. Craft et al.[1] tried to improve this weakness by introducing a non-linear constitutive relation with strain- and vorticity-invariant dependencies. Although the proposed model gave very encouraging improvements in a wide range of flow fields, its predictive accuracy near a wall needed further improvements.

2. APPROACH

DNS results [2] indicate that A2 has a large peak value and changes relatively smoothly in the buffer region. Thus, in order to capture near wall Reynolds stress behaviour, in addition to the S, Ω dependencies, it is helpful to introduce stress-invariant, A2, dependencies into the non-linear constitutive relation. The following functions and coefficients for the non-linear EVM are emerged through numerical experiments.

$$c_\mu = \frac{0.667 r_\eta}{1+1.8\eta}\left[1-\exp\left\{\frac{-0.145}{\exp\left(-1.3\eta^{5/6}\right)}\right\}\right], \eta = \max\left(\tilde{S},\ \tilde{\Omega}\right) r_\eta$$

$$r_\eta = 2-\exp\left\{-(A_2/0.5)^3\right\}+5\sqrt{\exp\left(-\tilde{R}_t/20\right)}$$

c_1	c_2	c_3	c_4	c_5	c_6
$-0.1 f_q/f_\mu$	$0.11 f_q/f_\mu$	$0.26 f_q/f_\mu$	$-0.8 f_c$	$-0.5 f_c$	$0.5 f_c$

$$f_\mu = \frac{1.1\sqrt{1-\exp\left(-\tilde{R}_t/20\right)}}{1+0.6A_2+0.2A_2^{3.5}}, f_q = \frac{r_\eta}{\sqrt{1+0.0086\eta^2}}, f_c = \frac{r_\eta^2}{1+0.45\eta^{2.5}}$$

A2 is obtained by solving its transport equation:

$$\frac{dA_2}{dt} = D_{A_2} - 2\frac{A_2}{k}P_k + 2\frac{a_{ij}}{k}P_{ij} + 2\frac{a_{ij}}{k}\phi_{ij} + 2\frac{A_2}{k}\varepsilon - 2\frac{a_{ij}}{k}\varepsilon_{ij}$$

by using the GGDH for the diffusion process, the cubic model of ϕ_{ij} and the ε_{ij} model of UMIST's new DSM. The GGDH is also employed in the k, ε equations. In the k equation, an additional modelled pressure-diffusion term, πk, is introduced while the ε equation has a new modelled gradient production term, $P_{\varepsilon 3}$, which is similar to Rodi-Mansour's [3], and a re-tuned f_2 function.

$$\Pi_k = 0.15\frac{\partial}{\partial x_k}\left(\nu f_k \frac{k}{\tilde{\varepsilon}}\frac{\partial \tilde{\varepsilon}}{\partial x_k}\right), f_k = \left\{1-\exp\left(-\tilde{R}_t/2\right)\right\}^{0.5}$$

$$P_{\varepsilon 3} = 0.9\nu\nu_t \frac{\partial^2 U_i}{\partial x_k \partial x_j}\frac{\partial^2 U_i}{\partial x_k \partial x_j} + 0.7\nu\frac{\nu_t}{k}\frac{\partial k}{\partial x_k}\frac{\partial U_i}{\partial x_l}\frac{\partial^2 U_i}{\partial x_k \partial x_l}, f_2 = \frac{1-0.3\exp\left(-\tilde{R}_t^{\,2}\right)}{\left\{1-\exp\left(-\tilde{R}_t/2\right)\right\}}$$

3. RESULTS

Fig 1 shows predictions of the fully developed channel flow at Re=14000 comparing with the DNS results. It is clear that the present model reproduces all the near-wall variables quite accurately. The predictive accuracy in the other complex flows is the same as that of the version of Craft et al.[1].

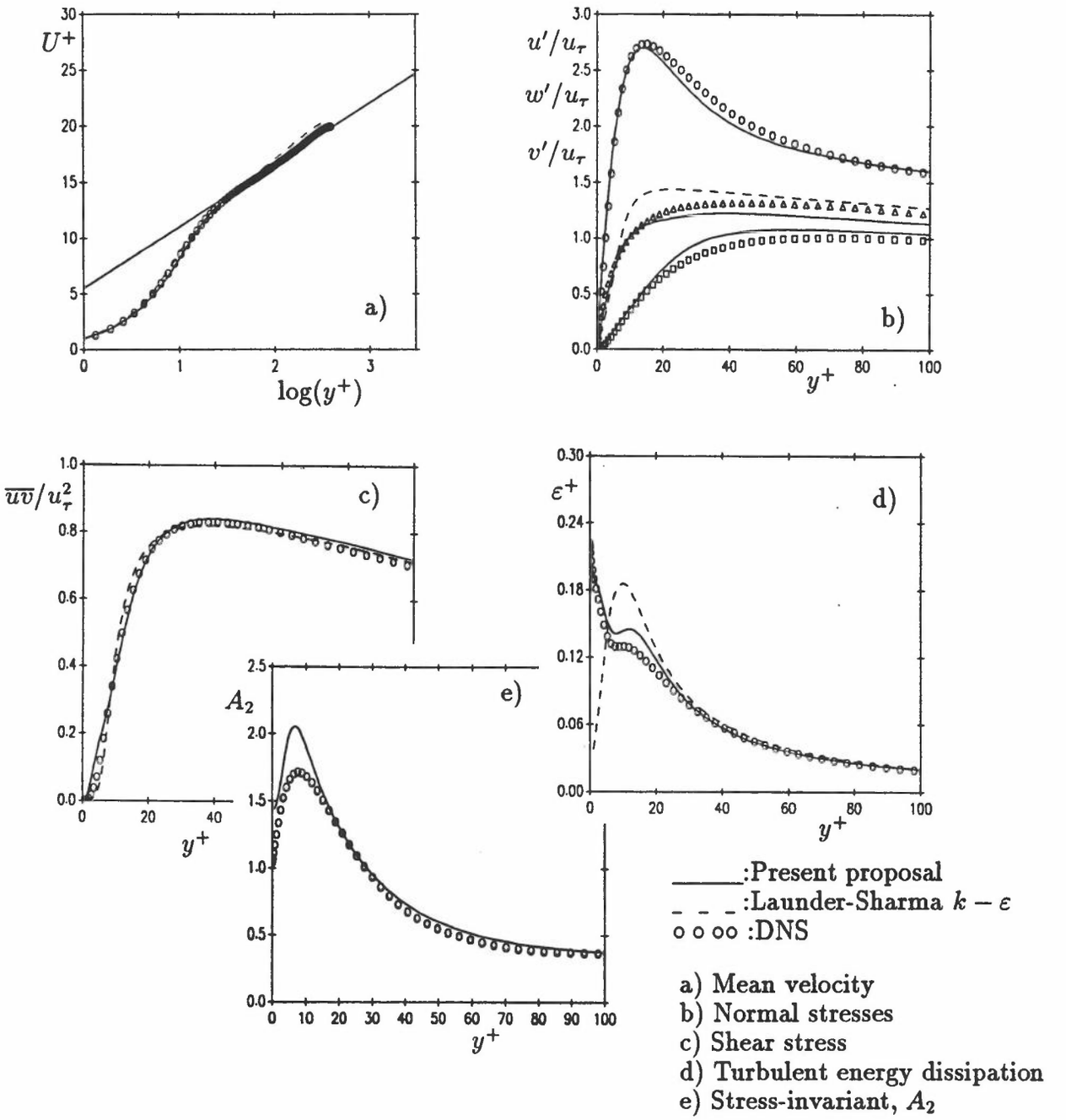

Figure 1 :Predictions of the fully developed channel flow at Re=14000.

4. REFERENCES

1. Craft,T.J., Launder,B.E., and Suga,K., 1993, 'Extending the applicability of eddy viscosity models through the use of deformation invariants and non-linear elements' Proc. 5th Int. Symp. Refined Flow Modelling and Turbulence Measurements, 125--132.
2. Kim,J., Moin,P., and Moser,R., 1987, 'Turbulence statistics in fully developed channel flow at low Reynolds number' J. Fluid Mech., 177, 133--166.
3. Rodi,W., Mansour,N.N., 1993, 'Low Reynolds number k-eps modelling with the aid of direct simulation data' J. Fluid Mech., 250, 509--529.

FURTHER DEVELOPMENT OF k-ω TREATMENT INCLUDING NON-LINEAR TERMS

Researchers : D. Sofialides, T.J. Craft
Supervisor : B.E. Launder
Sponsor : SERC

1. INTRODUCTION

One of the major difficulties in computing near-wall flows is the problem of modelling the dissipation rate of turbulent kinetic energy. The standard ε equation requires Re-number dependent damping functions and extra near-wall source terms which can lead to a less stable scheme. In addition, it is well known that the equation gives poor predictions in separating and stagnating flows. This latter problem can, to some extent, be overcome by including the Yap lengthscale correction, although it is not easily applied to complex topographies, since it involves prescribing the "distance to the wall".

A promising alternative was proposed by Wilcox (1991), who replaced the ε equation by a transport equation for what he termed the "specific dissipation rate" $\omega = \varepsilon/k$. Although, in the later paper cited, the model still employed Re-number damping functions, studies of boundary layers in adverse pressure gradients and, more searchingly, explorations of the impinging jet reported at the 5th CFD Colloquium, indicated that no equivalent of the Yap correction was needed. This has great potential advantages for studying complex flow geometries.

In fig. 3, comparisons of Wilcox's k-ω and the k-ε model with and without the Yap correction, shows that, although the k-ω model does considerably overpredict the impingement heat-transfer, the profile shape is quite promising, particularly as the model *does not* include a Yap correction. The current work has, therefore, focused on combining the k-ω scheme with some of the models reported in papers 1.1 and 1.2; in particular, introducing the strain-rate invariant as a parameter, and including a non-linear stress-strain relation.

2. MODELLING DETAILS

The k-ω equations can be written as

$$\frac{Dk}{Dt} = P_k - \omega k + \frac{\partial}{\partial x_j}\left((\nu + \nu_t/\sigma_k)\frac{\partial k}{\partial x_j}\right) \quad (1)$$

$$\frac{D\omega}{Dt} = c_{\omega 1}\frac{\omega}{k}P_k - c_{\omega 2}\omega^2 + \frac{\partial}{\partial x_j}\left((\nu + \nu_t/\sigma_\omega)\frac{\partial \omega}{\partial x_j}\right) \quad (2)$$

The forms adopted for c_μ, f_μ and $\overline{u_i u_j}$ are derived from [1] and [2]. After optimizing the model in high-Re-number pipe flow and the impinging jet at Re=23000, the following forms were arrived at:

$$\nu_t = c_\mu(S) f_\mu(R_t)\frac{k}{\omega} \quad (3)$$

$$c_\mu = 0.09\left[\frac{3.89}{S(1-(\exp(-80/S))^{0.6})} - 0.089\right]\left[1-\exp(-0.3S-0.015S^2)\right]\left[1-(\exp(-70/S))^{0.5}\right] \quad (4)$$

$$f_\mu = 1 - 0.72\exp(-0.0056R_t) \quad (5)$$

The various model coefficients, including those used in the expression for $\overline{u_i u_j}$ are given in table 1.

3. RESULTS

Pipe flow computations for Reynolds numbers between 10^4 and 10^5 produced skin-friction coefficients and Nusselt numbers broadly in line with experimental values. Fig. 1 shows the predicted log-law at Re=50000.

The impinging jet results at Re=23000, fig. 2, show that the present k-ω model gives

significantly better predictions than the original proposal, particularly in the stagnation point turbulence levels. As a result of this, the heat-transfer (fig. 3) is also well-captured. At a higher Re number of 70000, the dynamic field remains essentially the same, although fig. 4 shows that the Nusselt number predictions are not quite so accurate. The shape of the Nusselt number profile at the stagnation point is, however, reasonably well captured. The heat-transfer is mainly affected by the near-wall behaviour of the model, and thus a further refinement of the Re-number dependent terms could be expected to bring about further improvements.

References:

1. Wilcox D.C. (1991) "Progress in hypersonic turbulence modelling" AIAA Paper 91-1785.
2. Cotton M.A. & Ismael J.O. (1993) "Development of a two-equation turbulence model with reference to a strain parameter" Proc. 5th Int. Symp. on Refined Flow Modelling and Turbulence Measurements, Paris.
3. Craft T.J., Launder B.E., Suga K. (1993) "Extending the applicability of eddy-viscosity models through the use of deformation invariants and non-linear elements" Proc. 5th Int. Symp. on Refined Flow Modelling and Turbulence Measurements, Paris.

$c_{\omega 1}$	$c_{\omega 1}$	σ_k	σ_ω
$0.435 + 2.17\exp(-0.3R_t)$	$0.833 + 2.17\exp(-R_t/3)$	1.2	0.8

c_1	c_2	c_3	c_4	c_5	c_6
-0.08	0.08	0.18	-1.0	-0.1	0.1

Table 1. Model coefficients.

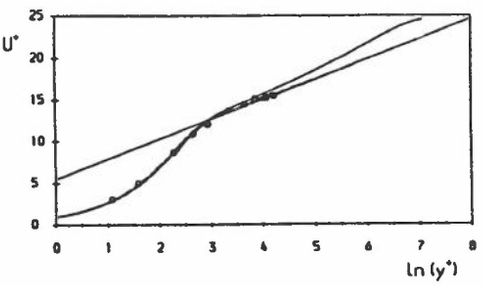

Figure 1. Log-law in pipe flow at Re=50000.

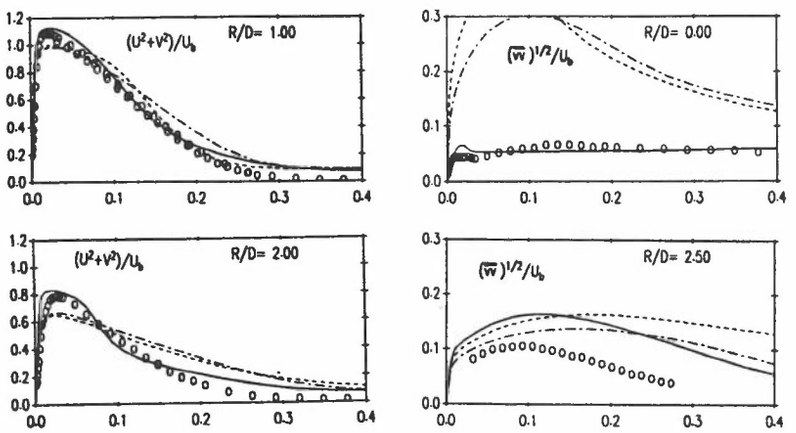

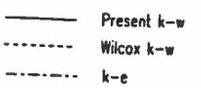

Figure 2. Mean velocity and stress normal to the wall.

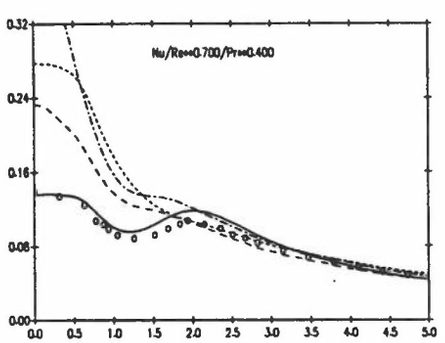

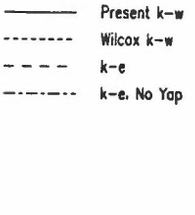

Figure 3. Nusselt number predictions at Re=23000.

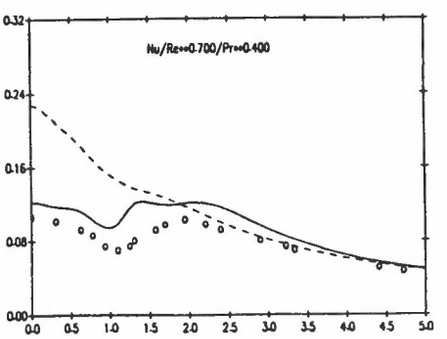

Figure 4. Nusselt number predictions at Re=70000.

AN IMPROVED SECOND MOMENT CLOSURE FOR PREDICTING TRANSITION.

Researcher : A.M. Savill
Sponsor : Rolls-Royce plc

Visiting Research Fellow, Mechanical Engineering Department, UMIST
& Senior Research Associate, Department of Engineering, University of Cambridge.

1. BACKGROUND

This contribution presents further validation and refinement of the Savill-Launder-Younis low-Re Differential Second-Moment Closure for prediction of by-pass transition [1].

2. LOW-Re EXTENSIONS TO THE BASIC DSM MODEL

The SLY RST Model employs the following low-Re extensions:

$$\varepsilon_{ij} = -2/3\delta_{ij}\,(1-f_s)\,\varepsilon + [\,(1+2.5v^2/k)^{-1}\,f_s\,\varepsilon\,\{u_iu_j + u_iu_k\,n_kn_j + u_ju_k\,n_kn_i + \delta_{ij}\,u_ku_l\,n_kn_l\}/k]$$

$$\& \quad D\varepsilon/Dt = d_\varepsilon + f_1\,C\varepsilon_1\,P_{kk} - f_2\,C\varepsilon_2\,\varepsilon^2/k + f_\mu\,C\varepsilon_3\,\nu\,(v^2/k)(k^2/\varepsilon)(d^2U/dy^2)^2$$

with: $f_s = (1+R_t/10)^{-1}$, $f_1 = 1$, $f_2 = [1 - (0.4/C\varepsilon_2)\,e^{-MIN\{(Rt/6),\,20\}}]$

and: $f_\mu = e\,[-3.4/\{1+(R_t/50)\}^2]$ with: $R_t = k^2/\varepsilon\nu$

and the model constants used are the same as in the basic high-Re model except:

$C\varepsilon = 0.15$, $C\varepsilon_1 = 1.275$, $C\varepsilon_2 = 1.8$ and: $C\varepsilon_3 = 0.25$ (optimised for transition [1])

3. TEST CASE COMPUTATIONS

This model has now been applied to a wider range of Simulated and experimental Test Cases of the ERCOFTAC Special Interest Group - see [2-4] - than the zero pressure gradient, 1-6% free-stream turbulence, and variable pressure gradient cases considered previously [1]. The effects of higher intensity isotropic fst and both weak and strong fst anisotropy, in zero pressure gradient, have been considered, together with the influence of off-design Reynolds numbers on transition in pressure-gradients representative of an aft-loaded turbine blade. In each case parabolic boundary layer computations have been performed; starting from specified initial and boundary conditions within the pseudo-laminar, pre-transitional layer. These computations were performed on the Cambridge IBM 3084Q, and required 0.03s cpu/x-step increment of 0.025δ, on an expanding 80 point grid with 30 points below $y+=10$ ($y_1+=0.04$) and a further 20 points below $y=0.1\delta$.

4. RESULTS & CONCLUSIONS

The results presented in Figures 1-4 show that the model continues to accurately predict the onset of by-pass transition up to free-stream turbulence intensities of 10%, in zero pressure-gradient flow, and can to a large extent capture the effects of free-stream anisotropy, variable pressure gradient and Reynolds number on transition location. The Transition Simulations have provided a justification for the adopted value of $C\varepsilon_3$. However a more detailed comparison of model predictions with the Simulated database have revealed deficiencies in the physical

modeling of the fst interaction and development of turbulence in the transitional layer. It is suggested that these might be corrected by introducing additional non-local or cross-diffusion terms into what remains an essentially local one-point closure model, and that the prediction of low fst transition could be improved by the addition of a transport equation for intermittency.

ACKNOWLEDGEMENT

This work would not have been possible without the continued active support of Rolls-Royce plc and many helpful discussions with other researchers at UMIST & Surrey University

REFERENCES

1. A.M.Savill (1992) A low-Reynolds number second moment closure for predicting by-pass transition. Abstr. 5th UMIST Collqum on Computational Fluid Dynamics.
2. A.M.Savill (1993) Some recent progress in the turbulence modelling of by-pass transition. In Near-Wall Turbulent Flows (Eds. R.M.C.So, C.G.Speziale & B.E.Launder; Elsevier) pp.829.
3. A.M.Savill (1993) Further progress in the turbulence modelling of by-pass transition. In Engineering Turbulence Modelling and Experiments 2 (Eds: W.Rodi & F.Martelli; Elsevier), pp.583.
4. A.M.Savill (1993) Transition Modelling for Turbomachinery. A Summary of ERCTOFTAC Transition SIG Progress for 1st BRITE-EURAM AERO-CT92-0052 Project On Transition in Turbomachinery Workshop, UMIST.

Figure 1: $T3B_{DNS}$ (5%fst, weak anisotropy)

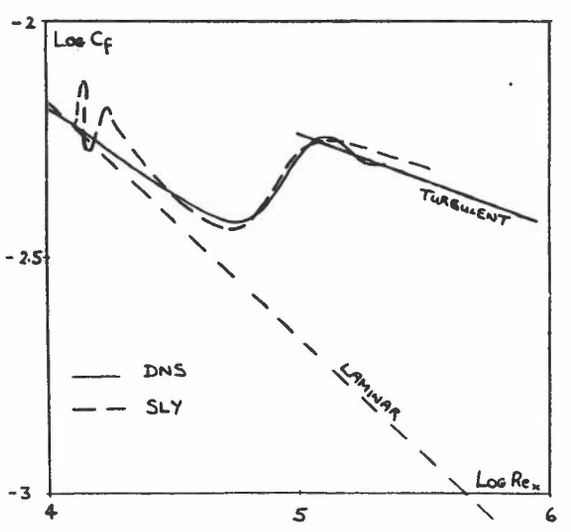

Figure 2: $T3B_{DNS}$ Test Case (strong anisotropy)

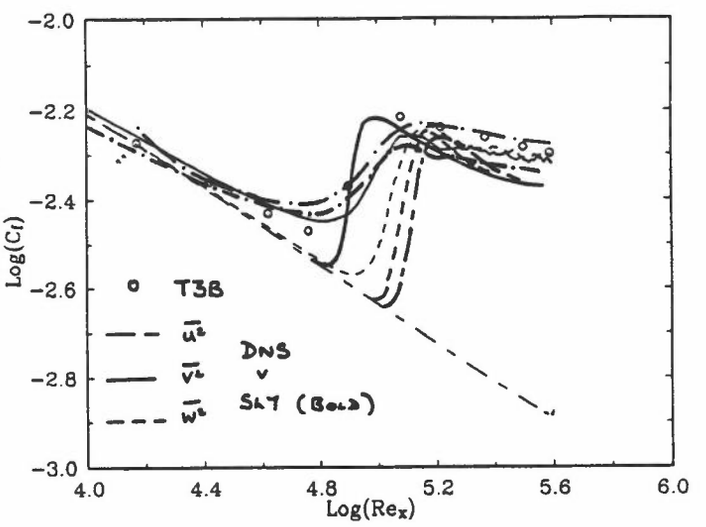

Figure 3:T3Test Cases (3-10% fst; zero p.grad)

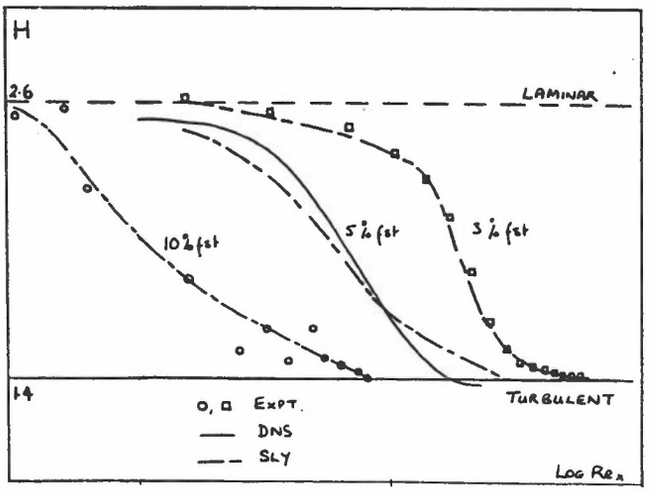

Figure 4: T3C Test Case (variable p.grad/Re)

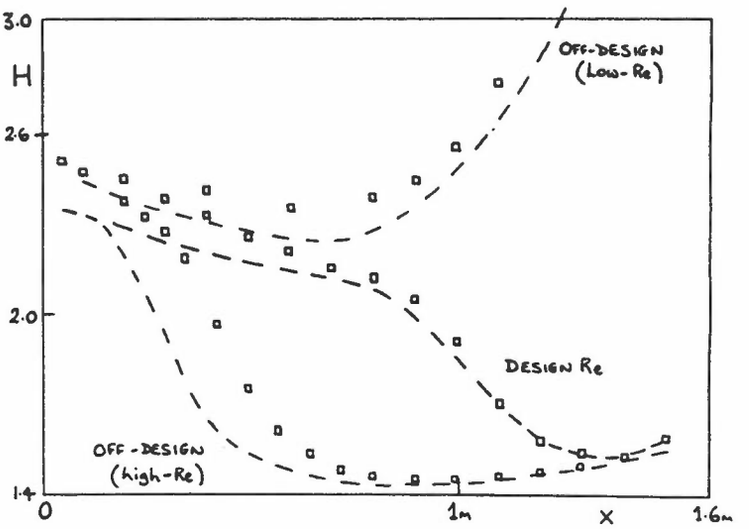

GENERALIZED LOW-RE 2nd-MOMENT CLOSURE WITHOUT WALL CORRECTIONS

Researchers: N.Z. Ince and S-P Li
Supervisor: B.E. Launder
Sponsor: SERC, FLAIR

1 BACKGROUND AND OBJECTIVE

Extending UMIST's New DSM model for free flows to the near-wall viscous sublayer has been one of the major tasks over the past few years. The 5th Colloquium reported a low-Re number form of second-moment closure [1] of the same general form which had been explicitly designed to satisfy several theoretical limiting constraints of wall turbulence and to comply with the stress profiles of direct numerical simulations. Like all the other model forms, however, that scheme also employed wall proximity/orientation parameters to ensure that the velocity fluctuations normal to the wall died out as the wall was approached faster than fluctuations parallel to the wall. The use of such devices renders the model unsuitable for application to surfaces of even moderately complex shape. The present research was therefore aimed at generalising this low-Re 2nd-moment closure model by removing the existing wall-topography parameters.

2 THE PROBLEM AREAS AND THE PROPOSED MODELLING

The approach followed has been to identify terms in the original proposal that contain wall-parameters and then to remove these parameters either by simply discarding the whole term while seeking a replacement that does not use such wall-parameters, or by replacing them with some other scalar quantities. For brevity, only the present proposed modifications are given here. The expressions for the original terms can be found in [1].

The Wall-Reflection Term ϕ_{ijw}

The 5th Colloquium reported satisfactory results for plane channel and duct flows obtained by a high-Re New DSM model for wall flow [2], in which the usually adopted ϕ_{ijw} model had been discarded. Instead, the wall-reflection effect was sensed via the local strain field, by suitably modifying the pressure-strain model ϕ_{ij2}, taking C_2' non-zero: with $C_2' = 0.6$ with $C_2 = 0.55$. The same approach has been adopted in the present study. That is to say ϕ_{ijw} is not employed.

The Inhomogeneity Correction

In the original model, a correction was applied to ϕ_{ij2} for strong *inhomogeneity* across the buffer layer by employing an effective velocity gradient in this process. To eliminate the use of $\overline{u_2^2}$, the mean square velocity fluctuations normal to the wall, the following form has been adopted:

$$\left(\frac{\partial U_n}{\partial x_m}\right)_{eff} = \frac{\partial U_n}{\partial x_m} + c_I l_t^2 \frac{\partial f(A)}{\partial x_k}\frac{\partial^2 U_n}{\partial x_m \partial x_k} \qquad (1)$$

where, $f(A)$ is taken as $A^{0.3}$ $(1 + 2.5A^3)$, $l_t = k^{3/2}/\varepsilon$ and the coefficient c_I takes the value 0.07.

The Dissipation Tensor ε_{ij}

The modified ε_{ij} takes the following form:

$$\varepsilon_{ij} = \left\{ \frac{\varepsilon \overline{u_i u_j}}{k} + \beta_1 \nu \frac{\partial k^{0.5}}{\partial x_k}\left[\frac{\overline{u_i u_k}}{k}\frac{\partial k^{0.5}}{\partial x_j} + \frac{\overline{u_j u_k}}{k}\frac{\partial k^{0.5}}{\partial x_i}\right] + \beta_2 \delta_{ij} \frac{\nu \partial k^{0.5}}{\partial x_m}\frac{\partial k^{0.5}}{\partial x_n}\frac{\overline{u_m u_n}}{k} \right\} / \left(1 + 5\frac{\nu \partial k^{0.5}}{\partial x_m}\frac{\partial k^{0.5}}{\partial x_n}\frac{\overline{u_m u_n}}{k}\right) \qquad (2)$$

We note that the choice $\beta_1 = \beta_2 = 2$ enables equation (2) to satisfy the limiting wall dissipation ratios of Launder Reynolds [3].

3 RESULTS

The validity of the present low-Re 2nd-moment closure has been tested through computations of fully-developed flows in a plane channel and a square-sectioned duct. In Figures 1-3, predicted near-wall variations of turbulent stresses and mean velocity profiles for the channel flow are compared with the corresponding DNS results of Kim et al [4]. Clearly, the present predictions are in very good agreement with the DNS data. The predicted primary velocity and turbulent kinetic energy profiles for the duct flow are also in reasonably good accord with the experimental data, shown in Figures 4 and 5 respectively.

REFERENCES

[1] B.E.Launder and D.P.Tselepidakis, AIAA 91-0219, 1991.
[2] S-P Li, PhD Thesis, University of Manchester, 1992.
[3] B.E.Launder and W.C.Reynolds, Physics of Fluid, 26, p.1157, 1983
[4] J.Kim et al, J. Fluid Mechanics, 117, p.133, 1987

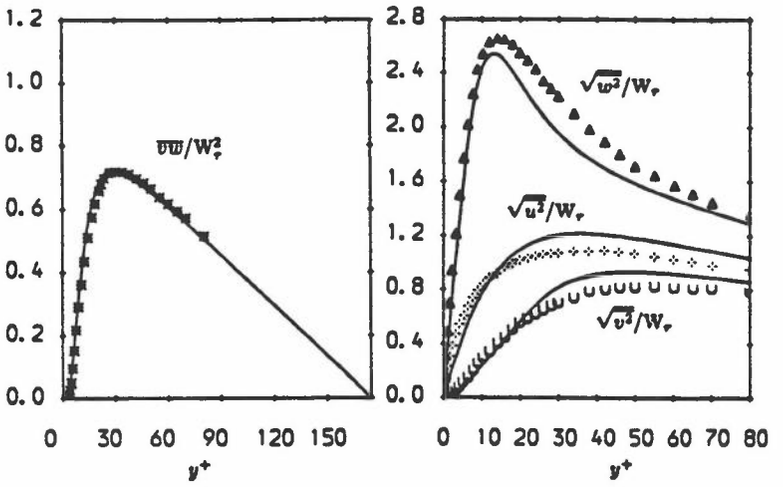

Figure 1 Shear stress profile

Figure 2 Normal stress profiles

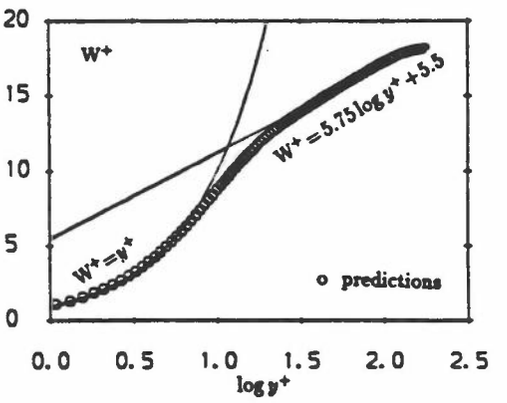

Figure 3 Mean velocity profile

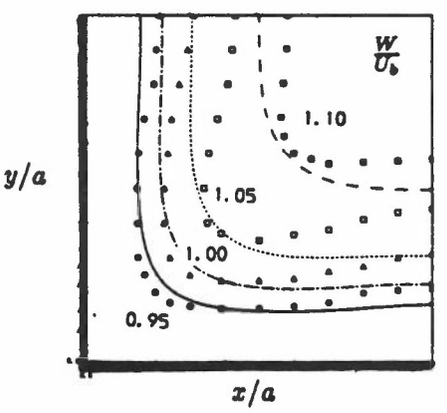

Figure 4 Primary velocity contours

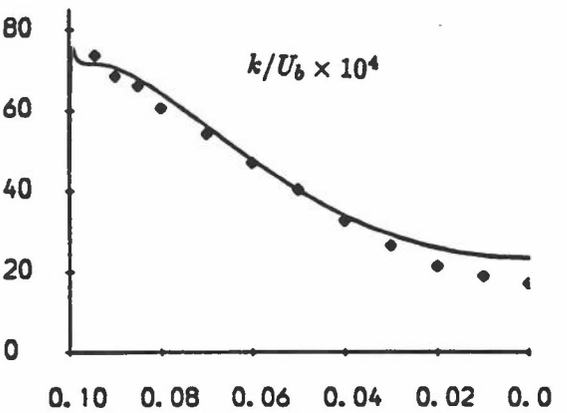

Figure 5 Turbulent kinetic energy along wall bisector

ADAPTING THE NEW '2D-LIMIT' REYNOLDS-STRESS MODEL FOR CURVED FLOWS

Researchers : A.M. Savill & D.P.Tselepidakis
Sponsors : Shell UK, Rolls-Royce & ICASE/NASA LaRC

Visiting Research Fellow, Mechanical Engineering Department, UMIST
& Senior Research Associate, Department of Engineering, University of Cambridge.

1. BACKGROUND

The ability of the New 2D-limit Differential Second-Moment Closure to predict simple curved shear flows has been examined [1] and a comparison of results with predictions obtained using the Basic Model [2] has allowed a small refinement to the present closure to be proposed.

2. CURVED FLOW COMPUTATIONS

Computations have been performed with both Basic and New RST Models for simple plane curved shear flows in the limit where Production and Pressure-Strain effects dominate Diffusion. Comparison has been made with experimental results obtained for approximately homogeneous shear flows subjected to both mild and strong longitudinal convex and concave curvature [3], the outer region of a convex curved boundary layer, and the concave side of a curved wake - where this condition is satisfied. It has been found that in the case of the homogeneous shear flows, the New model provides better predictions for the variation of turbulence energy and Reynolds stress anisotropy with changes in strength and sign of curvature than the Basic model, but still tends to over-predict the effect on the Reynolds shear stress - see [1] & Figure 1. The same is true for the curved boundary layer and wake flows where the Basic model produces quite respectable shear stress results. In an effort to improve the New model the idealised case of a homogeneous shear flow responding to a sequence of convex and concave curvature has been considered with both models - see Figure 2. The results suggested that some modification was required to the New model.

3. PROPOSED MODIFICATION TO THE NEW 2D-LIMIT RST MODEL

After testing previously proposed modifications to the constants $C_{\varepsilon 1}$ & $C_{\varepsilon 2}$ in the Production and Dissipation of Dissipation terms, which have been shown to ensure better predictions for a wide range of near-equilibrium free shear flows [4], it seemed likely that the deficiencies observed (particularly for strongly curved flows) could be attributed to out-of-equilibrium effects. The solution would appear to be to re-scale the Production of Dissipation term by a non-equilibrium parameter (P_k/ε) so that the two modified model constants become:

$$C_{\varepsilon 1} = 0.35\,[\,1 + \underline{\nu_t\,(dU_i)}\,]\,\underline{\varepsilon}$$
$$\varepsilon\ (dx_j)\ P_k$$

&

$$C_{\varepsilon 2} = \underline{1.92}$$
$$(1 + 1.65AA_2^{1/2})$$

Certainly the comparison with the Basic model shear stress predictions was very much improved when this modification was implemented - see Figure 2.

ACKNOWLEDGEMENT

This work would not have been possible without the support of Shell/UK (AMS), Rolls-Royce plc (AMS &DPT) and funding provided by an ICASE/NASA LaRC Workshop.

REFERENCES:

1. D.P.Tselepidakis, T.B.Gatski & A.M.Savill (1992) A comparison of turbulence models for homogeneous shear flows with longitudinal curvature. Proc. ICASE/NASA LaRC Workshop on Instability, Transition & turbulence (Eds: M.Y.Hussaini, A.Kumar & C.L.Streett; Springer-Verlag) pp.544.
2. T.B.Gatski & A.M.Savill (1989) An analysis of curvature effects for the control of wall-bounded shear flows. AIAA-89-1014.
3. A.G.L.Holloway & S.Tavoularis (1992) The effects of curvature on sheared turbulence. J.Fluid Mech.237 pp.569.
4. T.J.Craft (1991) Second-moment modelling of turbulent scalar transport. Ph.D Thesis, Faculty of Technology University of Manchester.

Figure 1: Predictions for homogeneous shear flow subjected to convex or concave curvature

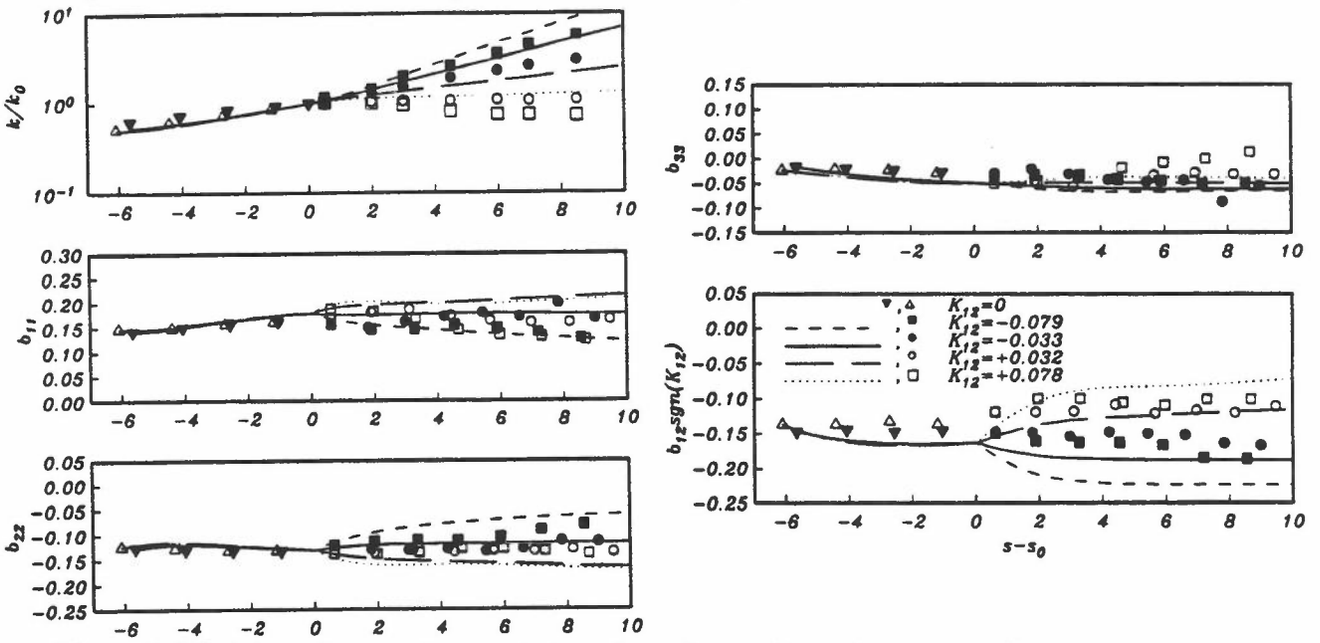

Figure 2: Model predictions for a turbulent shear flow subjected to convex & concave curvature.

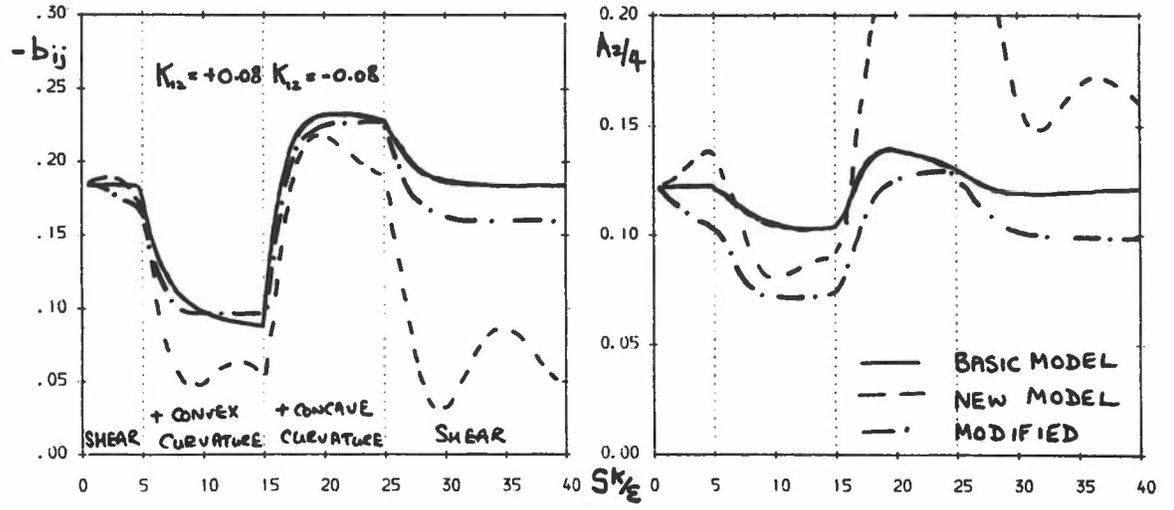

THE MODELLING OF DIFFUSION-CONTROLLED TRANSITION WITH THE NEW MODEL

Researcher: J R Cho
Supervisor: B E Launder
Sponsor: SERC/Rolls Royce plc

1 INTRODUCTION

The present research can be regarded as a continuation of that reported earlier in this session by Dr A M Savill. While even low Reynolds number EVM's can do a respectable job of modelling transition on a flat surface at turbulence levels of 3% or more, it is expected that, for the majority of situations arising in aeronautical practice, the surface will either not be flat or turbulence levels will be rather lower than 3%. Then one will need a more comprehensive model than is offered by EVM methodology. This type of test case is thus an excellent one to challenge and help refine the closure approach of the 'New Model'.

2 MODELLING

When the original near-wall form of the New Model (Tselepidakis, [1]) was applied to transition phenomena it was soon discovered that it was highly unstable for transitional flows. The model has thus been recast, introducing at the same time, new developments in low-Reynolds-number modelling. No entirely satisfactory form has yet been arrived at. However the results shown below adopted the following specific forms of the pressure strain model.

$$\bar{c}_1 = (1 + 3.38\sqrt{\min(A_{23}0.6)}A^{1/2}\,(1 - \exp[-R_t/150(1 + A_3)])$$

with 'wall refection' and viscous contributions to ϕ_{ij} as follows

$$\phi_{ij}^{wr} = 0.6\left(\frac{\partial \ell_A}{\partial x_m}\frac{\partial \ell_A}{\partial x_n}\phi_{mn2}\phi_{ij} - \frac{3}{2}\frac{\partial \ell_A}{\partial x_m}\frac{\partial \ell_A}{\partial x_i}\phi_{jm2} - \frac{3}{2}\frac{\partial \ell_A}{\partial x_m}\frac{\partial \ell_A}{\partial x_j}\phi_{im2}\right)$$

$$\phi_{ij}^{ws} = -0.05\,(2a_{ij}\varepsilon_{mm} + a_{mn}\varepsilon_{nm}\delta_{ij} - \frac{3}{2}a_{mi}\varepsilon_{jm} - \frac{3}{2}a_{mj}\varepsilon_{im})$$

$$\ell_A = k^{3/2}A^{1/2}/\varepsilon \quad ; \quad \varepsilon_{mn} = 2\nu\frac{\partial\sqrt{k}}{\partial x_m}\frac{\partial\sqrt{k}}{\partial x_n}$$

3 RESULTS

An important discovery made (with a simpler eddy viscosity model) was that the rapid change in velocity profile associated with transition itself induces local *pressure gradients* which themselves can have a significant effect on where transition occurs. While not strictly a 'turbulence modelling' effect, the discovery is important for modelling. It means that strictly one should use an elliptic scheme for computing the flow field; boundary layer approximations that treat the pressure as uniform across the layer are inappropriate. However for the present, all the reported results using a full second-moment closure have been obtained with a marching parabolic treatment.

Computations with the version of the New Model noted above are shown in Fig 1 for three levels of free stream turbulence. These capture reasonably well the dependence of the location of transition on the level of free-stream turbulence intensity. However, the transition process itself

is too abrupt. We suspected that the model of stress diffusion may have been the cause. This process is of little consequence in developed turbulence near walls and we thus conventionally adopt the simple GGDH model. There seemed good reason to suppose that for transition provoked by free stream turbulence diffusion could be of greater importance and we thus refined the model to the (still overly simple) HL version.

$$d_{ij} = 0.11\frac{\partial}{\partial x_k}\left(\frac{k}{\varepsilon}\left[\overline{u_k u_\ell}\frac{\partial \overline{u_i u_j}}{\partial x_\ell} + \overline{u_j u_\ell}\frac{\partial \overline{u_i u_k}}{\partial x_\ell} + \overline{u_i u_\ell}\frac{\partial \overline{u_j u_k}}{\partial x_\ell}\right]\right)$$

It is seen from Fig 2 that this change has indeed smoothed out the transition towards the type of behaviour found in the experiments.

4 CONCLUSION

There are good reasons to suppose that by-pass transition should in due course be predictable with the same low-Reynolds-number closure used to predict turbulent flows at low Reynolds number. Diffusive transport of stress is more influential in transitional flows than in fully developed wall turbulence and it appears that more attention must be paid to its modelling than hitherto.

REFERENCE

1 D P Tselepidakis, PhD Thesis, University of Manchester Faculty of Technology

Fig 1:

Predicted variation of c_f
for T3A, T3B test cases
(symbols - experiments; lines - computations)

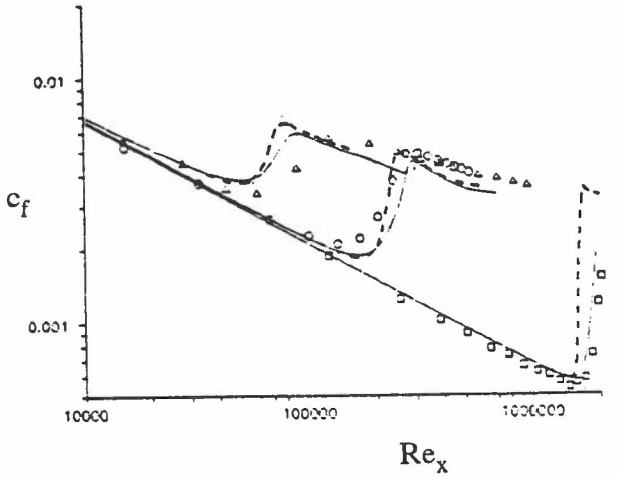

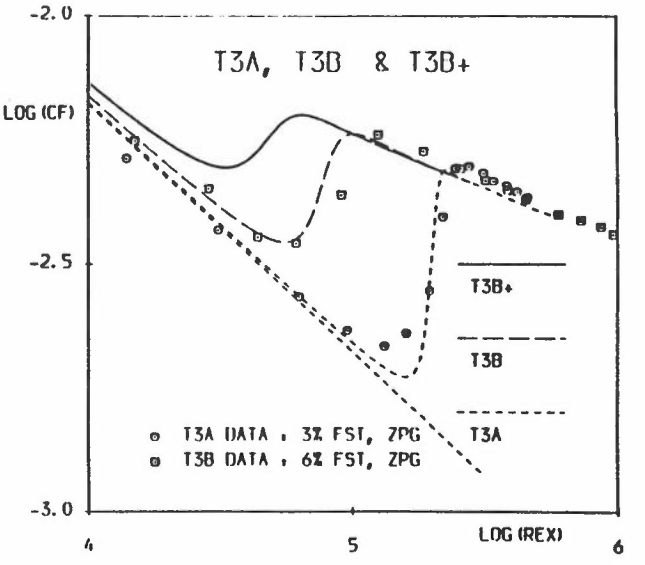

Fig 2:

Effect of stress-diffusion model:
---- GGDH;
____ KH Version

DIRECTIONS IN 2ND MOMENT MODELLING

Researchers : T.J. Craft and N.Z. Ince
Supervisor : B.E. Launder
Sponsors : SERC, Flair

1. INTRODUCTION

Over the past few years, the realizable, cubic model developed at UMIST has been widely tested over a range of free flows, buoyant flows and wall-affected flows. In these latter cases, since viscous effects are not included in the model, it has generally been used in conjunction with a much simpler near-wall model. Overall, the inclusion of non-linear pressure-strain terms and of stress anisotropy invariants into the ε equation have resulted in improved predictions compared to the basic model. However, as more flows have been tested, it has become more evident that a better modelling practice is needed in the near-wall, viscosity-affected region, particularly for flows involving heat-transfer through the wall.

A start in this direction was made by Tselepidakis [4], who modified the high-Re-number form of the cubic model in order to compute plane and rotating channel flows. The final form he adopted was not, however, entirely consistent with the high-Re-number form. Moreover, it still employed $\underline{\mathbf{n}}$, the unit vector normal to the wall, which becomes difficult, if not impossible, to define in complex geometries.

Our recent efforts have therefore been directed at building on Tselepidakis' experiences by looking at a wider range of flows encompassing plane channel, shear-free wall, transition and impinging flows.

2. MODELLING

Diffusion: In many of the shear flows studied, the turbulent diffusion process is relatively weak, and has simply been modelled using the GGDH. However, it takes on a greater importance in transition flows, and it seems likely that a more complex model taking explicit account of processes appearing in the third-moment transport equations including mean strain would be more appropriate.

Pressure-Strain: Significant steps have been taken in removing the conventional "wall-reflection" terms associated with ϕ_{ij2}. In channel flows, the inclusion of the c_2' terms and an inhomogeneity correction to $\partial U/\partial y$ can be used to achieve the desired effect [1]. However, there are still problems in applying these to the impinging jet: neither refinement significantly affects the stagnation region (where the stress normal to the wall is considerably overpredicted), and the inhomogeneity correction needs further refinement in order to reduce its influence in the initial wall-jet region around the velocity maximum.

The "slow" pressure-strain term, ϕ_{ij1}, includes non-linear terms, and the coefficient c_1 is taken as a function of A, A_2 and R_t. Realizability requires that $c_1 \sim A^n$ where $n \leq 1/2$ for small A, and experience suggests that this results in a more stable model than the variation $c_1 \sim A$ used by Tselepidakis. A further development would be the inclusion of inhomogeneity effects into ϕ_{ij1}. The shear-free boundary DNS data from Stanford [3] will undoubtedly prove very useful in the modelling of these terms.

Dissipation: We are currently using the form

$$
\begin{aligned}
\varepsilon_{ij} &= \varepsilon^*_{ij} f_\varepsilon + {}^2/_3 \varepsilon \delta_{ij}(1 - f_\varepsilon) \\
\varepsilon^*_{ij} &= \left[\varepsilon \frac{\overline{u_i u_j}}{k} + \frac{2\nu}{k} \frac{\partial \sqrt{k}}{\partial x_k} \left[\frac{\partial \sqrt{k}}{\partial x_i} \overline{u_j u_k} + \frac{\partial \sqrt{k}}{\partial x_j} \overline{u_i u_k} \right] + \frac{2\nu}{k} \frac{\partial \sqrt{k}}{\partial x_k} \frac{\partial \sqrt{k}}{\partial x_l} \overline{u_k u_l} \delta_{ij} \right] \Big/ \left[1 + \frac{5\nu}{\varepsilon k} \frac{\partial \sqrt{k}}{\partial x_k} \frac{\partial \sqrt{k}}{\partial x_l} \overline{u_k u_l} \right] \\
f_\varepsilon &= \exp\{-R_t A^{1/2}/100\}
\end{aligned}
\qquad (1)
$$

which reverts to the isotropic dissipation model at high Re numbers, and also satisfies the wall limit

$$\frac{\varepsilon_{11}}{\overline{u_1^2}} = \frac{\varepsilon_{33}}{\overline{u_3^2}} = \frac{1}{4}\frac{\varepsilon_{22}}{\overline{u_2^2}} = \frac{1}{2}\frac{\varepsilon_{12}}{\overline{u_1 u_2}} = \frac{\varepsilon}{k}$$

Fig. 1 shows that this captures the normal stress dissipation rates in channel flow reasonably well, although the ε_{12} component is overpredicted between y^+=10 and 50.

Another encouraging feature of eq.(1) is shown by the impinging jet Nusselt number distribution in Fig. 2. Although the stagnation heat-transfer is overpredicted (because of the absence of wall-reflection terms to damp $\overline{v^2}$ in the fully turbulent region) the strong near-wall dissipation of $\overline{v^2}$ results in a reasonable profile shape at the stagnation point *without* including the Yap correction in the ε equation. Since the Yap correction contains the "distance to the wall", this is another term whose inclusion causes severe difficulties in complex geometries, and which we would therefore like to eliminate.

In addition to introducing the invariants A_2 and A into the dissipation equation, another possibility is the inclusion of alternative source terms such as those suggested by [2], containing products of mean strains and dissipation anisotropies.

3. FURTHER WORK

The above ideas are currently being evaluated and tested over the range of flows mentioned. Geometrical quantities such as $\underline{n}$ are not being allowed, and this restriction, combined with the widely different flow configurations being studied, should result in a reasonably stable model that can be applied to complex flow topographies.

References:

1. Launder B.E, Li S.P. (1994) *Phys Fluids* 6, 999.
2. Oberlack, M. (1993) "Closure of the dissipation tensor and pressure-strain tensor based on the two-point correlation equations" Turbulent Shear Flows 9, Springer.
3. Perot J.B. Moin P. (1993) "Shear-free turbulent boundary layers: physics and modeling" Report TF-60, Stanford Univ.
4. Tselepidakis D.P. (1991) PhD Thesis, Faculty of Technology, Univ. of Manchester.

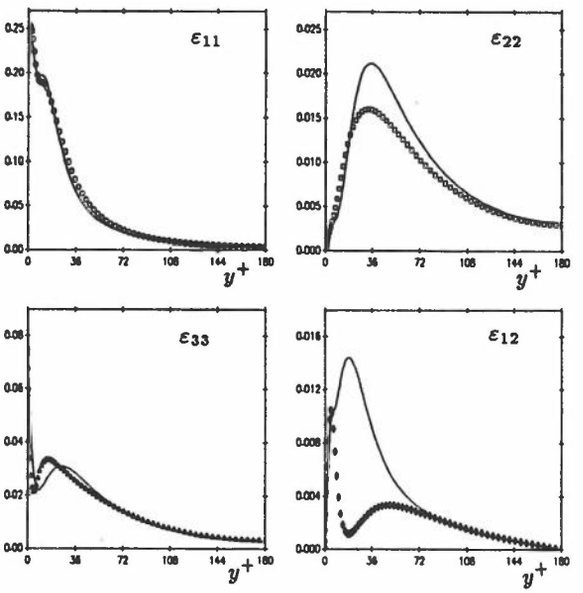

Figure 1. Reynolds stress dissipation rates in plane channel flow.

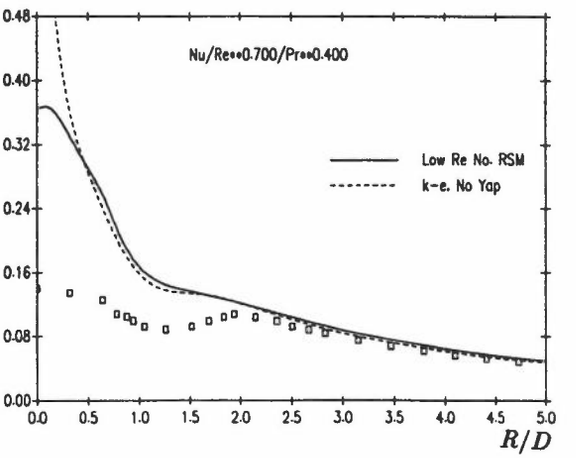

Figure 2. Nusselt number distribution in the impinging jet.

DIRECT NUMERICAL SIMULATION OF PREMIXED TURBULENT COMBUSTION

Researchers: Dr. M. C. Gallagher, Dr. R. S. Cant
Supervisor: Dr. R. S. Cant
Sponsors: EPSRC, NASA/CTR Stanford

1. INTRODUCTION

Direct Numerical Simulation (DNS) involves the numerical solution of the full Navier-Stokes equations governing turbulent fluid flow, without recourse to any form of turbulence modelling. This is enormously demanding of computing resources in terms of both CPU time and execution storage, due to the need to represent faithfully a three-dimensional and time-dependent phenomenon occurring over a very broad range of length and time scales. In DNS it is essential first of all to ensure adequate resolution of the smallest scales of motion, whereupon the largest problem that can be tackled is set by the size and power of the largest available computer. In practice this means that there is a severe restriction on the attainable Reynolds number and on the level of geometrical complexity that can be represented. Thus, for the foreseeable future, DNS is not viewed as a replacement for Reynolds-averaged modelling as a tool for the solution of industrial problems. Rather, DNS provides a novel means to carry out fundamental investigations of turbulent flow in order to obtain physical insight and statistical data which can be used to refine and develop existing Reynolds-averaged models.

The application of DNS to the treatment of turbulent combustion is an area where the unique advantages of DNS are particularly valuable. Turbulent flames contain strong mutual interactions between the effects of turbulent motion, molecular transport of heat and mass, strong heat release and combustion chemistry. Experimental measurement of important quantities in turbulent flames remains very difficult despite recent advances in laser diagnostic techniques, and many quantities of interest are simply inaccessible. In many cases, DNS offers the only possible route to the collection and analysis of data necessary for modelling.

The present work continues a line of research in combustion DNS begun at the 1990 Summer School of the Center for Turbulence Research at Stanford University [1]. An extensive set of raw data obtained from DNS of turbulent premixed flames was analysed in the light of the Bray-Moss-Libby model formalism [2] leading to the extraction of a great deal of useful information. Some of the principal results are discussed below. The success of this activity has led to the present project, supported by EPSRC, in which DNS of turbulent combustion is being carried out for the first time in the UK. The objective, as before, is to extract statistical data in support of modelling efforts.

2. PREVIOUS RESULTS

The impact of the early Stanford DNS on the modelling of turbulent premixed combustion has been considerable. The computations were carried out by Rutland [3] on a grid of 128 nodes in each direction, using a pseudo-spectral discretisation with periodic boundary conditions and a third-order Runge-Kutta algorithm for time advancement. The full Navier-Stokes equations were solved together with transport equations for two scalar variables representing a normalised temperature and species mass fraction. One-step Arrhenius reaction kinetics were employed, and heat release was not coupled back to the flow field which remained incompressible. Each run was initialised from a prescribed spectrum of turbulence and a settling period was allowed to elapse before the introduction of combustion. In order to preserve periodicity, two planar flames were initialised back-to-back near to the central plane of the domain and were allowed to propagate outwards. After a short initial acceleration the flames adjusted to the ambient field of decaying turbulence and propagated with decreasing speed to the ends of the domain. Each run of about 1500 time steps required about 15 hours of CPU time on a Cray Y-MP. Results in the form of full-field datasets were collected every 100 time-steps, and the results of four such runs made with different initial values of

turbulence intensity were available for analysis.

Extensive post-processing was carried out on selected datasets. The flame surfaces were located in space by a root-finding technique and quantities of interest were interpolated onto the surface using cubic splines. Gradients of velocity and scalar quantities were evaluated in spectral space for best accuracy. Surface distributions were obtained having a sample size of at least 128 by 128 for each flame surface. Principal results included surface pdfs of the tangential strain rate on the flame, and surface joint pdfs of the tangential strain rate and the local flame curvature [4]. Estimates of the integral length scale of flame surface wrinkling were obtained using a surface autocorrelation technique and several geometrical features of the flame were identified and quantified. On the basis of the results a revised model for mean turbulent reaction rate has been proposed [5] and is currently under test.

3. NEW APPROACH TO COMBUSTION DNS

The pseudo-spectral approach to DNS has some serious limitations which restrict its applicability to more general combustion simulations. In order to introduce realistic heat release rates it is necessary to replace the periodic boundary conditions in at least one spatial direction with an appropriate inflow/outflow condition. Much of the computational efficiency of the pseudo-spectral method is lost in this case, and this has led to the use of high-order finite differences instead. Recent DNS of non-reacting channel flow [6] has been carried out using low-order finite differences and has demonstrated minimal loss of resolution with respect to the higher-order methods which are much more complex and expensive. Thus, the new combustion DNS work now in progress at UMIST makes use of second-order central spatial differencing combined with a modified second-order Adams-Bashforth algorithm for time-stepping. A new code, known as ANGUS, has been developed locally and is currently undergoing validation tests against previous data. A parallel version of the code has been developed in conjunction with Daresbury Laboratory and is running on the Intel Hypercube. The standard combustion test problem involves a premixed turbulent flame located near a central plane of the computational domain, propagating in a statistically stationary manner against an oncoming turbulent stream of fresh reactants. A primary objective is to collect long-duration time-averaged statistics relating to the interaction of the pressure, velocity and density fields.

REFERENCES

1. Cant,R.S., Rutland,C.J., Trouve,A. (1990) "Statistics for Laminar Flamelet Modelling", Proceedings of the 1990 Summer Program, Center for Turbulence Research, Stanford.
2. Bray,K.N.C., Moss,J.B., Libby,P.A. (1985) "Unified Modelling Approach for Premixed Turbulent Combustion-Part I: General Formulation", Combust.Flame 61, 87-102.
3. Rutland,C.J. (1989) "Effects of Strain, Vorticity and Turbulence on Premixed Flames", Ph.D. Thesis, Stanford University.
4. Bray,K.N.C., Cant,R.S. (1991) "Some Applications of Kolmogorov's Research in the Field of Combustion", Proc. Roy. Soc. Lond. A, 434, 217-240.
5. Cant,R.S. (1994) "Direct Numerical Simulation for Premixed Turbulent Combustion Modelling", presented at the 74th AGARD FDP Meeting and Symposium, Chania, Crete, Greece, 1994; proceedings to appear.
6. Kristoffersson,R., Andersson,H.I. (1993) "Direct Simulations of Low-Reynolds-Number Flow in a Rotating Channel", J. Fluid Mech., 256, 163-197.

« Session 2 »

Numerical Methods

MULTI-BLOCK ALGORITM FOR GENERAL TURBULENT FLOWS

Researchers: W.L. Chen and F.S. Lien
Supervisor: M.A. Leschziner

1. INTRODUCTION

Geometric flexibility is one of the key ingredients in the mix of capabilities allowing CFD to be used as a practical aid to engineering design. It is also of increasing importance in the context of validation efforts focusing on complex flows, particularly in high-lift aerodynamics and highly-loaded turbomachine blades in which turbulence transport contributes significantly to primary operational characteristics.

Although a considerable level of flexibility can be attained with single-block structured grids - provided non-orthogonality is admissible - there are many applications, notably such involving multiply-connected domains, which cannot be meshed with a single structured grid. Alternative routes to increasing geometric flexibility are based on unstructured and block-structured grids. Both have strengths and weaknesses. With the latter option, local flow-driven adaptation is more difficult, but this option is well-disposed towards an accurate near-wall resolution, allows the use of well-established structured-grid solvers (e.g. ADI, ICCG, SIP, multigrid), is well-suited to parallel computing based on domain-decomposition methods and allows the retention of simple index connectivity which enhances transparency and eases programming. Adaptation can be implemented by the type of the grid-refinement technique introduced in a companion summary in this section.

This summary introduced a multi-block implementation of the general-flow code STREAM (Lien & Leschziner [1]). The block topology is essentially unstructured, with a block connectivity matrix generated to allow efficient inter-block communication. Within each block the grid is fully structured, however. One notable feature of the method is that the coordinate systems, governing equations and physical models need not be (indeed, are not) identical across the entire block family, which is particularly beneficial in external aerodynamics applications.

2. APPROACH

The base algorithm is STREAM - a general non-orthogonal co-located finite volume scheme incorporating higher-order discretisation, second-moment closure and applicable to incompressible as well as compressible conditions. The multi-block extension involves the following major steps:

(i) The flow domain is sub-divided into non-overlapping blocks and associated grids are generated for each block separately, by using either algebraic or differential grid generation;

(ii) A connectivity matrix is constructed which is used to communicate information across block boundaries with the aid of 'halo' data regions at boundaries. The connectivity matrix is in the form of 2D array MATRIX(IBLOCK,IFACE), where IBLOCK is the block number, and IFACE identifies a block face (out of 6). A typical example is given in Fig. 1, where for IBLOCK=1,

MATRIX(1,1)=0,
MATRIX(1,2)=0,
MATRIX(1,3)=2,
MATRIX(1,4)=0,
MATRIX(1,5)=7,
MATRIX(1,6)=0,

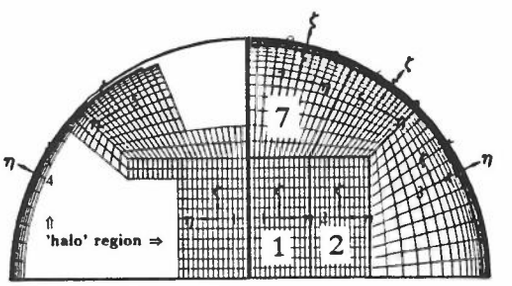

Fig. 1: Example of a 8-block arrangement

where '0' means that the neighbouring block is a physical boundary, while any other integer identifies the neighbouring block.

(iii) One 'inner iteration' consists of the solution in individual blocks, with block boundary conditions temporarily 'frozen', and an update of boundary conditions via the connectivity matrix. The outer iteration is, in effect, a 'Block Jacobi' method.

3. EXAMPLES

Fig. 2 shows the use of a multi-block system in the computation of a compressor blade considered in greater detail in a related summary in Section 5. The figure includes enlarged views of the grid arrangements at the rounded leading and trailing edges and a comparison between single-grid and multi-block solutions for the pressure coefficient using the Launder-Sharma low-Re k-ε model. Fig. 3 shows the 15-block grid and the predicted flow around a three-element high-lift aerofoil. Finally, Fig. 4 shows the transverse-velocity field downstream of a round-to-square transition in a duct obtained with a 8-block arrangement and a low-Re k-ε model.

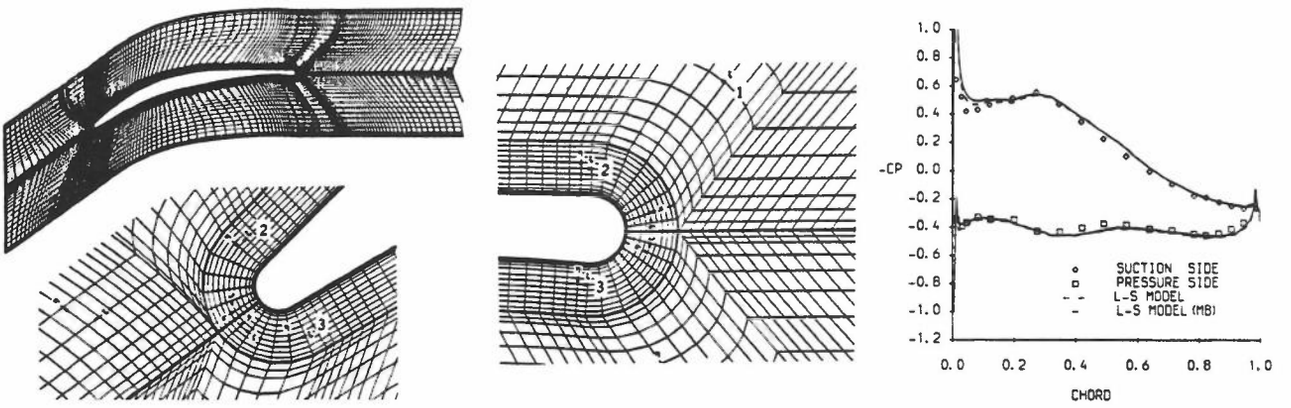

Fig. 2: Multi-block grid and pressure coefficient around a compressor-cascade blade

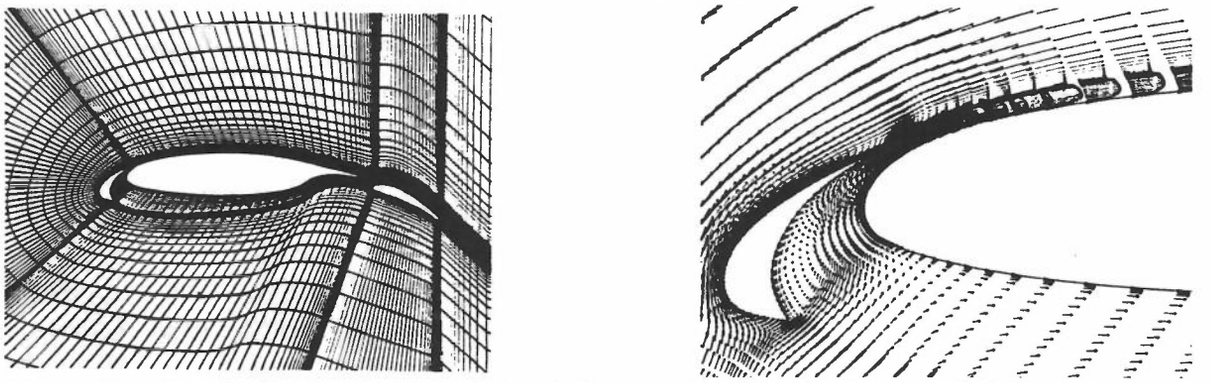

Fig 3: Multi-block grid and velocity field around a three-element aerofoil

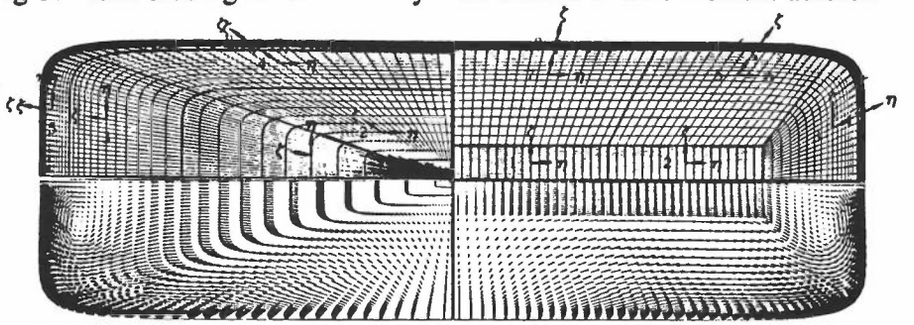

Fig. 4: Transverse velocity in a transition duct computed with 8 blocks

REFERENCES

1. Lien, F.S. and Leschziner, M.A., (1994), Comp. Meth. Appl. Mech. Eng., 114, p. 123.

ASPECTS OF LOCAL MESH REFINEMENT

Researcher: W.L. Chen
Supervisor: F.S. Lien and M.A. Leschziner
Sponsor: Rolls-Royce plc.

1. INTRODUCTION

In most flows, large gradients of flow properties are generally confined to some local portions of the whole spatial domain. In these regions, particularly fine grids are required to achieve a sufficiently accurate solution. In general, it is impractical to adopt a uniformly fine mesh over the entire spatial domain in an effort to meet accuracy constraints, for such a practice tends to give rise to serious resource problems, not only in terms of memory but also because CPU times tend to rise quadratically or even cubicly with mesh size.

The unstructured-grid approach, coupled with flow-sensor adaptation or enrichment is one possible route to local resolution control, but this technology is still at an embryonic stage, particularly in the context of complex turbulent flow. The other route, applicable to the structured-grid environment is local-grid refinement - the method considered here. This involves the selective insertion of additional grid nodes or cells in sub-domain. The insertion process may be pre-defined, but the true potential of mesh refinement can only be realised in combination with flow-related sensors which dictate the position and refinement level on the basis of solution error or local rates of change. Basic aspects of this approach are considered here in the context of the finite-volume framework. Parameters of the coarse grid solution are used to identify regions where finer grids need to be introduced. Of particular interest are the type of sensor, its critical value, at which refinement is initiated, and the role of the interpolation practices at coarse-mesh/fine-mesh boundaries in maintaining uniform accuracy. A more extensive account of the present work may be found in ref [1].

2. APPROACH

The present local mesh-refinement method consists of the following key elements:

(i) **Grid generation:** A property of the coarse-grid solution (or "sensor") is used to guide the grid refinement. The grid system generated consists of the background coarse grid and refined levels with the latter being irregular and confined to regions of high values of the refinement criterion.

(ii) **Treatment of interface between coarse and fine grids:** As there is no overlapping mesh portions at any coarse-grid/fine-grid interface, the values of near-interface cells must be obtained by interpolation. Three interpolation methods have been examined. The first uses area-average interpolation using the interface-cell locations shown in Fig. 1(a). The second and the third operates with the same interface-cell locations shown in Fig. 1(b). The second method employs linear interpolation, while the third implements Lagrange interpolation polynomials. Test computations show that the choice of the interpolation method has profound effects on the accuracy of solution.

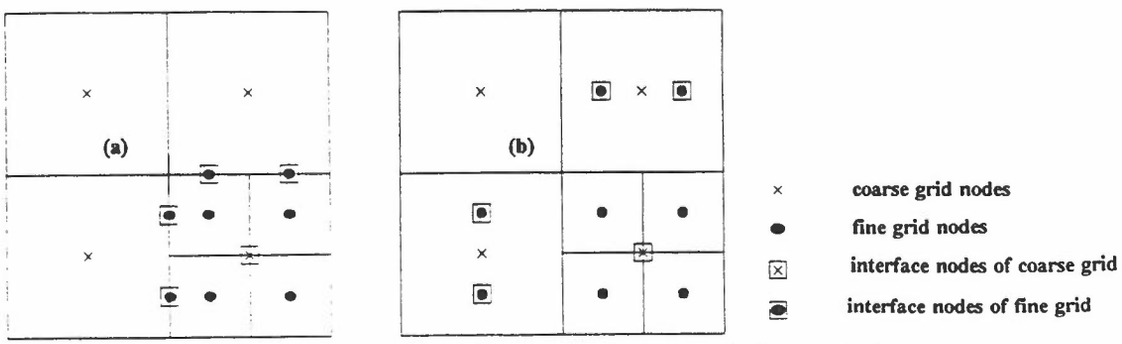

Fig. 1: Locations of near-interface nodes for intergrid interpolations

(iii) **The selections of refinement criterion:** The selections of the refinement criterion and its critical value used to flag the cell to be refined are very influential on the accuracy of refinement method. In calculations presented below, the sensor is based on the solution gradient and its critical value *'Cr'* is chosen as:

$$Cr = Gradient_{min} + f(Gradient_{max} - Gradient_{min})$$

where f is a value to be specified, and *Gradient* is the solution gradient of the coarse-grid solution. This type of sensor is, of course, based on the assumption that there is only one important gradient to which adaptation may be geared. In general flow, the choice of adaptation sensor is a non-trivial issue.

3. APPLICATION

The present technique has been applied to the Poisson equation proposed by Phillips et al (1984), which contains a source resulting in a steep increase in property around the region (1,0). Fig. 2(a) show the errors of full fine-grid simulation (20×20) which is used as a 'benchmark' against which to compare the accuracy of a one-level local mesh-refinement within a 10x10 grid (multi-level refinement is also possible). The results obtained with the three aforementioned interface-interpolation methods with the same fine grid pattern are given in Fig. 2(b,c,d). As seen, the interpolation practice has a crucial influence on the accuracy of this technique. With the sufficiently small value of f specified, the technique predicts the solution with as small a peak error as that of the full fine-grid solution, Fig. 3.

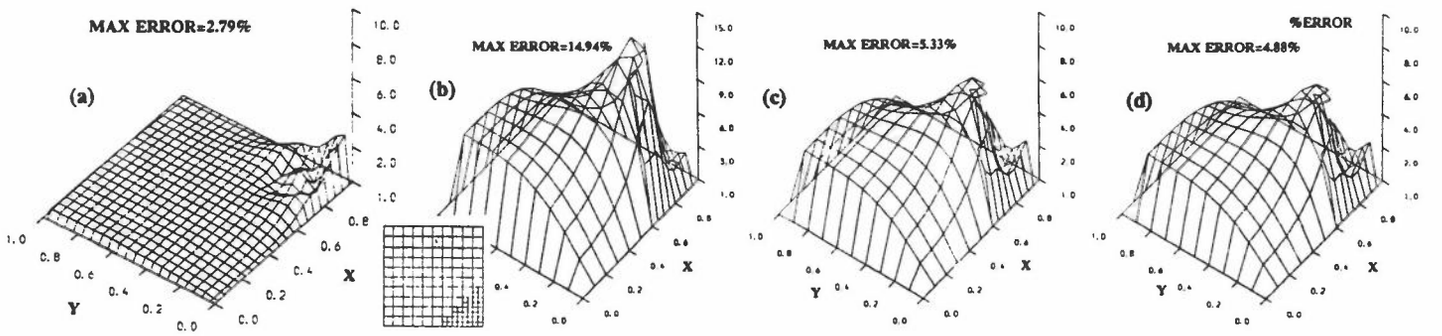

Fig.2: Solution error fields f=0.05 - (a) full 20x20 grid; (b),(c),(d) different intergrid interpolations

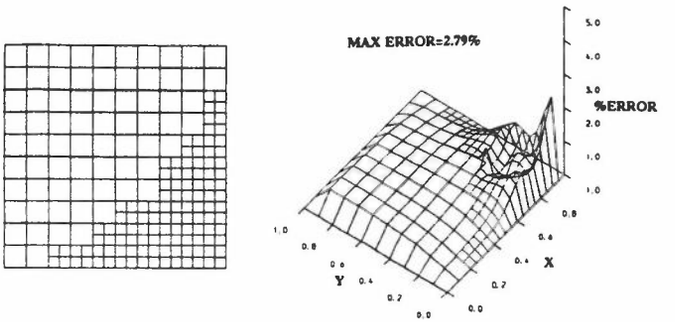

Fig. 3: Solution error field f=0.03

REFERENCES

1. Chen, W.L. (1994), PhD Transfer Report, UMIST, Dept. Mech. Eng.
2. Phillips, R.E. and Schmidt, F.W., (1984), ***Numerical Heat Transfer***, Vol. 8, p. 25.

AN UNSTRUCTURED-GRID ALGORITHM FOR INCOMPRESSIBLE FLOW

Researcher: M.P. Thomadakis
Supervisor: M.A. Leschziner
Sponsor: European Community (Human Capital and Mobility Programme)

1. INTRODUCTION

Unstructured-grid schemes are becoming increasingly popular in the computation of very complex geometries, especially in aerodynamics. Although not without challenges and drawbacks, the method offers, in contrast to block-structured approaches, total flexibility in respect of local grid-density control and flow-sensitised adaptation. With few exceptions, efforts made over the past few years have focused on compressible flow in which the conservation laws governing mass and momentum are solved with a time-marching scheme to yield density and velocity. For incompressible conditions, this is, at best, inefficient and, at worst, unstable. Indeed, it is only tenable in conjunction with an artificial compressibility linking density to pressure via a fictitious relationship. The widely used alternative in the structured-grid environment is the solution of the pressure or pressure-correction equation, which replaces the describing mass continuity.

The present summary reports on initial efforts towards the formulation of an unstructured finite-volume scheme for incompressible flow involving a pressure-correction algorithm. Major elements of work concern the manner in which pressure is determined, the discretisation of the convective and diffusive terms in an unstructured grid environment, and the implicit solution approach arising from the elliptic pressure field.

2. METHODOLOGY

The governing equations are integral forms of the steady 2D continuity and momentum equations for incompressible viscous fluid:

$$\oint \rho \vec{c}\vec{n} dE = 0$$

$$\oint_E \rho u \vec{c}\vec{n} dE = -\oint_E p n_x dE + \oint_E (\tau_{xx} n_x + \tau_{xy} n_y) dE$$

$$\oint_E \rho v \vec{c}\vec{n} dE = -\oint_E p n_y dE + \oint_E (\tau_{xy} n_x + \tau_{yy} n_y) dE$$

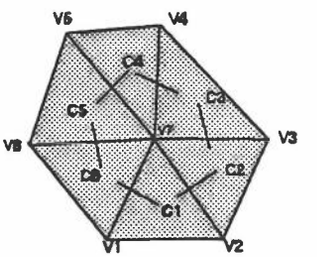

Fig.1: Control volume for the momentum equation (C_1...C_6)

Discretisation involves the transformation of the integrals into flux summations over the edges of the polygonal control volume which represents the numerical form of the closed surface E.

A SIMPLE-like, pressure-correction procedure is used to accommodate the coupling between pressure and velocity. Both velocity components are stored at the vertices of the triangular grid, while pressure is stored at the centres of the triangular cells. The momentum equations are discretised using the centroid duals of the primary triangular cells as control volumes (here called macro-volumes, Fig. 1). A provisional pressure field is given as input, and the corresponding provisional velocity field is obtained from the solution of the momentum equations. At this stage, a procedure similar to SOR for structured grids is used to solve the algebraic systems, with successive sweeps being performed over the central vertices in all the macro-volumes of the domain.

The continuity equation with the provisional velocity field is then discretised over the primary triangular cells. Replacement of corrections to the provisional velocities by pressure perturbations derived from the momentum equations, results in the system of the continuity equations being transformed into a system of equations for the pressure corrections. The solution of this system is also obtained in a SOR-like manner at this stage, although the implementation of a locally implicit solver is being investigated. The pressure correction field is then used to correct the pressure and velocity fields, which closes one iteration. The procedure is repeated until convergence.

To discretise the convective terms, approximations to products of the form $u_e^j * flux_e$ are required all the edges forming a macro-volume (centroid dual), where u^j one of the velocity components and the subscript 'e' denotes value on the edge. A first-order upwind approximation is then implemented for the velocities, in which the mean edge value of velocity is set to the appropriate upstream vertex value. More accurate TVD-type schemes will eventually replace this simple practice. For example, u_e on the edge C_1-C_2 (Fig. 1) is set equal to u_{V7} if the direction of the edge-normal velocity is from V7 to V2. In contrast, the mass-velocity values for the approximation of the fluxes on the edges are obtained as arithmetic averages of the corresponding values on the end-points of the edge (i.e. u_e on C_1-C_2 is set equal to $\frac{1}{2}(u_{C_1}+u_{C_2})$ in Fig. 1).

When descretising diffusion fluxes on macro-volume edges, we follow Stolcis [1] who suggests an approximation for the velocity derivatives on the edges which prevents odd-even point decoupling.

The present method, whilst involving staggering, deviates from a standard practice in that both velocity components are defined on the same points. Therefore, spurious oscillations can appear in the solution due to the poor coupling between velocity and pressure. This has motivated the introduction of artificial dissipation terms into the pressure-correction equation. Following Rhie and Chow [2], face velocity corrections forming the basis of the pressure-correction equation are sensitised to the pressure corrections at nodes straddling the respective faces by adding - say, for the x-velocity term on the edge C_1-C_2 of Fig. 1 - a pressure-gradient term of the form:

$$DP=\alpha\cdot\frac{1}{2}\left[\left(\frac{1}{L_{V7}}+\frac{1}{L_{V1}}\right)\right]\left(p^*_{C_1}-p^*_{C_2}\right)+\frac{1}{2}\left(\frac{1}{L_{V2}}\frac{\partial p^*}{\partial x}\Big|_{V2}+\frac{1}{L_{V2}}\frac{\partial p^*}{\partial x}\Big|_{V7}\right) \qquad (3)$$

where α is a user defined coefficient and the L's are the coefficients of the velocities on the corresponding vertex as they occur from the momentum equations.

3. RESULTS

Test cases computed so far include inviscid flow in a corner and over a channel bump, and viscous flow in a lid-driven cavity at Reynolds numbers of up to 3200. In all cases, a triangular-cell grid was created dy diagonalising a algebraically-generated structured body-fitted mesh. Fig. 2 presents a comparison between computed and the exact streamlines for the corner flow. Fig. 3 compares computed u-velocity profiles through the vertical centre-line of the cavity, at Re=100. The present 3121 vertex calculation is seen to agree well with other numerical solutions.

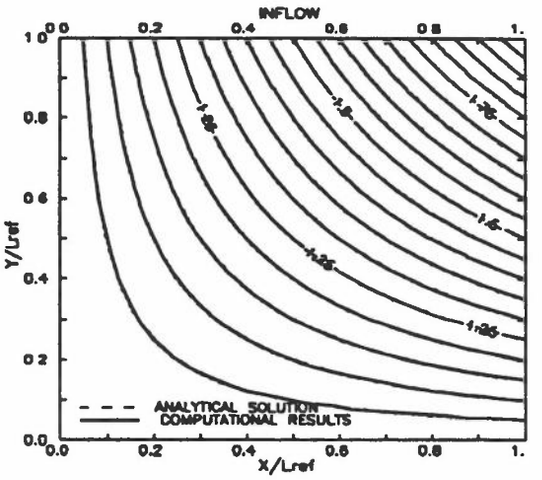

Fig. 2: Inviscid corner flow

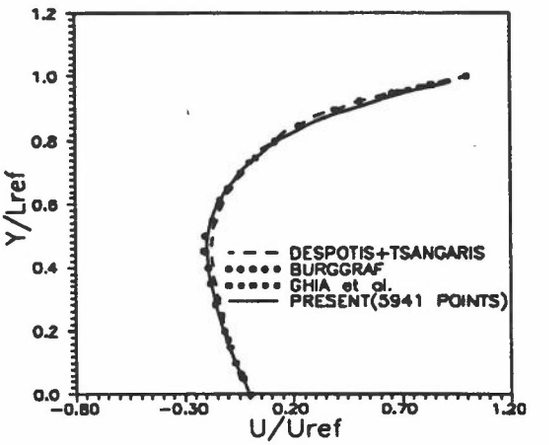

Fig. 3: Mid-cavity velocity profiles at Re=100

REFERENCES

1. Stolcis, L., and Johnston L.J. (1992), AIAA Paper 92-2368.
2. Rhie, C.M., and Chow, W.L. (1983), J. AIAA, 21, p. 1525.

UNSTRUCTURED - GRID FLOW ADAPTION FOR COMPUTATION OF TRANSONIC AERODYNAMIC FLOWS

Researcher : A.R. Jahangirian
Supervisor : Dr. L.J. Johnston
Sponsor : MCHEI

1. BACKGROUND

Mechanical high lift devices, such as trailing-edge flaps and leading-edge slats provide the additional lift necessary to fulfil the low-speed performance requirements associated with take off and landing. These devices can also be used to enhance the manoeuvrability of combat aircraft at transonic conditions. Deployment of flap and slat elements results in a multi-section aerofoil, the flow about which is much more complex than that of a single aerofoil. Additional complications are associated with the generation of a suitable computational grid for such a complex flow domain, which also contains sufficient points to resolve all relevant flow features. These requirements can be satisfied by using unstructured-grid flow adaption.

2. APPROACH

There are essentially three techniques that can be used to alter the computational grid: grid movement, grid enrichment and grid regeneration. In the present work a grid enrichment method is used in conjunction with grid movement to both generate new points in the regions where they are needed and improve the results near the flow features. The method is based upon the equi-distribution principle which intends to produce a grid in which the error is uniformly distributed in space. The pressure gradient along each edge is chosen as an error indicator to decide which edges (or cells) need to be subdivided. The information required for grid adaption is provided by a matrix which connects each cell to its forming edges, so that it is not necessary to search through the list of edges. A new point is then added in the middle of the longest edge of the cell which has been detected for refinement. The adaption cycle starts from a fully-converged flow solution on an initial coarse grid. The grid is adapted to the solution which is then re-converged. This procedure is repeated for a specific number of adaptions.

3. RESULTS

The time-dependent integral form of the equations are solved by means of a cell-centred, finite-volume spatial discretisation. The steady-state solution is achieved by using an explicit multi-stage scheme [1]. The preliminary work to date has concerned flow adaption for inviscid transonic flow around single aerofoils, but the ultimate objective is to develop a method for viscous transonic flow. The standard transonic AGARD case 1 (Mach 0.8, incidence 1.25) for NACA 0012 aerofoil was used to assess the validity and efficiency of the method. Fig. 1a shows the initial coarse grid generated around the aerofoil from a C-type structured grid having 1986 points and 3780 cells. The grid after five levels of adaption (7575 cells) is shown in Fig. 1b. The pressure contours obtained from these two grids indicates that the upper and lower surface shock waves have been suitably refined (Fig 2). The efficiency of the present method is demonstrated by the good comparison with the surface pressure distribution obtained from a globally fine mesh (with 12600 cells) in Figure 3.

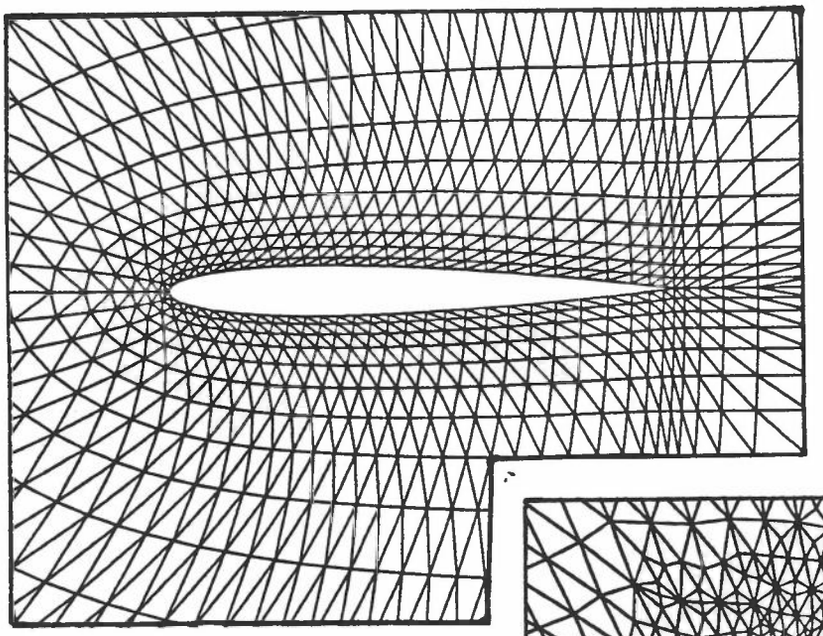

a)

b)

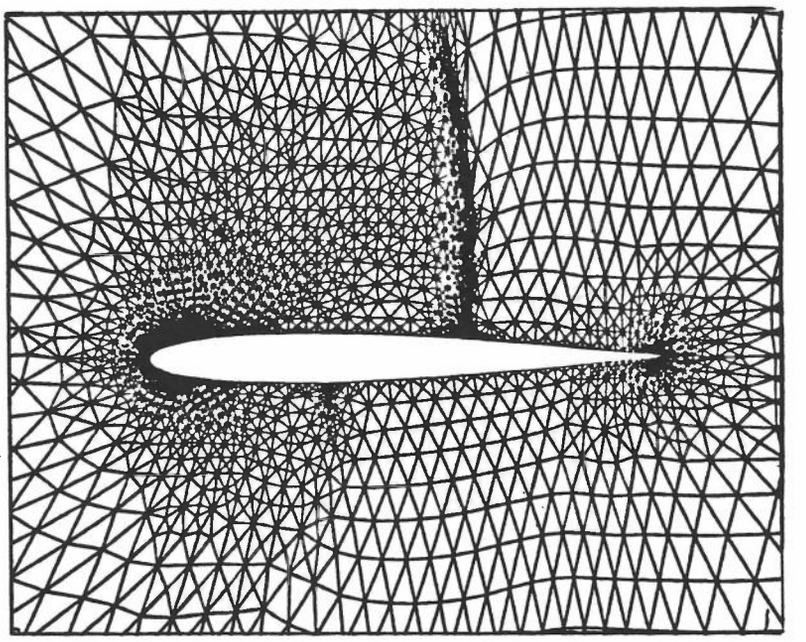

Fig. 1 - (a) initial coarse grid (b) adapted grid

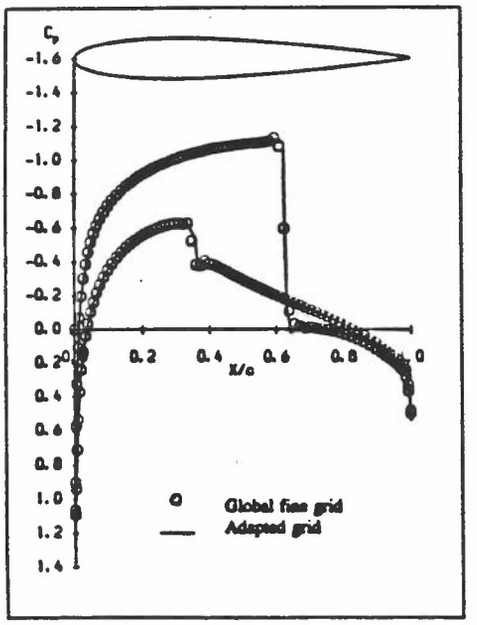

Fig. 3 - Surface pressure coefficient

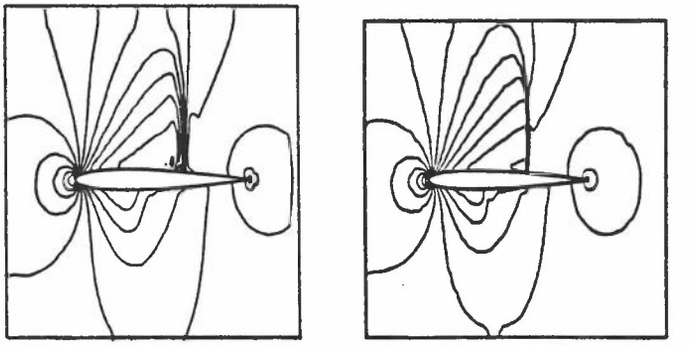

a) b)

Fig. 2 - Pressure contours a) Initial grid b)adapted grid

References

[1] Stolcis L., Johnston L.J. "Solution of the Euler equations on unstructured grids for two-dimensional compressible flow", Aeronautical Journal, Vol.94, pp 181-195, 1990

UPSTREAM MONOTONIC APPROXIMATIONS FOR TURBULENT FLOWS

Researchers: F.S. Lien and M.A. Leschziner
Sponsor: BAe (RAL, SRC), DRA

1. INTRODUCTION

The order of accuracy of the scheme approximating the convective fluxes in a general flow in which conditions vary at a high rate is of central importance to the overall accuracy of the numerical solution. First-order convection schemes tend to misrepresent the transport process through the addition of numerical viscosity to the physical level. Manifestations of this type of error include the smearing of shock waves in transonic flow and the underestimation of the size of recirculation zones in separated flow. Higher-order schemes offer, in principle, a route to improved accuracy, but tend to introduce spurious oscillations in regions of steep gradients due to the dominance of *dispersion errors* arising from odd-order truncation error terms. To avoid such oscillations and thus ensure unconditional *boundedness*, a non-linear limiter must be introduced which 'senses' oscillations and introduces, locally, a strictly controlled amount of dissipation, just sufficient to avoid the oscillation. This is referred to as a Total Variation Diminishing (TVD) constraint.

In the present study, the third-order QUICK scheme of Leonard [1] has been chosen to form the basis of a TVD scheme. To achieve boundedness, a new limiter, termed **UMIST** - Upstream Monotonic Interpolation for Scalar Transport (Lien & Leschziner [2]) - has been developed. Unlike other schemes, such as **SMART** (Gaskell & Lau [3]) and **SHARP** (Leonard [4]), this variant is computationally inexpensive, with the typical overhead being of order 15% relative to the unbounded QUICK approximation. The main purpose of the scheme is to permit uniformly high accuracy, iterative stability and efficiency to be achieved across the entire set of equations solved within a Reynolds-averaged procedure which incorporates the most general turbulence closures available.

2. APPROACH

In the context of an iterative solution for statistically steady flows within the finite-volume framework, the essential task is to approximate the volume-face variable ϕ_f. With the 3-node QUICK stencil (ϕ_U,ϕ_C,ϕ_D) shown in Fig. 1, a general bounded approximation scheme may be written:

$$\tilde{\phi}_f = \tilde{\phi}_C + \frac{1}{4}[(1+\kappa)\varphi(r_f)(1-\tilde{\phi}_C) + (1-\kappa)\varphi(\frac{1}{r_f})\tilde{\phi}_C] \qquad (1)$$

where

$$\tilde{\phi} = \frac{\phi - \phi_U}{\phi_D - \phi_U}, \quad r_f = \frac{\tilde{\phi}_C}{1-\tilde{\phi}_C}, \qquad (2)$$

If a symmetric limiter, satisfying $\phi(r)=r\phi(1/r)$ is chosen, then (1) becomes

$$\tilde{\phi}_f = \tilde{\phi}_C + \frac{\varphi(r_f)}{2}(1-\tilde{\phi}_C), \qquad (3)$$

A monotonic version of QUICK, satisfying the TVD constraint,

$$\begin{gathered}\tilde{\phi}_f \le 1, \quad \tilde{\phi}_f \le 2\tilde{\phi}_C, \quad \tilde{\phi}_f \ge \tilde{\phi}_C, \quad \text{for} \quad 0 < \tilde{\phi}_C < 1 \\ \tilde{\phi}_f = \tilde{\phi}_C, \quad \text{for} \quad \tilde{\phi}_C \le 0 \quad \text{or} \quad \tilde{\phi}_C \ge 1\end{gathered} \qquad (4)$$

can be achieved through the symmetric limiter:

$$\varphi(r) = \max[0, \min(2r, 0.25+0.75r, \underbrace{0.75+0.25r}_{\text{QUICK}}, 2)] \qquad (5)$$

which is termed here the UMIST limiter. The corresponding Normalised Variable Diagram (NVD) is shown in Fig. 2.

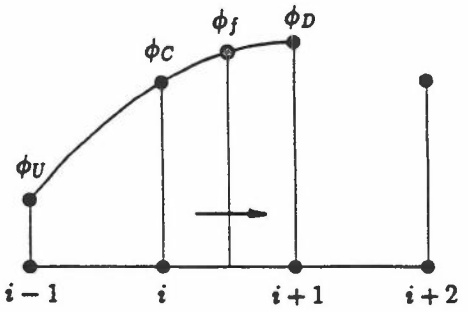

Fig. 1: QUICK/UMIST 1D stencil

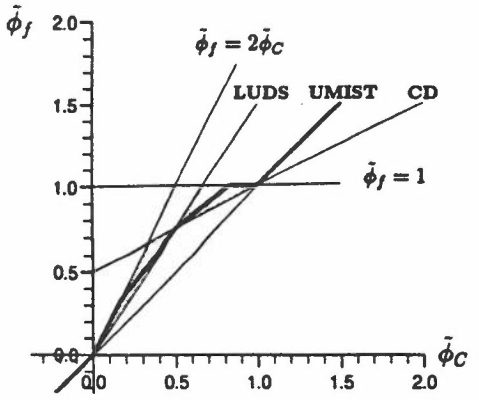

Fig. 2: NVD diagram for UMIST limiter

3. APPLICATION

In ref [2], the UMIST limiter is applied to a wide range of flows, spanning laminar, transonic and turbulent conditions. Here, two simple tests are included: a transonic Laval nozzle flow, illustrating shock-capturing capabilities, and the transport of a scalar near-discontinuity across a 2D Cartesian mesh by a prescribed rotational velocity field at Pe=10^6. In addition, Table 1 compares, for the latter case, the CPU resource requirements of the first-order upwind scheme UDS, QUICK and UMIST, all normalised by the UDS time.

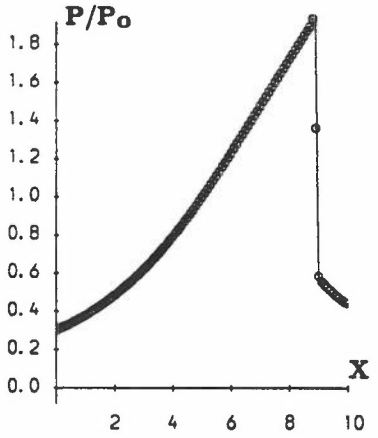

Fig. 3: Transonic Laval nozzle Flow

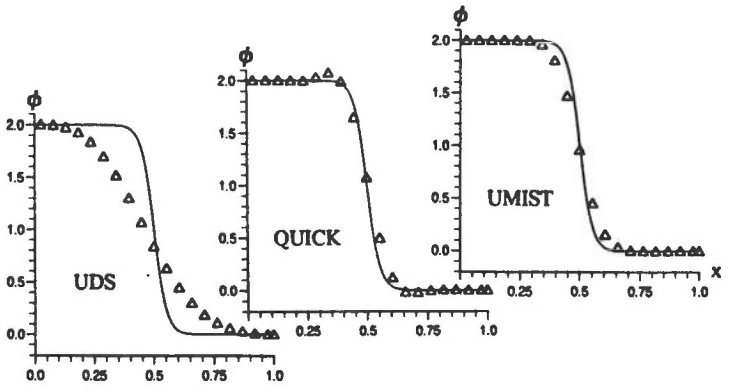

Fig. 4: Scalar transport by rotational velocity field

convection scheme	Pe=10^6			
	iterations	CPU (sec)	sec/per iteration	CPU ratio
UDS	95	13.997	0.1473	1.000
QUICK	89	15.010	0.1687	1.072
UMIST	89	17.364	0.1950	1.241

Table 1: Relative resource requirements of unbounded QUICK and UMIST schemes

REFERENCES

1. Leonard, B.P., (1979), Comp. Meth. Appl. Mech. Eng., 19, p. 59.
2. Lien, F.S. and Leschziner, M.A., (1993), Rep. TFD/93/12, Dept Mech. Eng., UMIST.
3. Gaskell, P.H. and Lau, A.K.C., (1988), Int. J. Num. Meth. Fluids, 8, p. 617.
4. Leonard, B.P., (1988), Int. J. Num. Meth. Fluids, 8, p. 1291.

NUMERICAL ASPECTS OF A LARGE EDDY SIMULATION ALGORITHM

Researcher: F. Archambeau
Supervisor: M.A. Leschziner
Sponsor: Electricité de France

1. INTRODUCTION

Large Eddy Simulation has been used extensively for fundamental research on turbulence and transition, but it also being applied with increasing frequency to high Reynolds-number flows allied to practical engineering problems in which influential large-scale organised motion co-exists with 'random' turbulence. In such cases the Reynolds-averaged Navier-Stokes framework often fails to return the periodic behaviour, because of excessive damping, and tends to misrepresent the time-averaged flow field due to its inability to distinguish between dispersion arising from the organised motion and diffusion.

In Large Eddy Simulation, the larger scales of the turbulent flow are resolved directly on a mesh whose size determines the smallest scales which can be captured, while unresolved small-scale processes are represented by a model returning the diffusive subgrid stresses. Because the small-scale motions tend to be more isotropic and less organised than large-scale ones, the task of modelling diffusive transport within an LES scheme tends to be less challenging than that of the full Reynolds stresses. Moreover, the time-averaged behaviour is considerably less sensitive to the realism of the modelling practice.

This summary reports on initial efforts directed towards the development of a general-coordinate, co-located finite volume algorithm for Large Eddy Simulation, able to compute transient flows in complex geometries with high accuracy and efficiency.

2. RATIONALE OF LARGE EDDY SIMULATION

The Navier-Stokes equations are first 'filtered' with a Gaussian function G so as to derive equations for the largest scales of the flow. The filter width Δ is, typically, twice the mesh size:

$$U = \overline{U} + U' \qquad \overline{U}_i(\underline{x}) = \int_{+\infty}^{-\infty} G(\underline{x} - \underline{x}')U_i(\underline{x}')\, d\underline{x}' \quad with \quad G(\underline{x}) = \left(\sqrt{\frac{6}{\pi}}\frac{1}{\Delta}\right)^3 \exp\frac{-6|\underline{x}|^2}{\Delta^2}$$

The filtered equations then read :

$$\frac{\partial \overline{U}_i}{\partial t} + \frac{\partial(\overline{U}_i\overline{U}_j)}{\partial x_j} = -\frac{1}{\rho}\frac{\partial \overline{p}}{\partial x_i} + \nu\frac{\partial^2 \overline{U}_i}{\partial x_j \partial x_j} - \frac{\partial \tau_{ij}}{\partial x_j}$$

The set of equations still needs to be closed as the tensor τ_{ij} does not depend only on the filtered variables. The widely used Smagorinsky's model is a closure example:

$$\tau_{ij} = -2\nu_t \overline{S}_{ij} \quad with \qquad \overline{S}_{ij} = \frac{1}{2}\left(\frac{\partial \overline{U}_i}{\partial x_j} + \frac{\partial \overline{U}_j}{\partial x_i}\right) \quad and \quad \nu_t = (C_s\Delta)^2\, |2\overline{S}_{ij}\overline{S}_{ij}|^{1/2}$$

3. COMPUTATIONAL APPROACH

The starting point has been the 3D general-coordinate code STREAM (Lien & Leschziner [1]). For LES, discretization is based on energy-conserving central differencing on a collocated grid, with Rhie & Chow interpolation for face velocities being used to circumvent pressure chequerboarding. The second-order accurate Adams-Bashforth scheme is used to advance convection, diffusion and subgrid stresses in time. The Crank-Nicolson scheme had initially been chosen to approximate the pressure-gradient terms to ensure second-order overall accuracy in time. However, a fully implicit approximation has been preferred in some cases for its much greater stability.

The pressure Poisson equation is discretised with a 27-points operator. The Bi-Conjugate Squared Gradient method, coupled to a line-Jacobi pre-conditioner performs well on a regular grid, but has been found to break down for non-symmetric matrices. Hence, the well known GMRES method has been preferred here, although it consumes twice as much CPU time.

4. RESULTS

At this stage, test calculations have been performed for various simple time-dependent flows to ensure that the numerical approach is correct. Results obtained with 32^2 and 64^2 grids and Courant numbers in the range 0.125 to 0.5 for a square-cavity flow driven by an oscillating lid, Fig. 1, compare well to computations by Nasser & Leschziner [2] with a time-space characteristics-based scheme. They also match results obtained with a staggered finite-volume LES code of Murakami et al [3].

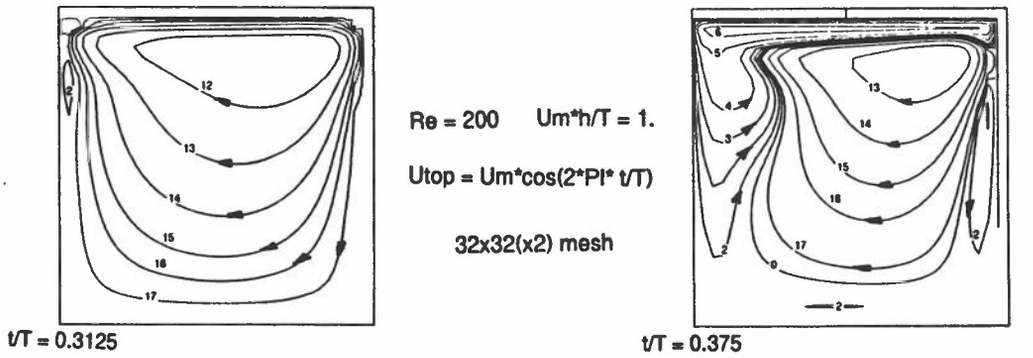

Fig. 1: Flow in cavity with sinusoidally-driven lid motion

Results for vortex shedding behind a square cylinder are contained in Fig. 2. The computed Strouhal number of 0.17 at Re=300 is in fair agreement with experiments (Okajima [4] and Davis & Moore [5] reports 0.14 and 0.17, respectively).

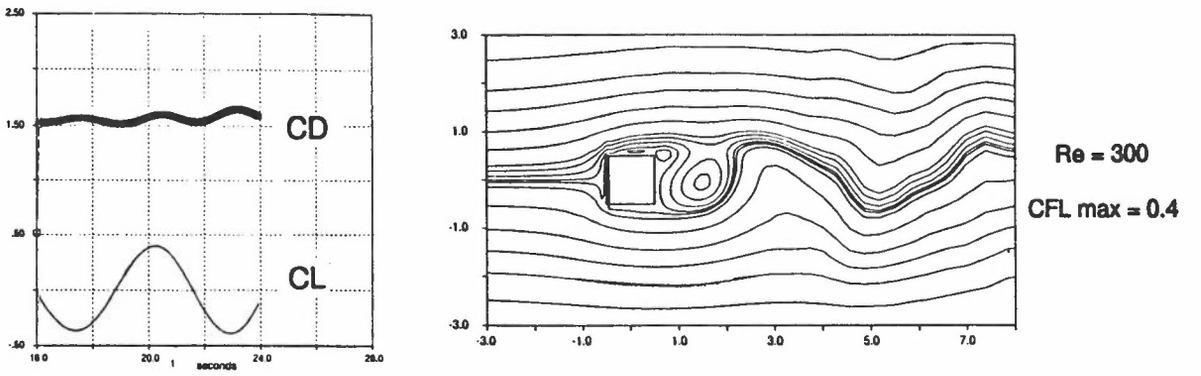

Fig. 2: Vortex shedding behind square cylinder

The major issue remains the large amount of CPU time needed. Half of the computing time is spent on solving the pressure Poisson equation. Hence, finding a fast and reliable iterative solver for non-symmetric, non-positive and non-definite matrices would be a major achievement.

REFERENCES

1. Lien & Leschziner (1994), Comp. Meth. Appl. Mech. Eng. (in press)
2. Nasser and Leschziner (1983), in Numerical Methods in Laminar and Turbulent Flow VIII, (C. Taylor, Ed.) p. 815, Pineridge Press.
3. Murakami, S., Mochida, A., Ooka, R., (1993), paper 13.5. Proc. 9th TSF, Kyoto.
4. Okajima, A. (1982), J. Fluid Mech., 123, p. 379.
5. Davis, R.W. and Moore, E.F. (1982), J. Fluid Mech., 116, p. 475.

PARALLEL COMPUTING ON DISTRIBUTED MEMORY MACHINES

Researcher: D. Golby
Supervisor: M.A. Leschziner
Sponsor: SERC

1. INTRODUCTION

Parallel computing is increasingly seen as the only promising route to securing the computing resources needed for large-scale 3D Navier Stokes computations, whether in the context of aircraft aerodynamics or direct numerical simulations. Given a MIMD (Multiple Instructions / Multiple Data) configuration of communicating processors with distributed, processor-specific memory caches, the usual approach to program execution is to decompose the solution domain into patches and assign these in some (usually predetermined) order to associated processors. Coupling is achieved by a controlled interchange of data between the processors. The principal challenges of this approach, particularly with large numbers of processors (MPP configurations) are, first, to account properly for data dependencies across processors/sub-domain boundaries; second, to minimise the amount of data exchanged between processors and optimise the manner of this exchange; and third, to avoid latency and thus achieve good load balancing. The better these objectives are met, the closer the correspondence between speed-up factors and the number of processors - an issue referred to as "scalability".

Parallel computing has been pursued at UMIST on a variety of architectures and with different numerical algorithms. One developing area of interest is the implementation of the multi-block scheme reported in Summary 2.4 on an Intel Hypercube and Cray T3D computers. The effort reported here involved the implementation of a time-marching NS scheme on a Transputer machine. The scheme, formulated principally in order to resolve shock/boundary-layer interaction in turbulent aerofoil flows, combines cell-vertex storage, Lax-Wendroff temporal discretisation, multigrid acceleration and various transport models of turbulence, including low-Re two-equation models and algebraic second-moment closure. The scheme is documented in detail in ref [1], while various aspects of parallel implementation and performance are reported in refs [2,3].

2. IMPLEMENTATION

Arising from the cell-vertex storage arrangement shown in Fig. 1 and the turbulence models implemented in the code, is the data-dependency stencil shown in the same figure. While this is not atypical of CFD codes based on regular structured meshes, the present data dependency is somewhat more extensive than in cell-centred schemes, and this has an adverse impact on inter-processor communication. This communication involves periodic exchanges of updated grid-node data shared between neighbouring sub-domains and the circulation of residual values over the processor array for global residual summations. The former step is responsible for a substantial proportion of the total communication overhead, while the latter, although using smaller packets of data, requires particular attention if the code is to run efficiently. Systolic loops running in parallel over each row of the processor array have enabled global communications to become a small overhead in the execution time, typically less than 1-2%. Particular difficulties arise in C- or O-type mesh topologies for aerofoils due to an unavoidable grid-index discontinuity across one 'radial' grid-line - typically a 'wake cut'. The logical connection between processors associated with sub-

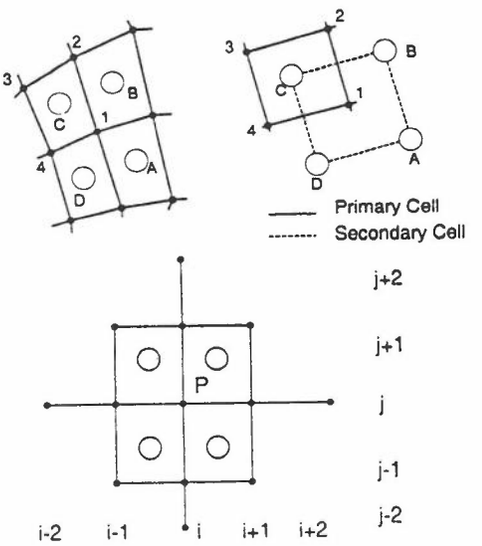

Fig. 1: Cell-vertex storage and data-dependency stencil

domains abutting this cut required careful attention. Problems are also posed by non-unity strides in the multigrid implementation, with grid-coarsening causing non-standard data dependencies and small numbers of nodes per processor, the latter decreasing parallel efficiency. In the present implementation, a minimum of one grid-node per processor has been imposed.

Most of the capabilities of the original code have been realised on the Transputer machine (a Meiko Computing Surface), with its ability to compute various aerodynamic flows with both low-Re two-equation models and the ASM being left intact.

3. RESULTS

Fig. 3 shows the performance of the code using three turbulence models for a flow around the RAE 2822 aerofoil using a 137x21 C-grid. Here, the measured program speed-up is compared with the maximum value estimated by eliminating the total measured communication time from the execution time value. For this particular flow problem, it is clear that the code runs efficiently only up to approximately 10 processors due to the coarseness of the grid being used. Further decomposition of the flow domain would serve to drive up the communications overhead to levels greater than 10%, which is generally unacceptable. The fact that the maximum execution time is less than the ideal value is an indication of the effect of load imbalance effects due to an uneven grid distribution over the processors as the mesh is further distributed. An improvement in performance would result if larger meshes were to be used here.

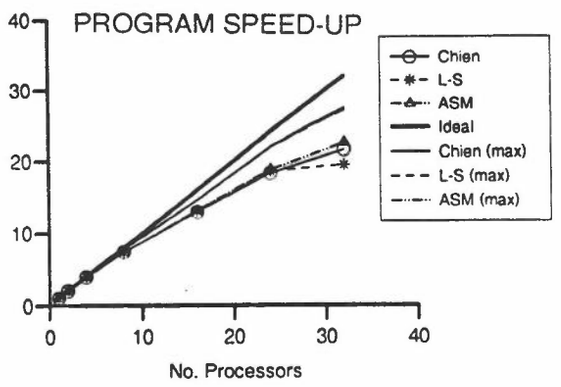

Fig.3: Speed-up profiles for RAE 2822 aerofoil

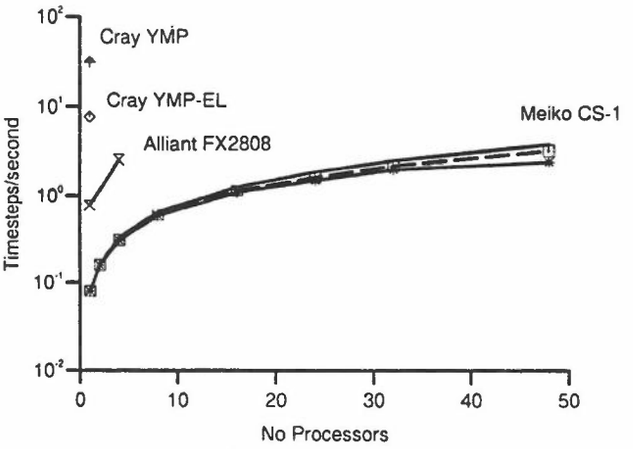

Fig. 4: Execution speeds for transonic bump

A comparison between the Meiko and a number of other machines is shown in Fig.4 for shock-induced separation over a channel bump using a 97x33 mesh. These results emphasize the rather low performance of the transputer when compared to more advanced microprocessors or vector systems. They indicate that approximately 50 transputers are required to attain even the speed of the four i860-processor cluster of the Alliant FX2808, while 500-600 nodes would be needed to reach the performance level of a Cray-YMP.

The study has indicated that the cell-vertex code is well suited to distributed memory systems, although communication overheads and load-imbalance problems do occur if the grid is rather coarse. While the Meiko is clearly outpaced by the Cray-YMP, the present parallel code can be run directly on the more advanced Meiko CS-2, and can be quickly adapted to other distributed memory systems using faster processing nodes.

REFERENCES

1. Leschziner, M.A., Dimitriadis K.P. and Page, G. (1992), The Aerodynamical Journal, 97, p. 43.
2. Golby D and Leschziner M.A. (1994), in Parallel CFD '93 (Ecer A, Hauser J, Leca P, Periaux J, eds), Elsevier (in press).
3 . Golby, D. and Leschziner, M.A. (1994), in Future Generations of Computer Systems, North Holland.

A SPECIAL NEAR-WALL ELEMENT FOR FINITE ELEMENT COMPUTATIONS OF DENSE-GAS DISPERSION OVER GROUND OF VARIABLE ELEVATION

Researcher: A.I. Sayma
Supervisor: P.L. Betts
Sponsors: Palestinian Students Fund, Arab-British Chamber, ORS

1. BACKGROUND AND OBJECTIVES

The Finite Element model, FEMSET [1], had earlier been developed to simulate environmentally hazardous dense gas dispersion in the atmosphere associated with accidental release of toxic or flammable gases. The model is based on the solution of the mean flow equations and a species concentration equation for the contaminant gas. A buoyancy extended anisotropic k-ε model is used to calculate eddy viscosity and turbulent diffusivities in the Reynolds averaged transport equations while standard wall functions were used to bridge the gap between the solution domain and the rough solid boundary, where variables vary steeply in logarithmic manner. The Galerkin finite element method is used to discretize the system of equations in space while the forward Euler method is used to advance the resulting system of ordinary differential equations in time.

Initial simulations with the code were successful in reproducing the major features of large scale dense gas releases over flat ground. However, simulation over an irregular topography diverged, even before injection of the heavy gas. Tests showed that the main cause of the problem, for the coarse mesh required in the 3D simulations and the resulting high grid Peclet number, was interaction of an oscillatory pressure mode near the ground with the velocity field through the wall function traction boundary condition. In the present study, this difficulty was eliminated by extending the solution domain up to the real boundary, where no slip boundary conditions can be applied with only minor increase in the computational costs.

2. APPROACH

The gap between the solid wall and the solution domain of all variables, except k and ε, is spanned by a one element thick layer of special elements which employ a logarithmic shape function. The special shape function is derived from the rough wall boundary layer profiles and resolves accurately the sharply varying quantities in the near wall region. The shape function in the direction normal to the wall takes the form [2]:

$$[\Phi_1,\Phi_2]=[1-A(n),A(n)] \qquad (1)$$

$$A(n)=\ln[\frac{\Delta(n+1)}{2z_o}+1]/\ln[\frac{\Delta}{z_o}+1] \qquad (2)$$

where n the is the element local coordinate in the direction normal to the wall, Δ is the average thickness of the element and z is the roughness height. The special shape function of the element is assembled by tensor multiplication of the special shape function in the n direction with the linear shape functions in the mutually perpendicular directions. The special shape function is used to represent the variables within the Galerkin formulation of the momentum and energy equations while the mother (linear) shape function is used to weight these equations and to represent velocities in the continuity equation, to retain symmetry of the pressure matrix.

Eddy viscosity is modelled by assuming that shear stress is constant across the special element with its value provided from the turbulent kinetic energy at the interface of the domain and the special element layer, where k and ε are treated in the usual wall law manner.

3. RESULTS

This approach was used successfully to simulate atmospheric boundary layers in two and three dimensions over flat and irregular grounds. Simulations of dense gas dispersion over flat ground were improved, owing to the better accounting for the dense gas cloud in the near ground region. Full three dimensional simulation of the Burro-8 [3] test over irregular topography shown in Figure (1) was successful in reproducing the trial qualitatively and quantitatively. Figure (2) shows a vertical section of the concentration contours at different times. Comparison with experimental results of maximum distance travelled by the lower flammability level is shown in the article about radiation in these proceedings and shows satisfactory agreement with the experiment.

REFERENCES

1. Betts P L and Haroutunian V, " Finite element calculations of transient dense gas dispersion", *Stably Stratified Flow and Dense Gas Dispersion*, ed. J.S.Puttock, IMA New Series 15, Oxford U.P., 349-384, 1988.
2. Betts P L and Sayma A I, "Improved near ground treatment in finite element simulation of dense gas dispersion", *Finite Elements in Fluids, New trends and applications*, ed. K.Morgan et al., Pineridge Press, 959-969, 1993.
3 Koopman R P et al., Burro series data report LLNL/NWC 1980 LNG spill tests, Lawrence Livermore National Laboratory, 1982.

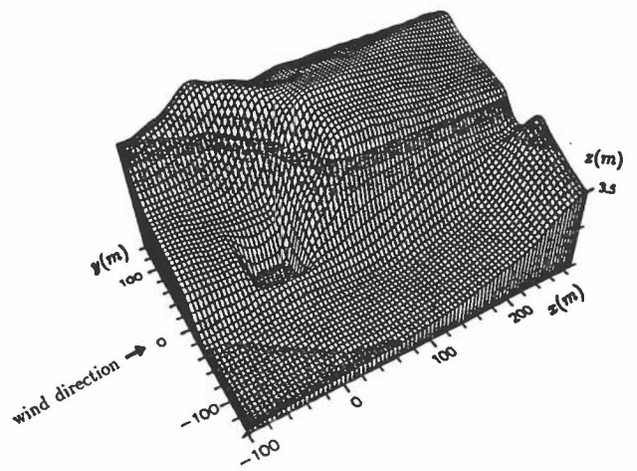

Fig 1 Topography of Burro Trials site. Note vertical scale exaggeration.

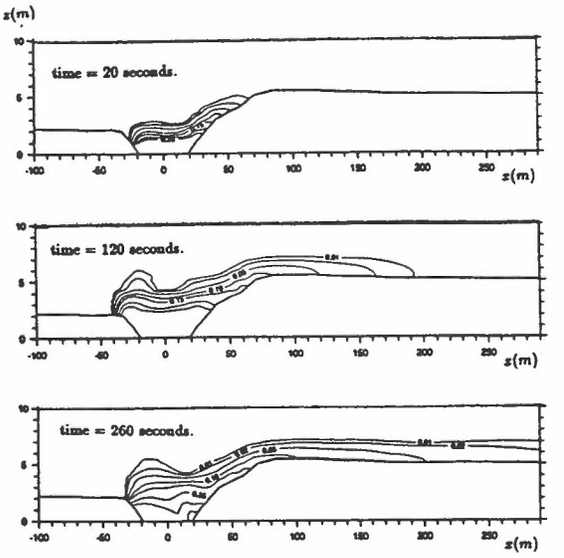

Fig 2 Centre-section predicted concentration contours at various times after start of dense gas release.

« Session 3 »

Turbulence Modelling - *Assessment & Validation*

SENSITIVITY OF 2D SEPARATION CHARACTERISTICS TO TURBULENCE MODELLING

F.S. Lien and M.A. Leschziner

1. INTRODUCTION

Separation, recirculation and reattachment are features encountered in numerous practical situations, and usually have profound consequences to pressure recovery, pressure drag, wall friction and heat-transfer characteristics. Recirculation is also a powerful generator of turbulence and hence mixing and losses. Separated flows have thus been the subjects of many studies, both experimental and computational.

By far the most popular separated-flow configuration for turbulence-model validation is the backward-facing step. Several high-quality experimental data sets exist for this flow, among them those of Driver & Seegmiller [1]. With the separation point being fixed, this case allows attention to be focused, principally, on the ability of turbulence models to predict the curved shear layer bordering the separation bubble, the reattachment process and the subsequent recovery of momentum in the wake.

The investigation summarised herein has arisen from the 1991/1992 Stanford validation initiative, coordinated by P. Bradshaw as a follow-up to the 1980/81 Stanford Conference on Complex Turbulent Flows. In this, the Driver & Seegmiller case featured as one of the central separated flows. The writers contributed solutions arising from five turbulence models, among them second-moment closure. Subsequently, two further models have been added to this range. A detailed exposition of the study may be found in ref. [2]

2. TURBULENCE MODELS and COMPUTATIONAL SCHEME

A total of seven turbulence model variants have been examined; these are listed below, each preceded by the identifier used in plots and the related discussion:

- STD k-ε - Jones & Launder's k-ε model [3];
- RNG k-ε - Yakhot et al's 'RNG' k-ε model [4];
- LL k-ε - Lien & Leschziner's low-Re k-ε model [5];
- N-L RNG k-ε - combining Speziale's non-linear [6] and Yakhot et al's 'RNG' models;
- RSTM-DH/ϕ_{ijw}^{GL} - standard Gibson & Launder's Reynolds-stress model [7];
- RSTM-DH/ϕ_{ijw}^{CL} - Gibson & Launder's model combined with Craft & Launder's wall-reflection term [8];
- RSTM-ED/ϕ_{ijw}^{GL} - Gibson & Launder's model combined with eddy-viscosity diffusion in the stress and dissipation equations, which replaces the usual Daly & Harlow GGDH form.

In the last variant, the Prantl numbers σ_k and σ_ε have been derived on the basis of constraints on the ratio of $\overline{v^2}/\overline{uv}$ implied by the standard second-moment closure applied to local equilibrium conditions, alongside the usual compatibility condition between Prantl numbers, the von Karman constant and the constants C_1 and C_2 in the ε-equation.

Numerical solutions with grids of up to 110x80 lines have been obtained with the general non-orthogonal co-located finite volume scheme STREAM of Lien & Leschziner [9], with the quadratic scheme QUICK used to approximate convection.

3. RESULTS

Solutions for streamfunction and skin friction on the lower step wall are presented in Figs. 1 and 2, respectively, for the case of a 6° channel expansion downstream of the step. Particularly noteworthy are (i) the importance of the wall-reflection term to the reattachment process; (ii) the considerable elongation of the recirculation zone arising from the isotropic diffusion of stresses and dissipation in the second-moment closure; (iii) the good representation returned by the non-linear

model when combined with the RNG modifications[1]; (iv) the elongation of the recirculation zone resulting from the low-Re form, apparently due to an improved representation of the near-wall length scale.

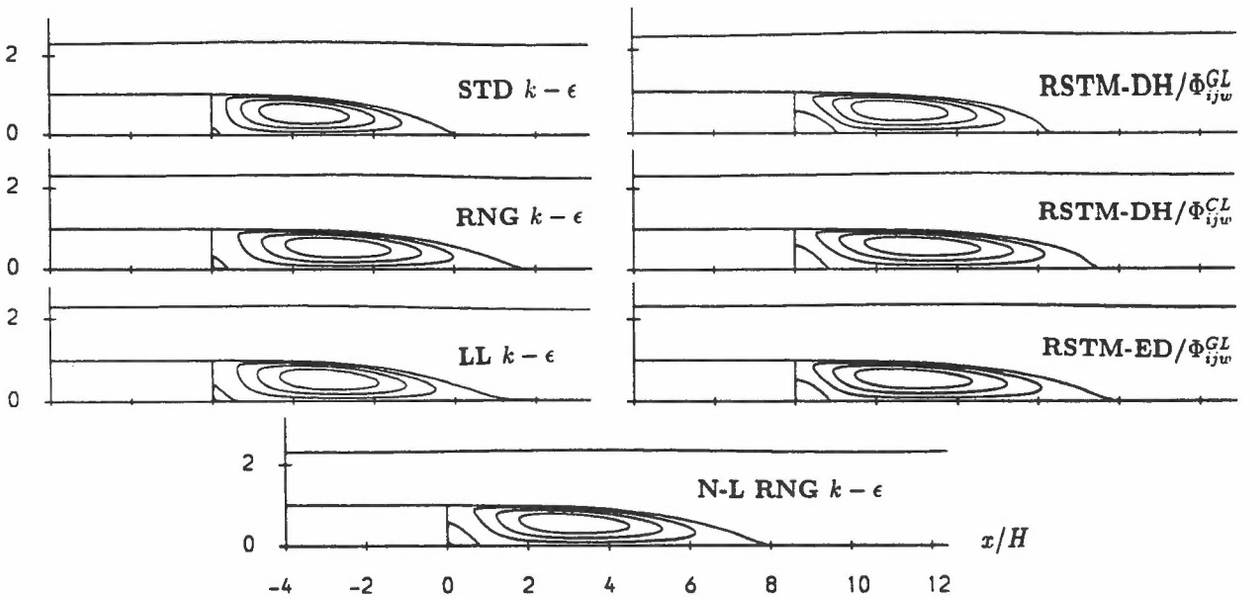

Fig. 1: Streamfunction contours in recirculation zone

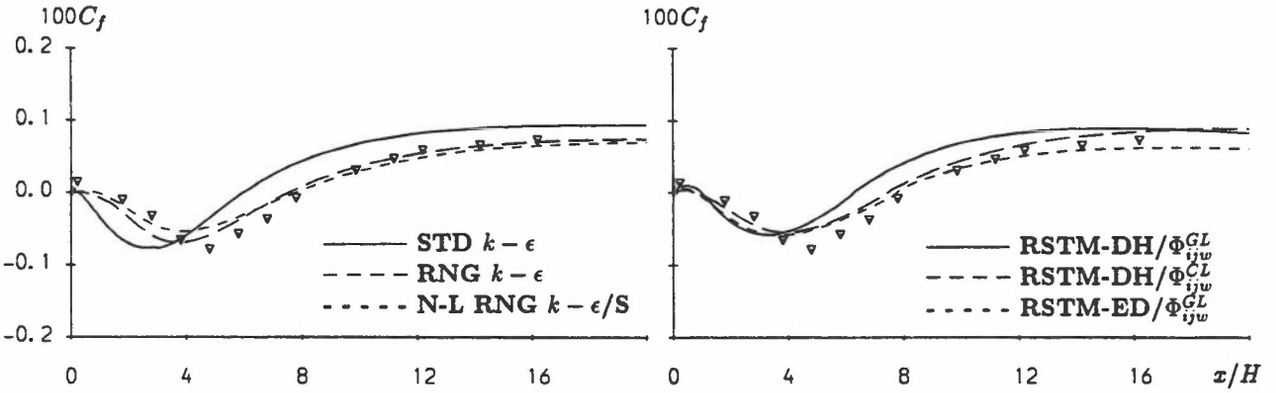

Fig 2: Skin-friction distribution on step wall

REFERENCES

1. Driver, D.M. and Seegmiller, H.L., (1982), AIAA Paper 82-1029.
2. Lien, F.S. and Leschziner, M.A., (1993), Rep. TFD/93/09, Dept. Mech. Eng., UMIST.
3. Jones, W.P. and Launder, B.E., (1972), Int. J. Heat Mass Transfer, 15, p. 301.
4. Yakhot, V., Orszag, S.A., Thangam, S., Gatski, T.B. and Speziale, C.G., (1992), Phys. Fluids A, 7, p. 1510.
5. Lien, F.S. and Leschziner, M.A., (1993), Engineering Turbulence Modelling and Experiments 2, (W. Rodi & F. Martelli, ed.), p. 217.
6. Speziale, C.G., (1987), J. Fluid Mech., 178, p. 459.
7. Gibson, M.M. and Launder, B.E., (1978), J. Fluid Mech., 86, p. 491.
8. Craft, T.J. and Launder, B.E., (1992), AIAA J., 30, p. 2970.
9. Lien, F.S. and Leschziner, M.A., (1994), Comp. Meth. Appl. Mech. Eng., 114, p. 123.

[1] Neither the non-linear model nor the RNG form returns, on its own, a satisfactory behaviour

MODELLING NON-EQUILIBRIUM BOUNDARY LAYERS WITH A MODIFIED k-ω MODEL

Researcher : T. Rung
Supervisor : M.A. Leschziner
Sponsor : European Community (Human Capital and Mobility Programme)

1. BACKGROUND and OBJECTIVES

The accurate prediction of non-equilibrium boundary layers which are close to incipient separation whilst developing on a continuous surface is important in many fluids engineering devices operating at high-load conditions where maximum performance (e.g. pressure recovery) is obtained. In such circumstances, separation may either be provoked or suppressed in response to even slight variations in the computational representation. Hence, the predictive quality of the flow's gross characteristics may hinge on seemingly subtle modelling details in apparently innocuous flow portions.

The simultaneous presence of shear and severe adverse pressure gradient in the near-wall region leads to a complex, highly anisotropic structure, where the assumption that all turbulence quantities scale with the friction velocity fails, because the near-wall flow is no longer universally controlled by the wall shear stress. Although a general approach to a satisfactory resolution of such complex near-wall phenomena would, arguably, be based on full second moment closure, which might include a tensorial representation of dissipation, a simpler, computationally cheaper approach involving scalar turbulence quantities is defensible, provided this approach returns the correct boundary-layer structure and its response to adverse pressure gradient.

The knowledge that the ε-equation is a major contributor to the misrepresentation of turbulence transport in adverse pressure gradients has motivated the adoption of a modified variant of Wilcox's ω-equation in the first stage of the present research effort which is directed towards incipiently separated ducted flows. The nature and rationale of the model modifications are outlined and results are reported for an attached boundary-layer in comparison to low-Re number k-ε solutions.

2. TURBULENCE MODELLING and COMPUTATIONAL APPROACH

Wilcox [1] has argued that the specific dissipation rate ω is more appropriate for predicting a proper wake strength and the near-wall length scale. Additionally, the transport equation for ω has the advantage of being less stiff in the near-wall region and is, at least in its classical form, able to return the correct structure inside the semi-viscous sublayer without any damping functions. However, this equation, as well as a low-Re version recently proposed by Wilcox [2] have been found to perform poorly when applied to non-equilibrium boundary-layers. Both variants significantly underpredict the turbulent length scale in the near-wall region and also seem to underestimate near-wall diffusion of turbulence energy.

In an effort to improve the performance of the equation, low-Re modifications have been incorporated into the classical model along a route suggested by Lien & Leschziner [3] in the context of k-ε modelling. This has involved four main elements:

(i) the coefficient β^* of the k-destruction term has been sensitised to the turbulent Reynolds number (based on k) so as to achieve the desired asymptotic near-wall behaviour of k (this is in line with Wilcox's approach in ref [2]);

(ii) the coefficient α in the ω-generation term has been similarly modified to ensure that the turbulent length scale declines in conformity with Wolfshtein's one-equation model [4] as the wall is approached;

(iii) the turbulent Prandtl numbers for k and ω have been sensitised to the turbulent Reynolds number in accord with recommendations by Nagano and Shimada [5];

(iv) a damping term, involving the turbulent Reynolds number, has been introduced into the eddy-viscosity relation to ensure consistency with the one-equation model close to the wall.

Finally, minor modifications have been applied to the one-equation-model terms in order to secure the

correct asymptotic behaviour of ω as the wall is approached.

Results reported below have been obtained with a 2D version of the general finite-volume code STREAM of Lien and Leschziner [6]. Although the algorithm does not require orthogonal meshes, a boundary-orthogonal grid was generated, for improved accuracy, by a consecutive application of transfinite-hermitian and differential techniques.

3. RESULTS and CONCLUSIONS

The modified k-ω model and the Lien-Leschziner (LL) k-ε model have been applied to a non-equilibrium boundary layer developing over a circular centre-body in an annular passage, Fig. 1(a), which is being investigated experimentally at the University of Berlin [7]. The k-ω variant performs consistently better, has slightly better stability properties and is relatively insensitive to the grid distribution inside the viscous sublayer. The model has also been validated for simple channel flow and a free jet.

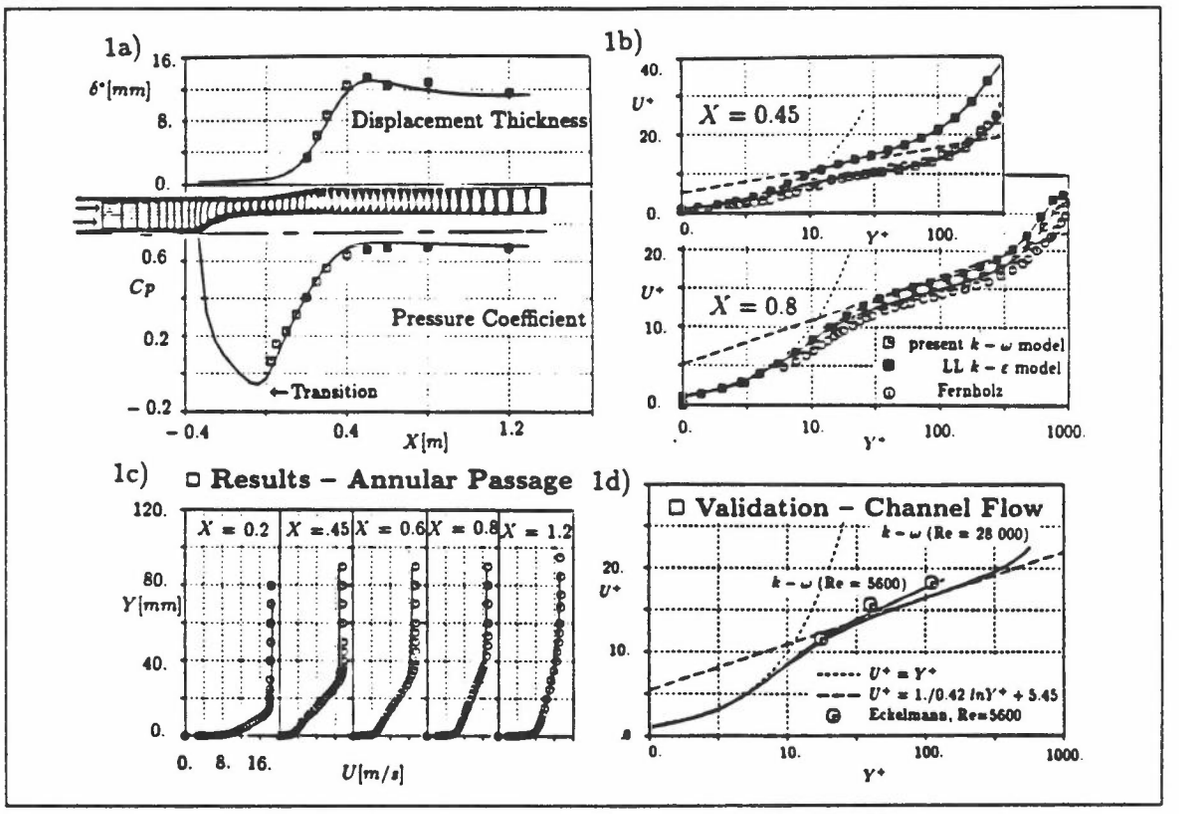

Fig. 1: Application of LL k-ε and present k-ω models to boundary layer developing on circular ducted centre-body and channel flow - (a) flow geometry; (b),(c) velocity profiles; (d) validation for channel flow

REFERENCES

1. Wilcox, D.C., (1988), AIAA Journal, Vol.26, NO. 11, p. 129.
2. Wilcox, D.C., (1994), AIAA Journal, Vol.32, NO. 2, p. 248.
3. Lien, F.S. and Leschziner, M.A., (1993), Engineering Turbulence Modelling and Measurements 2, Elsevier, p. 217.
4. Wolfshtein, M. (1968), Int. J. Heat Mass Transfer, 12, p. 301.
5. Nagano,Y. and Shimada, M., (1993), Paper 23-2, 9th Symp. on Turbulent Shear Flows.
6. Lien, F.S. and Leschziner, M.A. (1994), in Turbulent Shear Flows 8, Springer, p. 205.
7. Fernholz, H.H. and Kalter, M. (1994), Private communication.

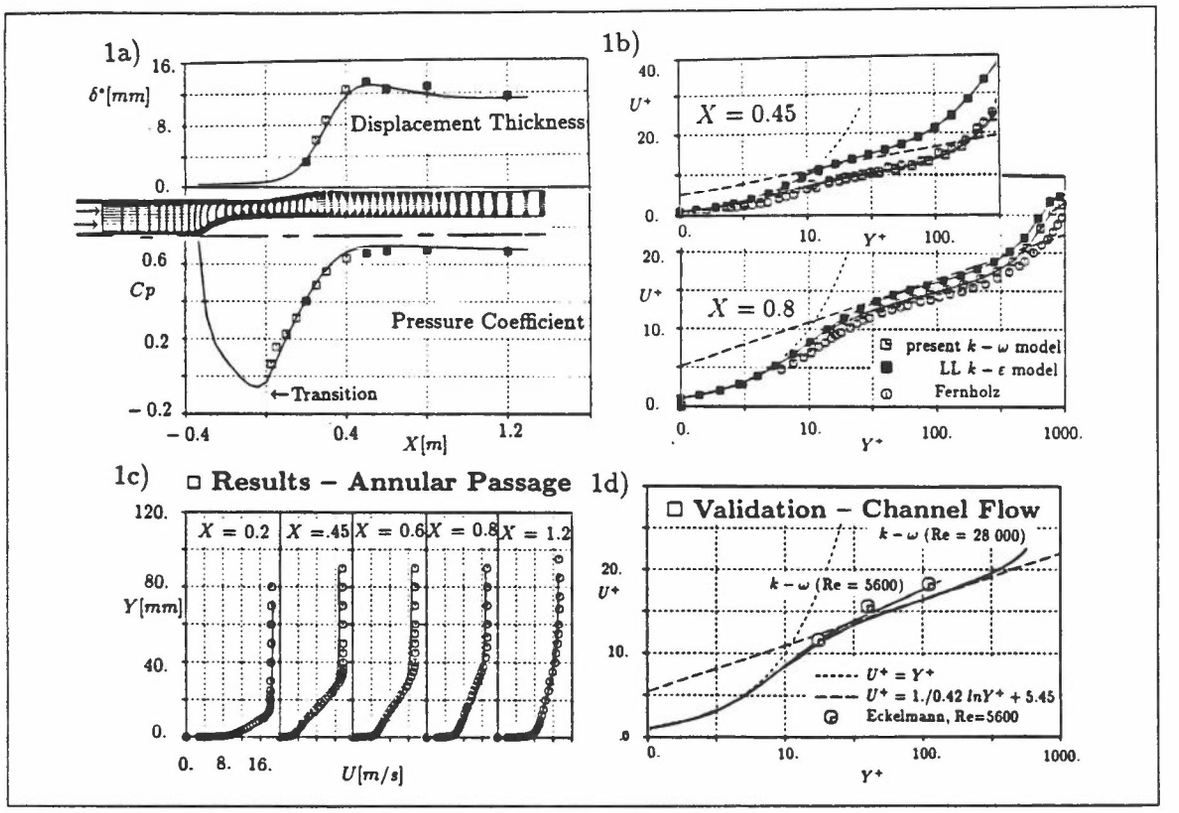
1a)
16.
$\delta^*[mm]$
8.
0.
Displacement Thickness
0.6
Cp
0.2
− 0.2
Pressure Coefficient
←Transition
− 0.4
0.4
1.2
X[m]
1b)
40.
U^+
20.
0.
X = 0.45
0.
10.
Y^+
100.
20.
U^+
10.
0.
X = 0.8
present k − ω model
LL k − ε model
Fernholz
0.
10.
100.
1000.
Y^+
1c)
□ Results – Annular Passage
120.
80.
Y[mm]
40.
0.
X = 0.2
X =.45
X = 0.6
X = 0.8
X = 1.2
0. 8. 16.
U[m/s]
1d)
□ Validation – Channel Flow
k − ω (Re = 28 000)
20.
U^+
k − ω (Re = 5600)
10.
$U^+ = Y^+$
$U^+ = 1./0.42\ lnY^+ + 5.45$
Eckelmann, Re=5600
0.
10.
100.
1000.
Y^+

REYNOLDS-STRESS AND PDF TRANSPORT MODELLING FOR NON-PREMIXED TURBULENT COMBUSTION

Researcher: A.R. Soltani
Supervisor: R.S. Cant

1. INTRODUCTION

In the vast majority of practical devices for combustion, the turbulent diffusion (or non-premixed) flames are of central concern. Generally, the combustion in gas turbines and furnaces is idealized as a turbulent diffusion flame. Confident numerical predictions of such flames are desirable for design of equipment, diagnosis of malfunction problems and development of modifications for improvement of performance. As a consequence, models of turbulent reacting flows are needed that are able not only to predict the flow field, but allow equally well for an accurate prediction of temperature and the species concentrations throughout the flame. As a result, calculation methods for practical combustion have been developed to incorporate the conservation equations, numerical solution methods, turbulence models, and combustion models. This approach is the focus of the present work.

2. COMPUTATIONAL APPROACH

In this study a time and direction correlated model for fluid particle dispersion is employed to uncouple the turbulent flow field from the highly non-linear chemistry of combustion which is described by the composition joint pdf- that is, the joint pdf of a set of scalars that describes the thermochemical state of the fluid. The dispersion of fluid particles, tracked by Lagrangian method within a continuous flow field modelled by an Eulerian scheme, is effected by imposing on the fluid particle turbulent velocity perturbations of the flow field. The approach to modelling dispersion is to extract the turbulent velocity fluctuation from the predicted flow field, taking both correlation in time between successive perturbations and directional correlation in space arising from the normal and shear components of the Reynolds stresses into account. From statistical information provided by the turbulence closure, these perturbations must be extracted by a sampling method. This sampling scheme is a modelling framework for calculating the turbulent velocity fluctuations of the particles from the statistical correlations of the flow field. The remaining task is to model the chemistry of combustion to complete the statistical description of the fluid state. In this study the Direct Closure approach is adopted. This implies that, in addition to equations describing the conservation of overall mass and momentum and the equations of turbulence model, the conservation equations for the species mass fractions are solved. The solutions of these equations are Lagrangian and no further modelling is required. As a consequence, the mean rate of production of species may be obtained as a solution of a modelled joint pdf equation. A major difficulty appeared to be that pdf equation was prohibitively difficult to specify and solve, due to its large dimensionality, therefore, the Monte Carlo method has been used. In the Monte Carlo method, the reaction processes are simulated on each particle as it advances from the previous time to the current time, leading to a discrete representation from which the pdf is constructed.

The present model is applied to the dispersion of fuel and air fluid particles in a free shear layer with turbulent mixing of a fuel jet in air. The flow field calculations were first performed for solutions of governing flow equations incorporating conventional second-moment closure. Each fluid particle at the initial plane was identified by its position, mass fraction of fuel, mass fraction of oxygen, mass fraction of products, and temperature at the inlet boundary. For each fluid particle at each location in the flow field the rate of production of fuel, oxygen, and products are then calculated. To account for the effect of temperature fluctuations on the reaction rates, the standardized enthalpy equation for a

gas mixture is solved assuming constant specific heat for all species. The ideal gas equation of state is then used to evaluate the mixture density which is fed to the solution of the flow field to complete the closure.

3. RESULTS

The validity of the present sampling method may be verified by constructing a discrete joint pdf representation of the fluctuating velocities of the field obtained from 1000 fluid particles discharged into the field and tracked over 80 time steps. On the basis of the joint Gaussian distribution which governs the nature of the velocity fluctuation pdf, one would expect the sampling method, if accurate, to reproduce a joint Guassian pdf with zero mean and the specified variances. The result shown below is a 2D contour plot of the sampled joint pdf of the fluctuating velocities (u,v) with normal and shear components of the field Reynolds stresses set to (0.05,0.04,0.0). The mean and variances are well reproduced, as is the anisotropy of the turbulence, revealed by the elliptic shape of the graph. The lack of correlation between the stresses is demonstrated by the alignment between the axes of the ellipse and the axes of the co-ordinate system.

Fig. 1 A turbulent diffusion flame.

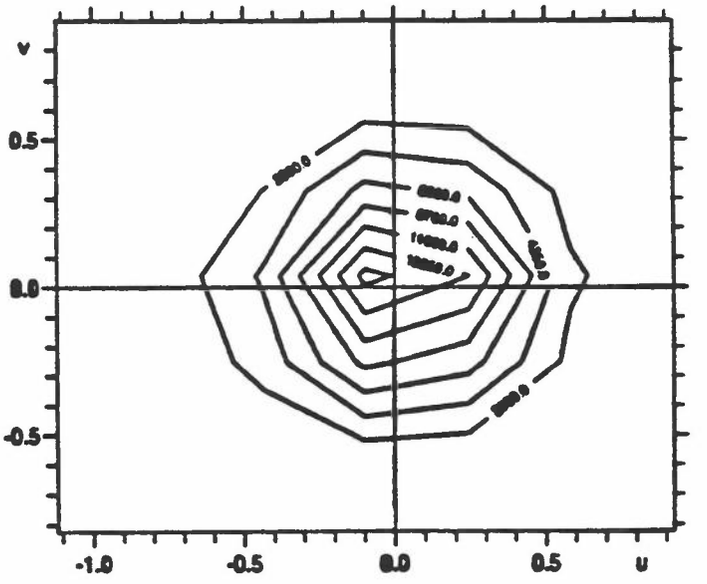

Fig. 2 2D contours of density-weighted joint pdf for fluctuating velocities (u,v) with normal and shear components of Reynolds stresses (0.05,0.04,0.0). (No. of particles: 1000, No. of samples: 80000).

REFERENCES

1. Zhou, Q and Leschziner, M.A., (1991), 8th Turbulent Shear Flow Symp., Munich.

SECOND-MOMENT MODELLING OF BUOYANT FLOWS IN CAVITIES

Researcher : N.Z. Ince
Supervisor : B.E. Launder
Sponsor : FLAIR

1. BACKGROUND

Over the last few years at UMIST extensive research has been carried out on the computation of turbulent buoyant flows in cavities. Significant improvements have been achieved using Generalised Gradient Diffusion Hypothesis (**GGDH**) in the modelling of heat fluxes. In the present re-consideration two issues relating to experimental boundary conditions have been addressed and a set of results using a closure based on transport equations of the turbulent stresses, in place of the eddy-viscosity hypothesis, have been obtained. The questions of boundary conditions addressed were the adequacy of the adiabatic conditions applied to the horizontal (and side) insulated surfaces and the three-dimensionality of the flow field.

2. APPROACH

3-D computations were made for 5:1 and 28:1 aspect ratio cavities, using the eddy-viscosity model described in ref.[1] An important refinement to the original predictions[1] were that now the heat losses from the top, bottom and side walls were now included in this calculations.

The second moment closure used is an extension of the basic Gibson-Launder model to the low-Reynolds-number regions by simple adaptations entailing the use of turbulent Reynolds number and the stress anisotropy invariants. The model coefficients were tuned by reference to the direct-numerical-simulation data for channel flow at Re=5600. The following form was employed.

$$\frac{D\varepsilon}{Dt} = c_{\varepsilon 1}\frac{(P_{kk}+G_{kk})}{2T} - c_{\varepsilon 2}\frac{\varepsilon}{T} + \frac{\partial}{\partial x_k}\left(c_\varepsilon \overline{u_k u_l}\frac{\partial \varepsilon}{\partial x_l}\right)$$

$$c_{\varepsilon 1} = 1.0 + 0.25 f_\varepsilon \qquad c_{\varepsilon 2} = \frac{1.92}{1. + 0.6A_2^{0.5}A} \qquad T = max\{(\frac{k}{\varepsilon}, 5(\frac{\nu}{\varepsilon})^{0.5}\}$$

$$\varepsilon_{ij} = \varepsilon^*_{ij} f_\varepsilon + {}^2/_3 \varepsilon \delta_{ij}(1 - f_\varepsilon)$$

$$\varepsilon^*_{ij} = \left[\varepsilon\frac{\overline{u_i u_j}}{k} + \frac{2\nu}{k}\frac{\partial\sqrt{k}}{\partial x_k}\left[\frac{\partial\sqrt{k}}{\partial x_i}\overline{u_j u_k} + \frac{\partial\sqrt{k}}{\partial x_j}\overline{u_i u_k}\right] + \frac{2\nu}{k}\frac{\partial\sqrt{k}}{\partial x_k}\frac{\partial\sqrt{k}}{\partial x_l}\overline{u_k u_l}\delta_{ij}\right] \Big/ \left[1 + \frac{5\nu}{\varepsilon k}\frac{\partial\sqrt{k}}{\partial x_k}\frac{\partial\sqrt{k}}{\partial x_l}\overline{u_k u_l}\right]$$

$$f_\varepsilon = \exp\{-R_t A^{1/2}/225\}$$

$$\phi_{ij} = -c_1\frac{\varepsilon}{k}(\overline{u_i u_j} - {}^2/_3\delta_{ij}k) - c_2(P_{ij} - {}^1/_3\delta_{ij}P_{kk}) - c_3(G_{ij} - {}^1/_3\delta_{ij}G_{kk})$$

$$c_1 = [2.5A_2^{0.5}+1]A^{0.5}min(1.0, A^{0.5}R_t/150.0) \qquad c_2 = min(0.75A^{0.5}, 0.6) \qquad c_3 = min(1.0, R_t/100.0)$$

The usual algebraic model (GGDH) was used for the calculation of heat fluxes.

3. RESULTS

Fig (1) shows the variation of the velocity and temperature profiles at the mid-height of the 5:1 aspect ratio cavity. With the inclusion of the heat losses in the calculations, the core region temperature, (which is lower than the average of the hot and cold wall temperatures) and the asymmetry in the velocity field are correctly predicted.

The results obtained with the low-Re number version of the DSM model for the tall cavity, fig(2),illustrates the ability of this model to capture the high level of anisotropy of the stress field.Good agreement with the experimental data was also obtained for 5:1 aspect ratio cavity, fig(3).

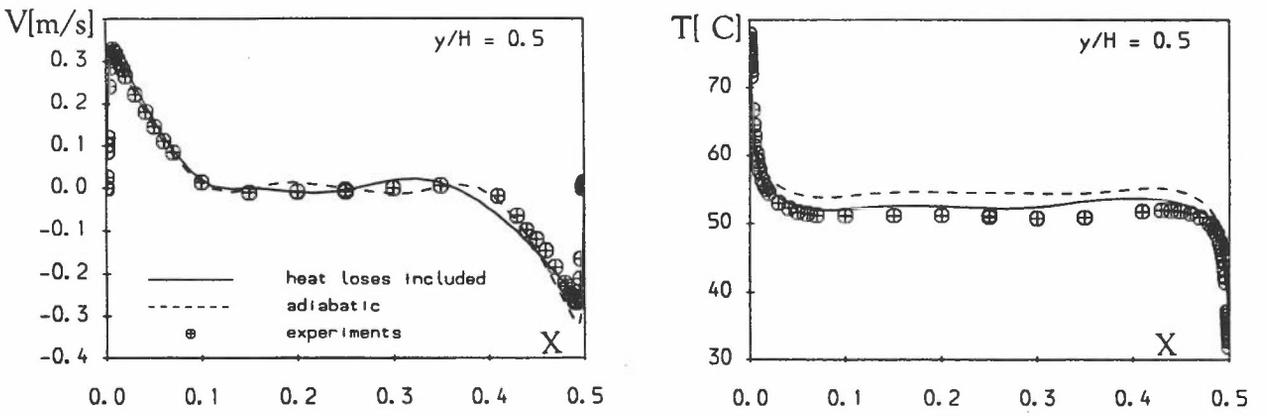

Fig[1] Velocity and temperature profiles across the mid-height of 5:1 cavity

Fig[2] Turbulent stress profiles across 30:1 cavity

- - - - - - vv
——— uu
symbols exp.

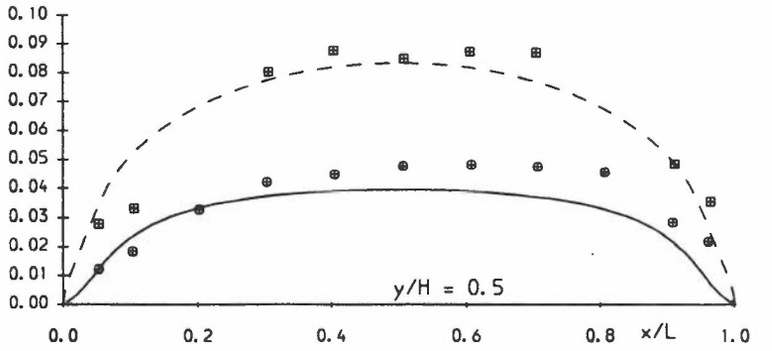

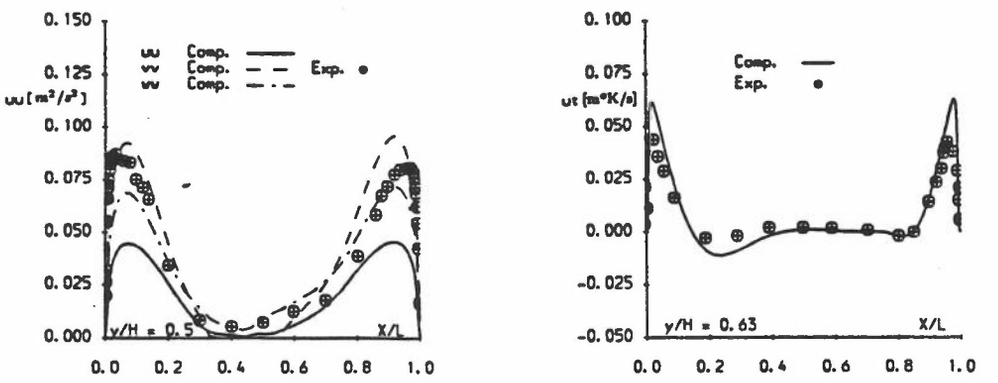

Fig[3] Turbulent stress and heat flux profiles in 5:1 cavity

REFERENCES

1. Ince,N.Z. and Launder,B.E. I.J.H.F.F, Vol 10, No 2, 110-117, 1989.

SECOND-MOMENT MODELLING OF FLOW IN FLUTED TUBES

Researcher : T.J. Craft
Supervisors : B.E. Launder, M.A. Leschziner
Sponsor : SERC

1. INTRODUCTION

The geometry of Yampolsky's spirally-fluted tubing[3] is shown in fig. 1. What is remarkable about it is that experimental studies show it to increase heat-transfer coefficients by up to 200% over smooth tube values, whilst not increasing (and sometimes decreasing) friction factors[2]. This makes it extremely useful in heat exchanger equipment. From a model validation point of view, it is a very interesting case, combining near-wall effects, swirl, and impingement; all of which affect the heat-transfer through the wall.

2. APPROACH

The flow has been computed using an extended version of the STREAM code. The solution domain consists of a segment containing one flute, and the fully-developed flow is computed by applying a periodic boundary condition between the edges of the segment, and setting gradients of dependent variables to zero in the direction aligned with the flutes. A portion of a typical 100x60 grid is shown in fig. 2. To improve convergence rates, the inner region ($r/R < 0.4$) was treated as a purely 1-dimensional (radial) region.

Over most of the domain a full RSM has been used. However, this has been interfaced to the simpler low-Re-number k-ε model used in the near-wall region. In applying wall-reflection models, it is necessary to define the unit vector normal to the wall, $\underline{n}$. This has been prescribed so as to vary from the radial vector in the core region, away from the flutes, to a vector that follows the "radial" grid-lines as the wall is approached. For heat-transfer calculations, a constant heat-flux has been applied through the wall.

3. RESULTS

Fig. 3 is a typical plot of the secondary velocity relative to the flute, showing the recirculation pattern that is set up within the flute. Profiles of mean streamwise and swirl velocity, together with normal stress components at Re=26400 are shown in fig. 4. In addition to the Basic and Cubic models, results are also shown using the Cubic model without any wall-reflection terms, but including the c_2' terms (see paper 1.5). These give further encouragement to the development of a model which does not use geometrical quantities such as $\underline{n}$. All the models give reasonable agreement with the experiments of [1], although they tend to underpredict turbulence levels within the flute valley. The anisotropy in the normal stresses enables the models to capture the non-linear swirl velocity profile in the core region.

Nusselt number profiles around the flute using the Cubic model are shown in fig. 5, and friction factors and mean Nusselt numbers are summarised in table 1. The general trend of increased heat-transfer without an associated friction factor rise is predicted (particularly at higher Prandtl numbers). However, experimental data suggests that the increase should be even greater than it is. To capture this, a better near-wall modelling would be required, probably involving a low-Re-number second-moment closure or, possibly, a non-linear EVM.

References:

1. Cheah S.C., Cheng L., Cooper D., Launder B.E (1993) "On the structure of tubulent flow in spirally fluted tubes" Proc. 5th Int. Symp on Refined Flow Modelling and Turbulence Measurements, Paris.
2. Perera K.K.C.K. (1993) "Local heat-transfer measurements in spirally fluted tubes" PhD Thesis,

Univ. of California, Davis.
3. Yampolsky J.S. (1979) "Spiral fluted tubing" Report GA-A15524.

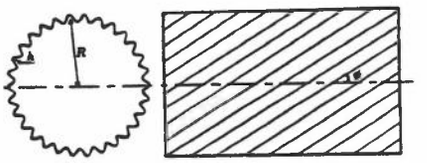

Figure 1. Geometry of spirally fluted tube.

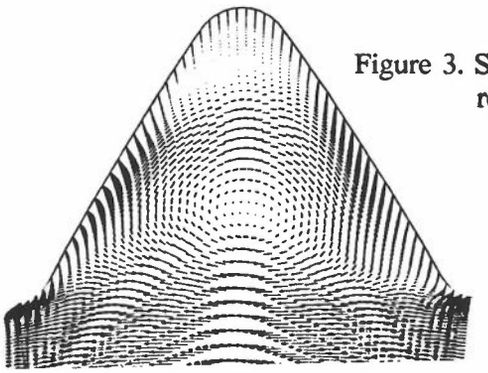

Figure 3. Secondary velocity relative to flute.

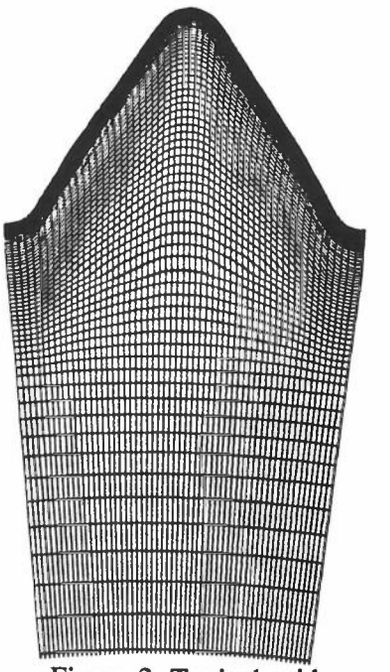

Figure 2. Typical grid.

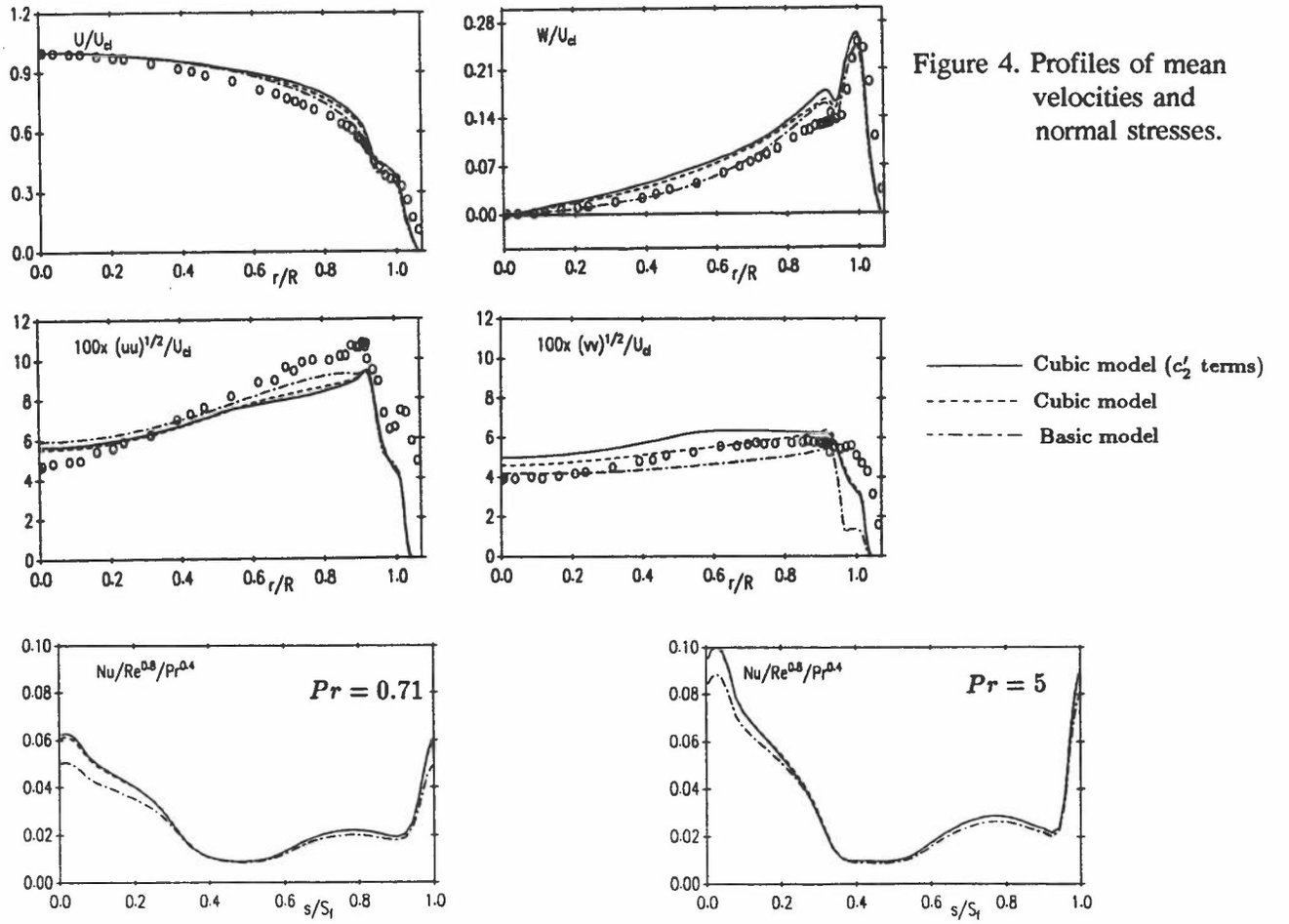

Figure 4. Profiles of mean velocities and normal stresses.

Figure 5. Nusselt number profiles at Pr=0.71 and 5.

	f	$Nu\ (Pr = 0.71)$	$Nu\ (Pr = 5)$
Smooth tube	0.025	66.1	144.3
Basic model	0.0239	70.5	214.4
Cubic model	0.0267	80.2	233.8
Cubic model (c_2' terms)	0.0254	80.8	232.7

Table 1. Friction factors and Nusselt numbers.

TURBULENCE MODELLING FOR HIGHLY-LOADED CASCADE BLADE

Researcher: W.L. Chen
Supervisors: F.S. Lien & M.A. Leschziner
Sponsor: Rolls-Royce plc.

1. INTRODUCTION

Although the flow through a turbine-blade passage is driven, principally, by inviscid process, some important operational characteristics and parameters are strongly influenced by turbulence transport and its manifestations. Even in design conditions, the boundary layer developing on the blade can grow rapidly as a consequence of adverse pressure gradients, and this will have a considerable influence on the pressure field in the passage. In the presence of shock waves and in off-design or high-load conditions, the boundary layer may separate, in which case pressure recovery may collapse. The response of the boundary layer to geometry- or shock-induced pressure gradient depends sensitively on the position of transition which may be provoked by laminar leading-edge separation or the diffusion of free-stream turbulence into the boundary layer triggering turbulence (by-pass transition). The key message is, therefore, that a realistic representation of turbulence effects is an important contributor to the predictive capabilities of any numerical procedure for turbomachinery flows. The quality of this representation in the computation of compressor-cascade passages is the focus of the this summary.

The present study is part of a wider research programme involving flow in turbine-blade passages, the modelling of transition and the computation of stagnation flows of the type encountered around blade leading edges. Various aspects of this broad study are documented in other summaries contained in this book. A broader exposition of the present research is given in ref. [1].

2. COMPUTATIONAL APPROACH

The ultimate objective of the study is to investigate and to identify the predictive capabilities of low-Re non-linear eddy-viscosity and full second-moment closure proposals for turbomachine flows arising in operation close to or beyond the upper end of the design range. At the present early stage of the programme, various low-Re linear eddy-viscosity models have been investigated. These include a new two-equation low-Re-number variant recently formulated by Lien & Leschziner [2]. The rationale of this model is rooted in the experimental observation that the turbulence length scale associated with the energetic eddies is fairly insensitive to adverse pressure gradient, whereas traditional low-Re k-ε models predict a steep rise in length scale in boundary layers subjected to such gradient. The model has thus been formulated so as to adhere, close to the wall, to length-scale constraints implied either by Wolfshtein's or Norris and Reynolds' one-equation models.

Calculations reported below have been performed with the general non-orthogonal fully co-located finite-volume scheme STREAM of Lien & Leschziner [3]. In this, convection is represented by bounded (monotonic) variants of second-order or third-order schemes. The solution is iterated to convergence using a pressure-correction approach which is applicable to both incompressible and compressible conditions, the latter including shocks. Versions of the code apply to 2D and 3D conditions and embody a variety of turbulence closures including Reynolds-stress-transport and RNG models. The algorithm used herein is a single-block variant using a single H-type mesh to cover the solution domain. A multi-block version allowing much greater flexibility in terms of controlling grid resolution and skewness, particularly at the rounded leading and trailing edges, is summarised in Section 2 of this book.

3. APPLICATION

The principal geometry considered is shown in Fig. 1 in terms of the 154x82 passage mesh and the mesh portions around the leading and trailing edges of the blade. Experimental data for flows

at 40°, 43.4° and 46° incidence at inlet have been obtained by Elazar and Shreeve [4]. As shown in Fig. 2, the computed C_p distributions are in good agreement with the experimental data at the lowest inlet angle (β=40°). However, at high incidence, significant discrepancies arise between computed and measured C_p distributions, Fig. 3, as well as velocity profiles, Fig. 4. This is due to a failure of all models to capture the leading-edge separation bubble, which is of considerable influence to the suction-side flow at high inlet angle, and a failure to simulate transition correctly on the pressure side. The real flow around the leading edge is laminar and a thin separation bubble ensues, which then provokes transition on reattachment. No part of this process is resolved by any of the present models because of the large generation of turbulence energy returned ahead of the leading edge in response to the high irrotational strain associated with stagnation. Hence, although the Lien-Leschziner model appears to perform considerably better than the other variants, this does not reflect a fundamental superiority in the sense identified above. Multi-block computations with finer leading-edge grids have confirmed that numerical issues do not contribute to this deficiency. To achieve improved performance, it is imperative to introduce a mechanism which drastically reduces the generation of turbulence energy by irrotational strain. One route is the model by Kato & Launder [5] which replaces the strain by vorticity in the turbulence production term. A fundamentally sounder route is second-moment closure which tends to respond more realistically to irrotational straining. Both routes are being persued.

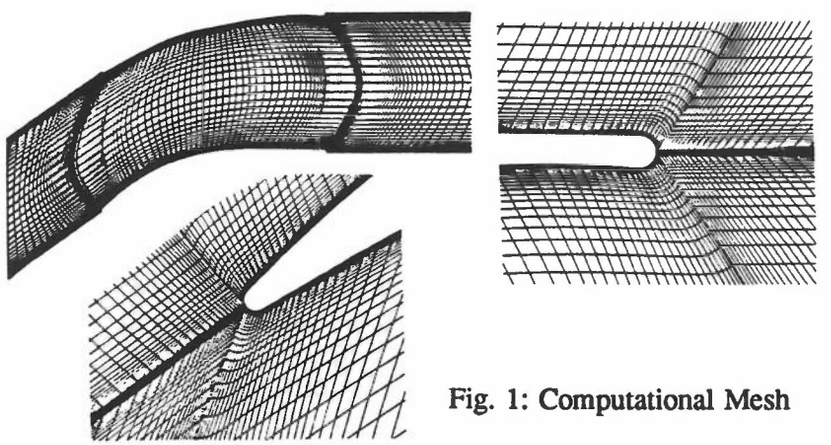

Fig. 1: Computational Mesh

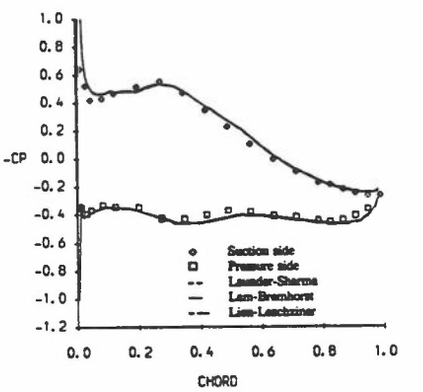

Fig. 2: Cp Distributions (β=40°)

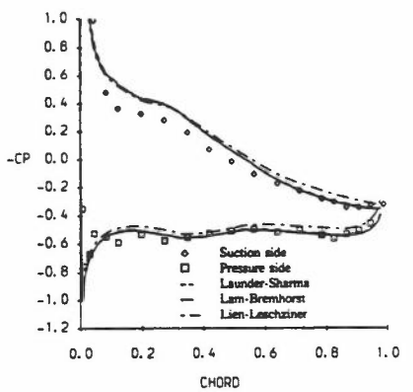

Fig. 3: Cp Distributions (β=46°)

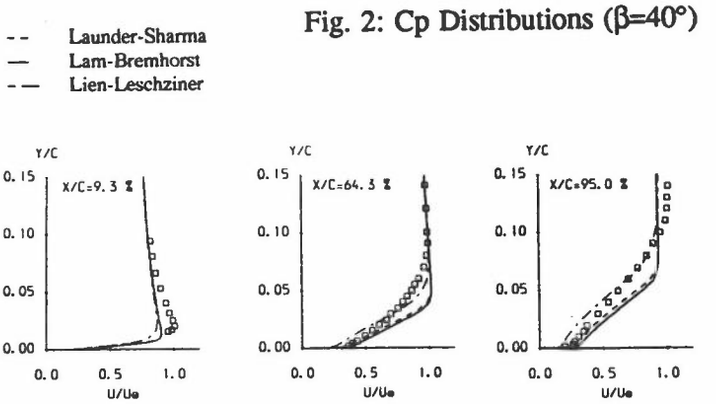

Fig. 4: Boundary-Layer Velocity Profiles ((β=46°)

REFERENCES

1. Chen, W.L. (1994), Ph.D. transfer report, UMIST, Mech. Engg. Department.
2. Lien, F.S. and Leschziner, M.A. (1993), Engineering Turbulence Modelling and Experiments 2 (W. Rodi & F. Martelli, ed.), p. 217.
3. Lien, F.S. and Leschziner, M.A. (1994), Comp. Meth. Appl. Mech. Eng., 114, p. 123.
4. Elazar, Y., and Shreeve, R.P., (1989), ASME paper 89-GT-131
5. Kato, M, and Launder, B.E.(1993), 9th Symp. on Turbulent Shear Flows, Kyoto.

DIFFERENTIAL STRESS TRANSPORT MODELLING OF SWIRLING I.C. ENGINE FLOWS

Researcher: T. Bo
Supervisor: A. P. Watkins
Sponsor: SERC

1. BACKGROUND AND OBJECTIVES

The two time scales k-ε-τ and differential stress(DSM) models have been used in IC engine in-cylinder flow simulations[1,2]. The former model takes the compression effects on turbulence into account through the introduction of the turbulence time scale τ[3]. The latter model offered greater benefits for accurate calculation of such flows. However, the above researches are basically on 2D non-swirl engine flows. The objectives of this work are to extend the application of DSM to 2D swirling engine flows, incorporate the τ transport equation into the DSM model and explore its capabilities in engine flows.

2. APPROACH

A 2D transient code was used which allows for piston and valve motion. Computations were carried out based on a four-stroke model engine whose valve is centrally located and whose piston can be specified to incorporate a bowl(Figure 1). All transport equations, discretised in a polar cylindrical translating grid, are solved using the finite volume method. First order fully implicit and second order CRANK-NICOLSON temporal schemes, and HYBRID, QUICK and MUSCL spatial schemes have been adopted for the discretization of convection. A 45×45 grid arrangement(Figure 2) and time steps of 1/2°, 1/4°, 1/8° and 1/16° crank angle intervals were used. At each time step the SIMPLE algorithm was employed. DSM and DSM-τ turbulence models were used. Before the DSM-τ was adopted for the in-cylinder flows, the transport equations for the turbulence time scale τ, and for ε, were tuned in parabolic free shear flows and elliptic impinging flows. Computations have been performed with three ressure-strain models: (1) Basic model without wall reflection terms; (2) Basic model with the Craft/Launder wall reflection term[4]; and (3) Cubic Φij2 without wall reflection terms. Wall functions were used in the wall boundary treatment.

3. RESULTS

High order spatial schemes were found to be necessary for non-swirling engine in-cylinder flow simulations[2]. It was shown that a high order temporal scheme is also important in the numerical simulation of swirling in-cylinder flow employing second moment closure: first order fully implicit scheme returns an over-estimated swirl level. Compared with measurements, the main error appears in the intake stroke while in subsequent strokes predictions are general satisfactory. The Basic DSM model with or without wall reflection terms returns a lower turbulence level than measurements in the intake stroke(Figure 3). Inclusion of the τ equation into the DSM may improve its performance in free shear flows and impinging flows. In in-cylinder flows, the refinement of two-time scales modelling brings a small improvement (Figure 3). In the intake stroke, Figure 4, different pressure-strain models give different turbulence levels in the valve-flow impinging area whose position shown in Figure 5. The Basic model returns higher turbulence in the stagnating region while the Craft/Launder wall reflection term and the Cubic Φij2 brought lower turbulence. The turbulence field in this region strongly affects the developments of velocity and turbulence profiles close to the upper cylinder wall. This in turn affects the flow in the core region after the fluid impinging on the piston. The predicted distribution of swirl velocity component is shown in Figure 6.

4. REFERENCES

1. M. Z. Gul, PhD Thesis, UMIST, 1994.
2. C. J. Lea, PhD Thesis, UMIST, 1994.
3. C. T. Wu, J. H. Ferziger and D. R. Chapman, Technical Report TF-21, Thermoscience Div., Dept. of Mech. Eng., Stanford Univ., Stanford, California, 1985.
4. T. J. Craft and B. E. Launder, AIAA J., Vol. 30, No 12: Technical Notes, Dec. 1992.

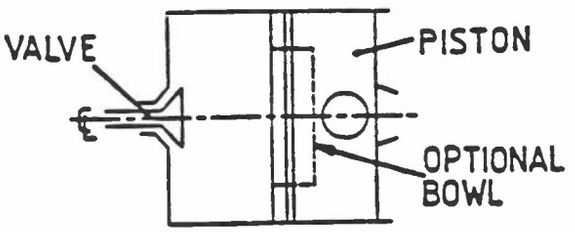

Figure 1. Diagram of Piston-Cylinder Assembly

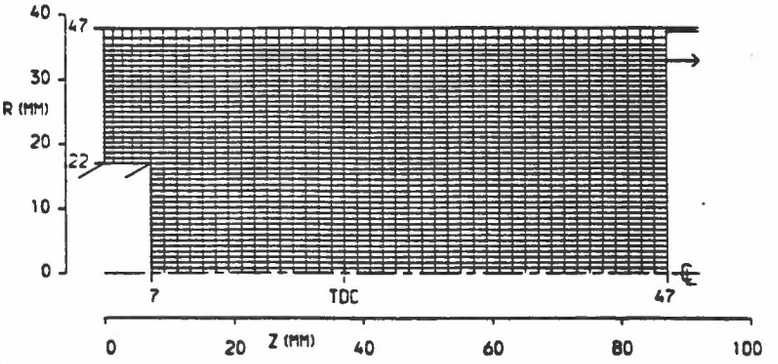

Figure 2. Grid Arrangement (45×45)

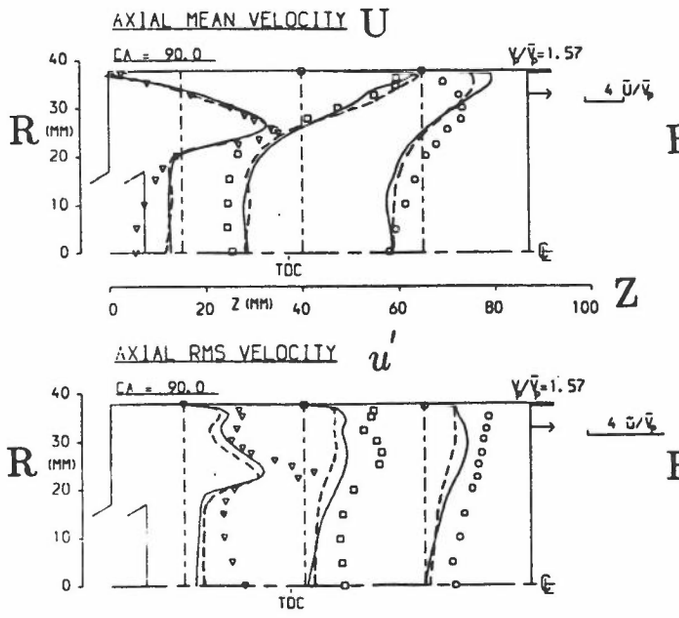

Figure 3. DSM and DSM-τ model predictions at 90° ATDC, intake stroke

DSM — — — DSM-τ —— experiment ▽ □ ○

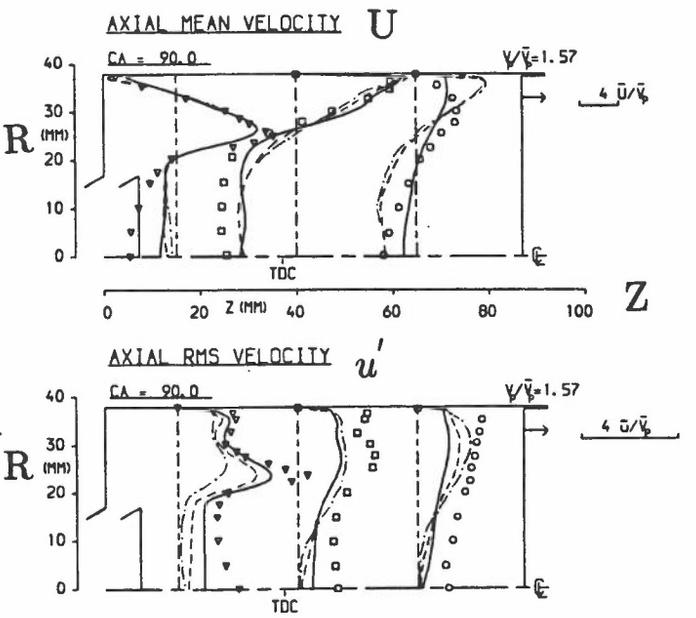

Figure 4. Predictions with different pressure-strain models at 90° ATDC, intake stroke

Basic no wall ref. —— Basic+CL wall ref.— — —

Cubic no wall ref. — · — experiment ▽ □ ○

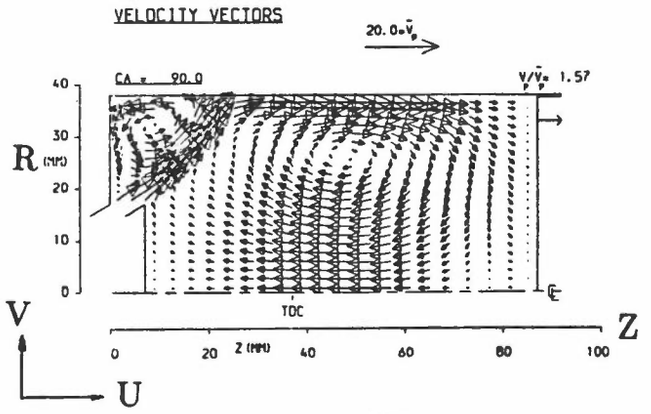

Figure 5. Velocity vectors of $U - V$ components

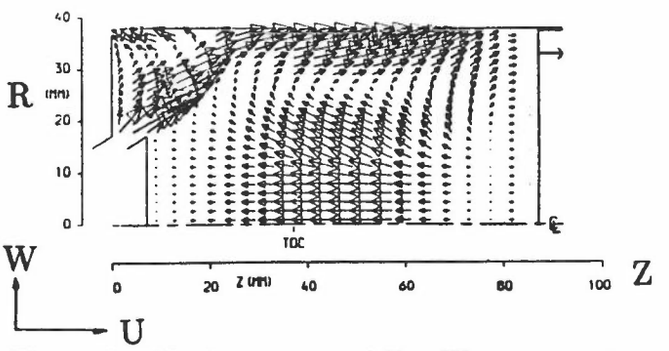

Figure 6. Velocity vectors of $U - W$ components

« Session 4 »

Aerodynamic Flows

MODELLING FLOWS AROUND HIGH-LIFT SUBSONIC AEROFOIL

Researchers: F.S. Lien and M.A. Leschziner
Sponsor: BAe (RAL and SRC), DRA, CEC

1. INTRODUCTION

Separated flow region, even if small, can have profound consequences to the overall behaviour of the flow containing these regions, and thus to the performance characteristics of the associated fluid-engineering device. One typical example is the loss of lift of an aerofoil at high incidence due to suction-side separation. Modelling separation at a such a gently curved surface is a particularly challenging task. The key issue is to represent the curved and decelerating boundary layer approaching the separation point faithfully, and it may be expected that effects of curvature-induced attenuation, anisotropy, streamwise momentum diffusion and turbulence enhancement due to normal-stress / normal-strain production all need to be accounted for properly.

In order to capture these processes in separated flow around a high-lift aerofoil, we resort to second moment closure and a particular form of non-linear eddy-viscosity model. As will be shown, the two models in their original form fail to capture the separation process at the correct incidence angle because of a slight overestimation of near-wall anisotropy and shear stress. To overcome this weakness, tentative modifications have been introduced to both models, which lead to a slight reduction in shear stress and hence to separation at the correct position. To demonstrate that the modifications do not adversely affect the predictions of attached conditions, calculation have also been performed at low incidence.

2. TURBULENCE MODELS

Three turbulence models feature in computations presented below, the linear low-Re k-ε model of Lien & Leschziner [1], the non-linear high-Re k-ε model of Shih et al [2] and the high-Re second moment model of Gibson & Launder [3], the last two combined with the one-equation k-l model of Wolfshtein [4]. The novel feature of Shih et al's model, comparing to an earlier non-linear form of Speziale [5], is that C_μ and coefficients in the stress-strain constitutive relation are sensitized to strain and vorticity invariants. Moreover, the former also adheres to 'realizability' constraints.

It is informative to express the Reynolds-stress components predicted by Shih et al's model for local equilibrium condition and contrast this to the stresses arising from the second-moment closure. Thus,

For Shih et al's model:

$$\frac{\overline{u'^2}}{k} = \frac{2}{3} + \frac{9.33}{C_\mu(1000 + 1./C_\mu^{1.5})} \qquad \frac{\overline{v'^2}}{k} = \frac{2}{3} - \frac{5.67}{C_\mu(1000 + 1./C_\mu^{1.5})} \qquad \frac{-\overline{u'v'}}{k} = \sqrt{C_\mu} \tag{1}$$

where C_μ is given, implicitly, by $C_\mu = \frac{2/3}{A_1 + 1.9/\sqrt{C_\mu}}$. If A_1=1.25, as suggested in the original model, then

$$\frac{\overline{u'^2}}{k} = 0.770, \quad \frac{\overline{v'^2}}{k} = 0.604, \quad \frac{-\overline{u'v'}}{k} = 0.294. \tag{2}$$

For Gibson & Launder's model (with Craft and Launder's model for ϕ^w_{ij2} [6]):

$$\begin{aligned} \frac{\overline{u'^2}}{k} &= \frac{4C_1 + 2C_1^2 - 4C_1C_2 + 3C_1C_2' + 6C_1' + 6C_1C_1' - 6C_2C_1' - 4C_1'C_4'}{3C_1(C_1 + 2C_1')} = 1.071 \\ \frac{\overline{v'^2}}{k} &= \frac{2(-1 + C_1 + C_2 - 3C_2' - 2C_4')}{3(C_1 + 2C_1')} = 0.229 \\ \frac{-\overline{u'v'}}{k} &= \sqrt{\frac{2(1 - C_2 - 1.5C_4')(-1 + C_1 + C_2 - 3C_2' - 2C_4')}{3(C_1 + 1.5C_1')(C_1 + 2C_1')} + \frac{C_4'}{C_1 + 1.5C_1'}} = 0.248 \end{aligned} \tag{3}$$

Two modifications are tested here to reduced the shear stress. In the case of Shih et al's model, the coefficient A_1 in C_μ is increased to 4.0, in which case,

$$\frac{\overline{u'^2}}{k} = 0.824, \quad \frac{\overline{v'^2}}{k} = 0.571, \quad \frac{-\overline{u'v'}}{k} = 0.235. \tag{4}$$

while for Gibson & Launder's model, the 'rapid' part of the pressure-strain model is truncated, in which case,

$$\frac{\overline{u'^2}}{k} = 1.055, \quad \frac{\overline{v'^2}}{k} = 0.333, \quad \frac{-\overline{u'v'}}{k} = 0.228. \tag{5}$$

3. APPLICATION

The above models have been applied to the ONERA-A high-lift aerofoil of Piccin & Cassoudesalle [7], the geometry of which is shown in the inset of Fig. 1. Lift polars are given in Fig. 1, and Fig. 2 shows velocity profiles on the suction side at 96% of chord. Clearly, the modifications, while not argued to be fundamentally profound, return a much better representation than the original forms. The low-Re k-ε model is seen to fail badly (like other forms) due to a serious over-estimation of turbulence transport.

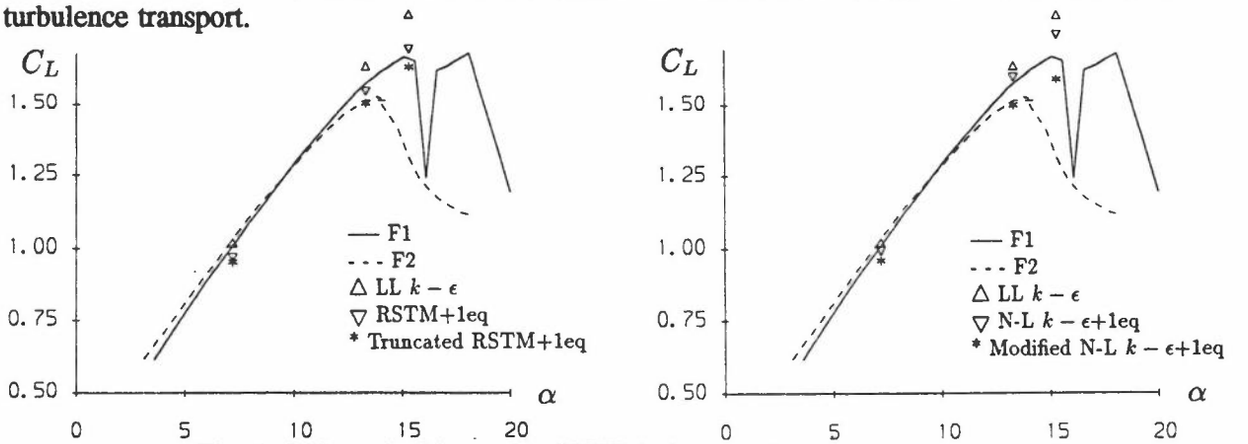

Fig. 1: Lift vs. incidence for ONERA-A aerofoil

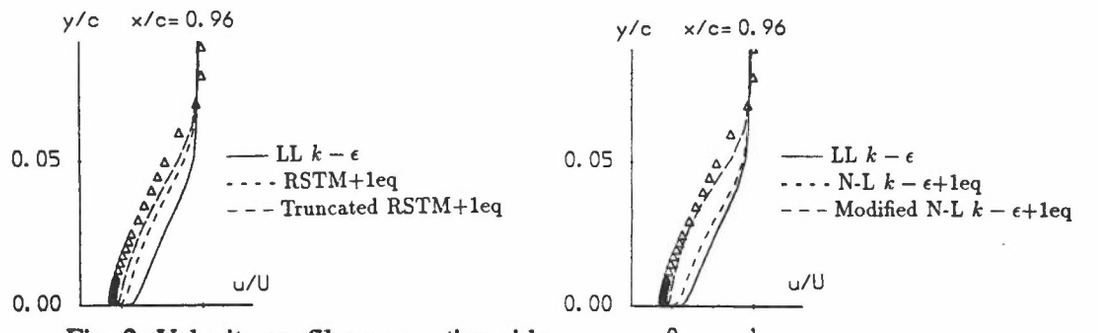

Fig. 2: Velocity profiles on suction side

REFERENCES

1. Lien, F.S. and Leschziner, M.A., (1993), Engineering Turbulence Modelling and Experiments 2 (W. Rod & F. Martelli, eds.), p. 217.
2. Shih, T.H., Zhu, J. and Lumley, J.L., (1993), NASA TM 105993.
3. Gibson, M.M. and Launder, B.E., (1978), J. Fluid Mech., 86, p. 491.
4. Wolfshtein, M.W., (1969), Int. J. Heat Mass Transfer, 12, p. 301.
5. Speziale, C.G., (1987), J Fluid Mech., 178, p. 459.
6. Craft, T.J. and Launder, B.E., (1992), AIAA J., 30, p. 2970.
7. Piccin, O. and Cassoudesalle, D., (1987), Rep. P.V. 73/1685 AYG, ONERA.

REYNOLDS-STRESS MODELLING USING AN UNSTRUCTURED TRANSONIC NAVIER-STOKES SOLVER

Researcher : Mr F. Cantariti
Supervisor : Dr L.J. Johnston
Sponsor : EEC

1. BACKGROUND AND OBJECTIVES

In Computational Fluid Dynamics, the accurate prediction of the viscous flow development around two-dimensional single- and multi-element aerofoils at transonic conditions remains an important goal. Indeed, such flows are dominated by viscous effects with thick turbulent boundary layers, shock-wave/boundary layer and wake/boundary layer interactions. The flow development is further complicated by the presence of large pressure gradients, flow curvature and separated flow regions. Therefore, it is generally acknowledged that such flowfields are only likely to be accurately predicted by solving the Reynolds-averaged Navier-Stokes equations, in conjunction with a turbulence model to close the set of governing flow equations. Eddy viscosity turbulence models have been successfully used in the past for fully-attached flows, but are deficient for flows close to and beyond separation. With the above as background, and following the work of Stolcis[3], the present work is aimed at the development of a computational method solving the Reynolds-averaged Navier-Stokes equations, together with a Differential Reynolds Stress turbulence Model (DRSM). It is expected that solving modelled transport equations for the Reynolds stress components themselves will improve the modelling of the complex flow physics and so improve the accuracy of the predictions, especially around maximum lift conditions.

2. COMPUTATIONAL APPROACH

The Reynolds-averaged Navier-Stokes equations applicable to compressible, two-dimensional turbulent flows are solved using a cell-centred, finite volume spatial discretisation. A multi-stage, explicit, time-marching scheme is used to advance the unsteady flow equations in time to a steady-state solution. Additional numerical dissipative terms are added explicitly to the discretised equations in order to obtain a smooth solution. Also, the geometric complexity of multi-element configurations is addressed by adopting unstructured computational grids. The DRSM used here follows the work of Launder *et al.*[1] and two turbulence model closures are available in the molecular viscosity-dominated near-wall region: the so-called wall function approach and a low-Reynolds number formulation[2] using an algebraic length scale for the ε-equation. The discretisation of the turbulence transport equations follows the same approach as for the mean-flow equations, except for the convective transport terms where a first-order upwind scheme is used for numerical stability reasons.

3. RESULTS

Results are presented for two single-element aerofoils, comparing calculations using the present DRSM and a two-equation k-ε turbulence model (using either wall functions or a one-equation near-wall formulation) with experiments. Firstly, the predicted surface pressure distributions and upper surface velocity profiles for the RAE 2822 aerofoil - Case 9 - are shown in figure 1. There is good agreement between the computations using the DRSM with both near-wall treatment and with experiment, which was expected for such a fully-attached flow. The method was then applied to the MBB A3 aerofoil. Figure 2 shows the surface pressure distributions for Run 113, indicating improved predictions from the DRSM compared to the k-ε model. Also, the use of wall function boundary conditions seems to over-constrain both turbulence models to fully-attached equilibrium flow conditions (figure 2a) whereas the low-Reynolds number closures further improve the calculations, (figure 2b). In particular, use of the low-Reynolds number DRSM results in a substantially-improved

prediction of shock-wave position and of pressure levels in the extensive downstream shock-separated flow region. Future work will include applications to multi-element aerofoil configurations and further improvements to the low-Reynolds number DRSM.

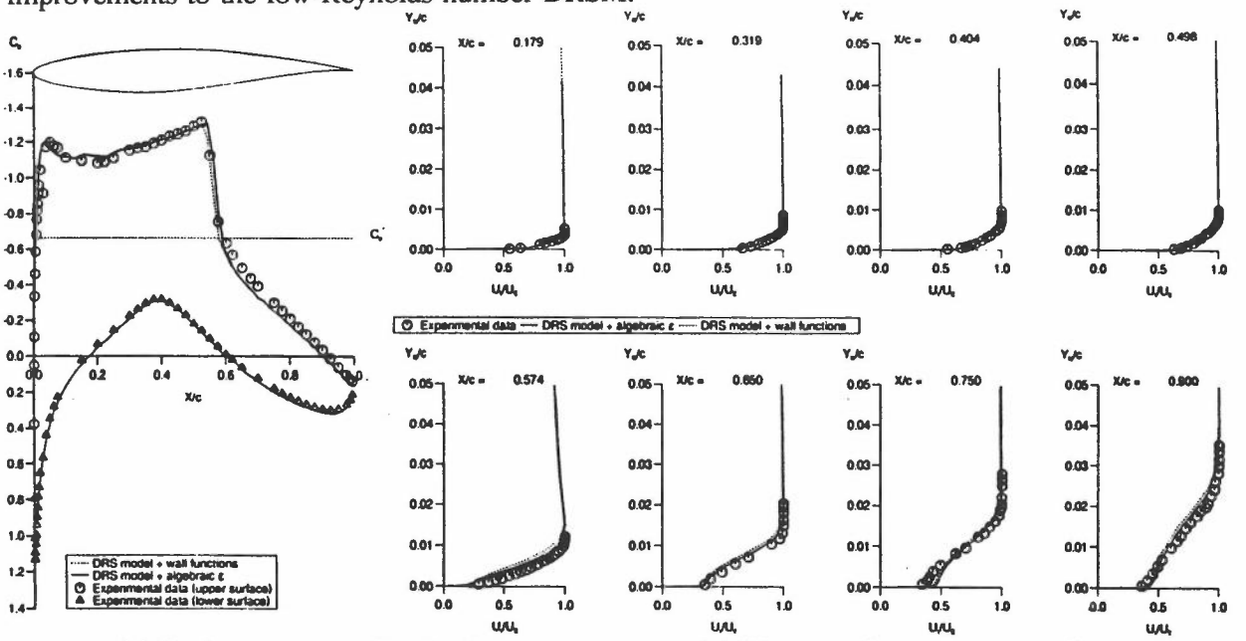

(a) Surface pressure distributions (b) Upper surface velocity profiles

Fig. 1 RAE2822 aerofoil at M=0.73, α=2.79°, Re=6.5x10^6

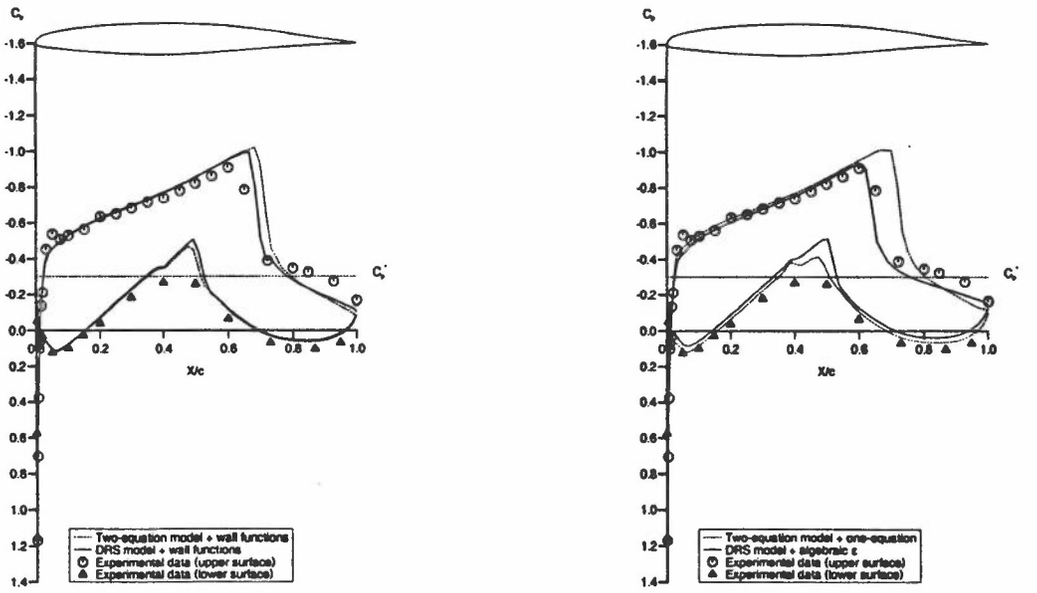

(a) Wall functions closure (b) Low-Reynolds number closure

Fig. 2 MBB A3 aerofoil at M=0.85, α=1.78°, Re=6.08x10^6

REFERENCES

(1)LAUNDER, B.E., REECE, G.J. and RODI,W., 'Progress in the Development of a Reynolds-Stress Turbulence Closure', Journal of Fluid Mechanics, vol 68, pp 537-566, part 3, 1975.

(2)LAUNDER, B.E. and SHIMA, N., 'Second Moment Closure for the Near-Wall Sublayer: Development and Application', AIAA Journal, vol 27, No 10, pp 1319-1325, 1989.

(3)STOLCIS, L., 'Computation of the Turbulent Flow Development Around Single- and Multi-Element Aerofoils', PhD Thesis, University of Manchester, Institute of Science and Technology (UMIST), 1992.

AN EMBEDDED CARTESIAN GRID APPROACH TO THE COMPUTATION OF AERODYNAMIC FLOWS

Researcher : Richard J. Smith
Supervisor : Leslie J. Johnston
Sponsors : EPSRC/British Aerospace Defence

1 Background and Objectives

Computational Fluid Dynamics (CFD) analysis is finding increasingly widespread use within the aerospace industry. However, the application of CFD to complex configurations is still a long way from being a routine process. The main limiting factor is the unacceptable turn-around time of most current methods. More specifically the problem centres on the elapsed time taken to generate a computational grid of adequate quality, starting with the initial CAD geometry. This problem becomes more acute with the increase in complexity of the configuration. The accepted methodology of most existing grid generation techniques is to first explicitly generate a surface grid and then generate the field grid. It is in the area of surface grid generation where excessive user interaction is generally required.

The aim of the present method is to provide the capability to quickly analyse complex geometries within the engineering design environment, by identifying and providing an alternative to existing grid generation techniques.

2 Approach

The basic requirement of any grid generation method is to provide a discretised flow domain upon which to implement the physical flow model and associated boundary conditions. The final accuracy of the flow solution is greatly influenced by the surface and the field definition of the flow domain provided by the grid generation method. The resolution of the surface within the grid generation method is essential for accurate loads predictions and to this aim there are two important aspects to consider. Firstly an adequate number of points is required to implement accurately the surface boundary conditions. Secondly clustering points on the surface, especially in regions of high curvature and shock waves, is required to resolve the large flow gradients that exist there. The field grid resolution is a compromise between having a globally fine grid to resolve all flow field gradients sufficiently accurately and a coarse grid to allow an acceptable computation time.

The majority of existing grid generation techniques, be they unstructured or block-structured, have two distinct stages. Firstly a surface grid is generated and then the field grid is generated. By the use of a Cartesian cell embedding technique in the present work, a method has been developed that reduces grid generation to a single automatic stage. The technique starts with an initial single outer boundary cell. This cell and subsequent cells are then subdivided if they contain or intersect the geometry. Following this procedure, cells are clustered around the geometry surface, thus satisfying surface definition requirements. To ensure adequate field definition, a constraint is imposed that prevents any two neighbouring cells differing by more than one level of subdivision. This also has the benefit of preventing abrupt changes in cell area which is deemed to be desirable in the interests of flow solution accuracy. Upon finishing the subdivision process, grid points that lie within the geometry are moved onto the geometry surface as shown in Figure 1. The Cartesian grid is then

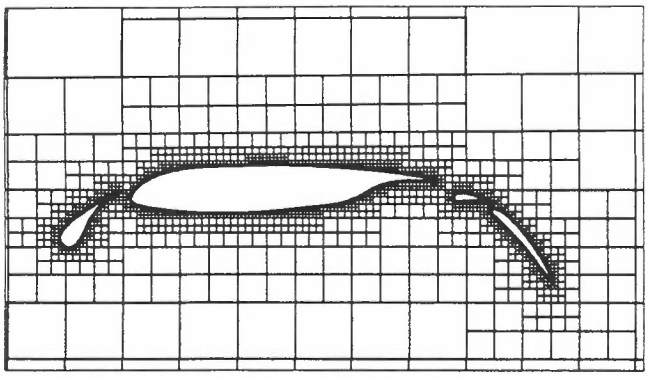

Figure 1 Cartesian Grid

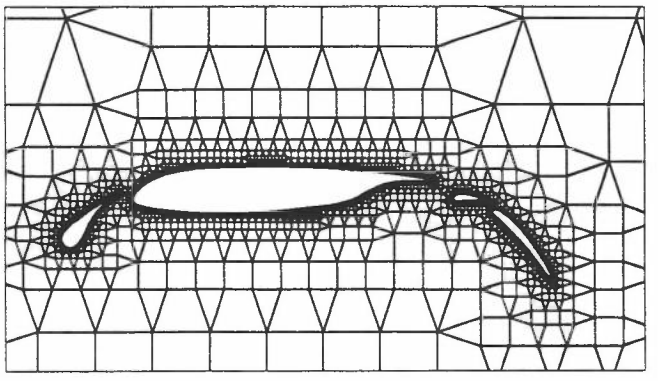

Figure 2 Dual Grid

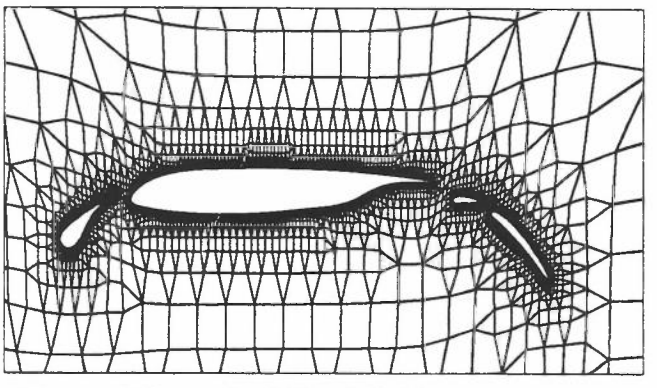

Figure 3 Smoothed Dual Grid

reconnected to form the dual grid shown in Figure 2, this then avoids special treatment within the flow solver of the hanging nodes present in the Cartesian grid. Finally the grid is smoothed to improve the accuracy of the flow solution, as shown in Figure 3.

3 Results

Initial results from a 2D compressible, inviscid feasibility study are presented in ref.[1]. The method employs a typical cell centred Jameson type finite volume approximation[2] to the governing Euler flow equations. To demonstrate the ability of the method to produce a flow solution on the grids shown earlier a test case for the 4 element, high lift aerofoil configuration, of Mach number 0.2 and angle of incidence 16° was chosen and the resulting pressure contours are shown in Figure 4. Based upon the 2D success, further work will be focused on a 3D feasibility study.

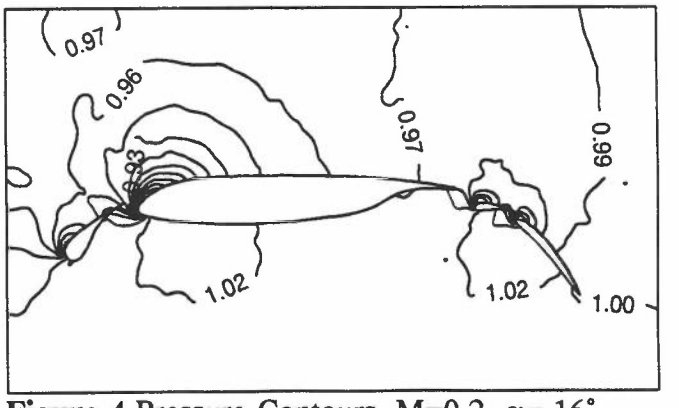

Figure 4 Pressure Contours, M=0.2, α= 16°

References

1 SMITH, R.J. & JOHNSTON, L.J. - A Novel Approach to Engineering Computations for Complex Aerodynamic Flows, **Proc. 4th International Conference on Numerical Grid Generation in Computational Fluid Dynamics and Related Fields**, Ed. Weatherill, N.P., Eiseman, P.R., Häuser & Thompson, J.F., pp271-285, April 1994.

2 JAMESON, A., BAKER, T.J. & WEATHERILL, N.P. - Calculation of Inviscid Transonic Flow Over a Complete Aircraft, **AIAA Paper 86-0103**, Jan 1986.

COMPUTATION OF AERO-ENGINE THRUST-REVERSER FLOWS

Researcher: Mr P Lardy
Supervisor: Dr L J Johnston
Sponsor: Hispano-Suiza, France

1 BACKGROUND

Engine thrust-reversing systems are commonly used on transport aircraft to augment the braking action of the wheel brakes after landing. This reduces the reliance on the wheel brakes which can increase safety in iced runway conditions, and also minimises the length of runway required. Fig 1 shows a door-type thrust reverser of the type developed by Hispano-Suiza for application to Airbus aircraft. After touchdown, doors forming part of the outer nacelle structure rotate open to block the fan flow, deflecting it forward to provide a retarding force. The objective of the present project is the development of computational methods to predict the aerodynamic performance of door-type thrust-reversing systems. An important consideration in the project development has been that the resulting methods must be applicable within an industrial design environment.

2 COMPUTATIONAL APPROACH

Work to date has indicated that a combination of two-dimensional and three-dimensional methods provides the most cost-effective approach to the analysis of thrust-reversing flows. A two-dimensional, inviscid, compressible flow method has been developed, based on a solution of the Euler equations in time-dependent integral form; see Lardy and Johnston [1]. The Euler equations are solved by an implicit time-marching procedure with a finite-volume spatial discretisation. Convective fluxes are computed using either the flux-difference splitter of Roe, or the polynomial flux-vector splitter of Lardy and Deconinck [2]. The latter approach is computationally much more efficient than the approximate Riemann solver of Roe. Computational girds are of block-structured form and are generated by algebraic procedures.

3 RESULTS

Typical results are presented for the flat fan-ramp configuration of Fig 2, which includes a kicker plate and flow leakage under the door. The velocity vectors for a nozzle pressure ratio of 1.5 indicate the main features of the thrust-reversing flow, Fig 3. Predicted mass flow rates agree with experiment within 7.6% (Roe first-order scheme), 3.8% (Roe second-order scheme), 6.7% (Lardy first-order scheme) and 4.8% (Lardy second-order scheme). Such levels of accuracy are within industrial design requirements and, in fact, the first-order schemes results are sufficient for preliminary design purposes. Finally, Fig 4 shows an adequate level of agreement with experiment for surface pressure distributions, required to compute the aerodynamic loads used for the structural design.

REFERENCES

[1] Lardy P and Johnston L J, "Two-Dimensional Subsonic Thrust-Reversing Flow Computations with an Upwind Scheme", AIAA Paper 94-1811, June 1994.

[2] Lardy P and Deconinck H, "A Polynomial Flux Vector Splitting Applied to Viscous Hypersonic Flow Computation", Lecture Notes in Physics, Vol 371, pub Springer-Verlag.

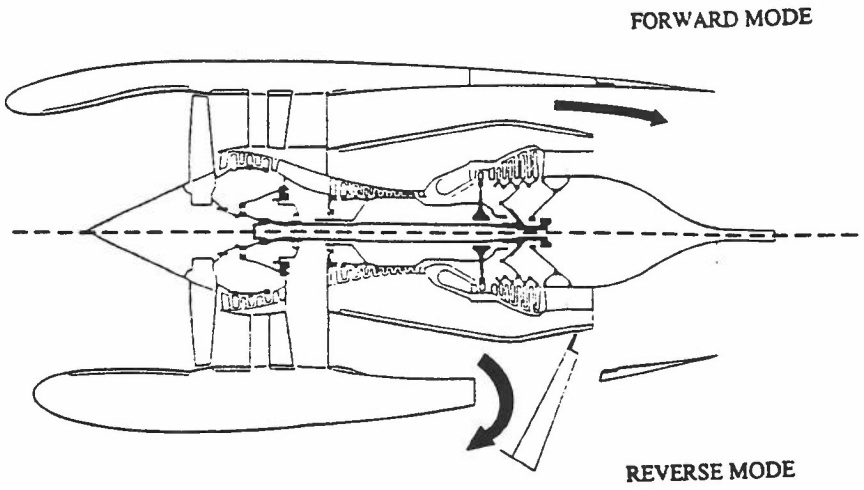

Fig 1 Door-type Thrust Reverser

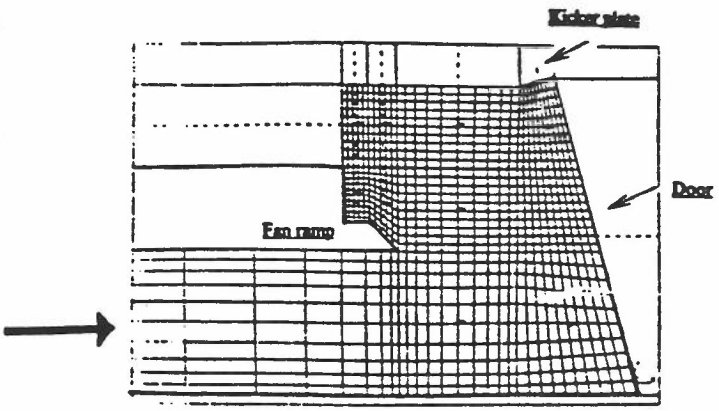

Fig 2 11-Block Computational Grid

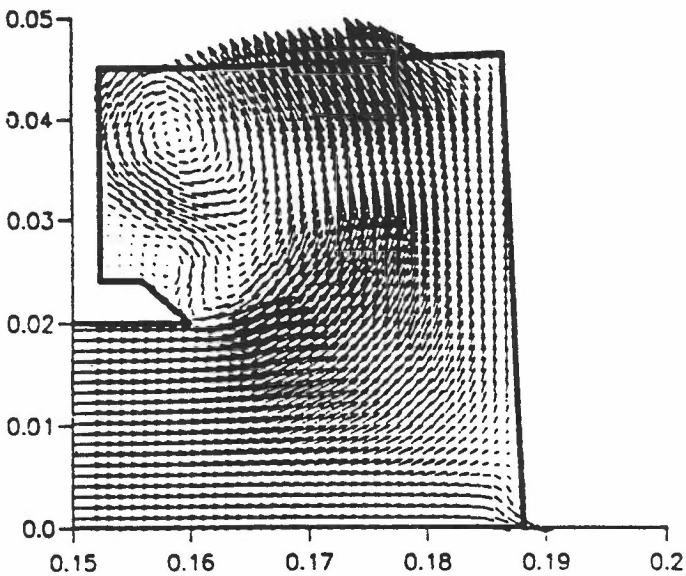

Fig 3 Velocity Vectors

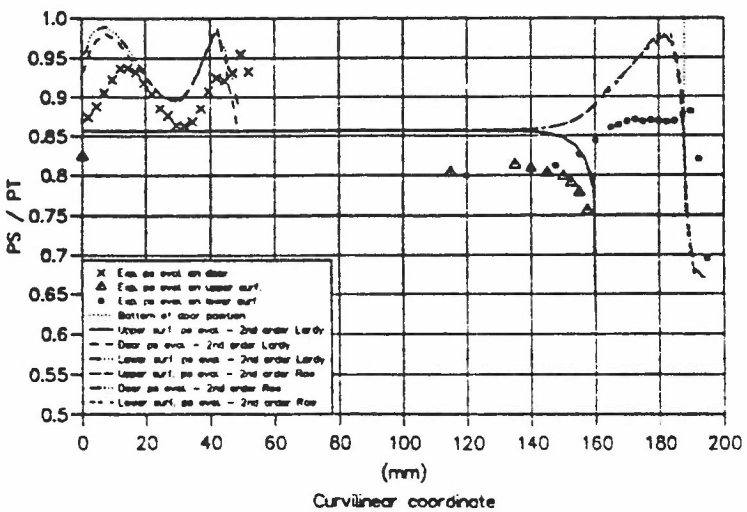

Fig 4 Surface Pressure Distributions

SECOND-MOMENT-CLOSURE MODELLING OF OPEN SEPARATION FROM PROLATE SPHEROID AT HIGH INCIDENCE

Researchers: F.S. Lien and M.A. Leschziner
Sponsor: BAe (RAL, SRC) and DRA, CEC

1. INTRODUCTION

The lift of and the drag on streamlined bodies operating at high incidence - for example, an aircraft fuselage in climb - are strongly affected by the relatively thick boundary layers developing on the body. If incidence is sufficiently large, the boundary layer will separate from the leeward upper surface. At moderate incidence angles, this separation will be "open", i.e. of the vortex-type, in which the magnitude of the skin friction does not change sign. As incidence increases, the open separation patterns becomes increasingly complex, with several vortices separating from the surface. Eventually, at very high incidence, a closed recirculation zone will form.

The successful prediction of any of the above types of separation hinges on a faithful representation of the structure of the curved and decelerating boundary layer approaching the separation line, for this will have a strong effect on the location of separation and hence on any ensuing recirculation pattern. In the rapidly varying boundary layer, turbulence transport, curvature-induced turbulence attenuation, streamwise momentum diffusion and turbulence enhancement due to normal-stress/normal-strain production are all influential. Moreover, processes very close to the wall may be important, due to the strongly non-planar (skewed) nature of the flow, and need to be resolved in detail. Finally, high numerical accuracy must be maintained, which clearly poses serious problems here as a result of the disparities of the boundary-layer and geometric scales.

This summary reports on a numerical study of open separation from a prolate spheroid using a low-Re k-ε model and second-moment closure. Two incidence angles have been investigated at DLR by Kreplin et al [1], namely 10° and 30°, the former involving fixed transition and the latter free transition. Both have been computed.

2. COMPUTATIONAL APPROACH

Calculations have been performed with the single-block version of the algorithm STREAM (Lien & Leschziner [2]) over a 170'000-node conformal grid generated with the aid of the closed potential-flow solution for the spheroid, Fig. 1. The scheme employs a fully co-located storage arrangement for all transported properties, including the Reynolds-stress components, and marches the solution towards a steady state by way of a pressure-correction scheme applicable to incompressible and compressible conditions. Advective volume-face fluxes are approximated using either the QUICK scheme or a TVD MUSCL scheme, the last applied in scalar form (rather than in a form applicable to the coupled set of conservation laws), principally to the turbulence-model equations.

Turbulence effects are represented by the low-Re k-ε model of Lien & Leschziner or by Gibson and Launder's high-Re second-moment closure, applied in conjunction with the the former model in the semi-viscous sublayer. The low-Re model has been formulated, subject to length-scale constraints implied by Wolfshtein's low-Re one-equation form, to be less sensitive than other models to adverse pressure gradient and to require fewer grid lines in the sublayer in support of a grid-independent solution.

4. RESULTS

For 10° incidence, Fig. 1 shows a representative nose-to-tail distribution of pressure coefficient at one azimuthal angle, azimuthal variations of skin friction and its direction at one axial position, and profiles of azimuthal velocity components in the leeward region of the spheroid in which the flow is most complex. While it is evident that the Reynolds-stress model does not return an entirely satisfactory representation of the separation process, the predicted behaviour may be said to be

encouraging and is certainly superior to that achieved with the low-Re k-ε model. Variations of pressure, skin friction and its direction at 30° incidence are shown in Fig. 2. These demonstrate that the calculations, while returning a fair representation in the separated region, not unexpectedly fail to resolve the transition process. This is a serious obstacle which remains to be addressed.

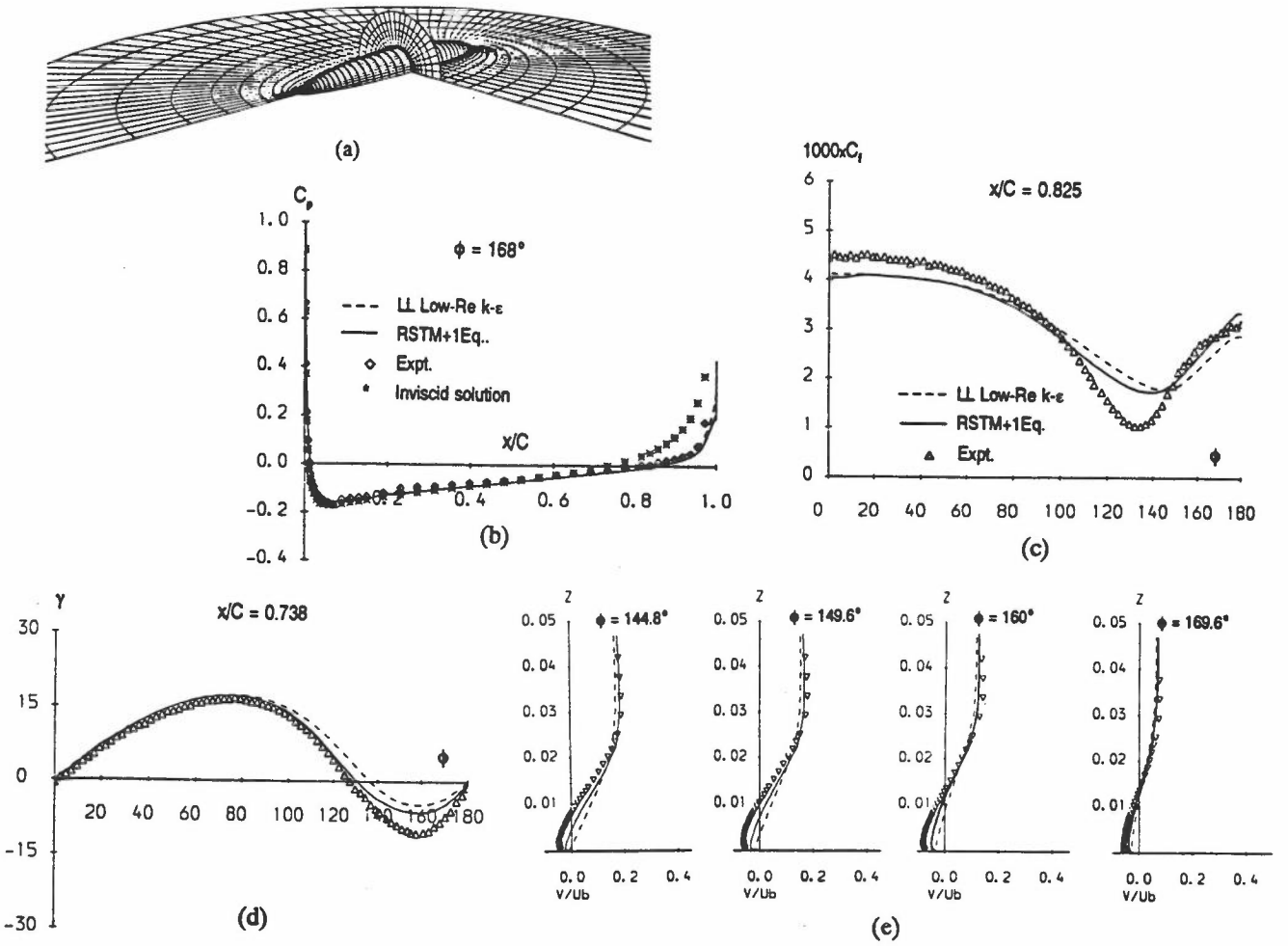

Fig. 1: Prolate spheroid at 10° incidence: (a) mesh; (b) pressure coefficient; (c) skin friction; (d) skin-friction direction (e) azimuthal velocity on rear leeward side

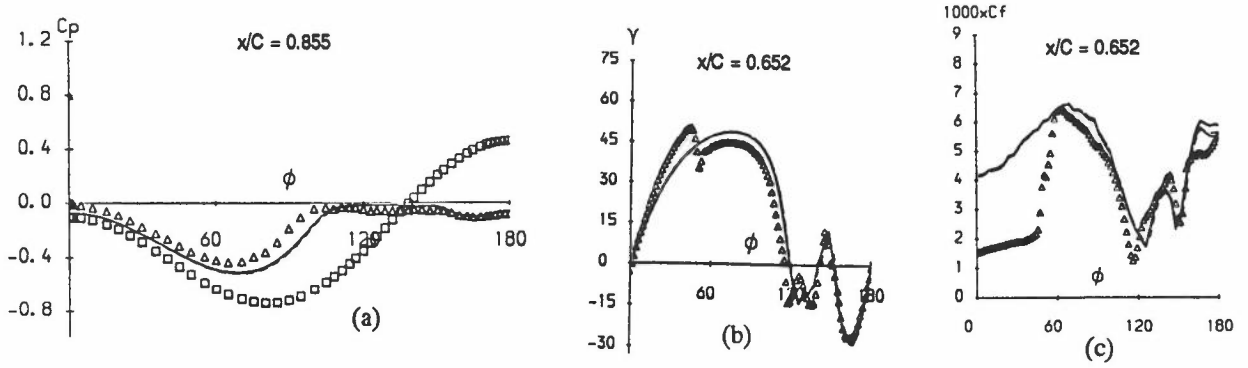

Fig. 2: Prolate spheroid at 30° incidence: (a) pressure coefficient; (b) skin friction; (c) skin-friction direction

REFERENCES

1. Kreplin, H.P., Vollmers, H. Meier, H.U. and Kuhn, A., 1985, DLR Report.
2. Lien, F.S. and Leschziner, M.A., 1993, Paper 13.1, Proc. TSF9, Kyoto.

COMPUTATION of COMPRESSIBLE and INCOMPRESSIBLE IMPINGING MULTIPLE JETS

Researcher : N.Z.Ince
Supervisor : M.A.Leschziner
Sponsor : BAe (MAL).

1. INTRODUCTION

Near-ground operation of vertical take-off and landing aircraft entails a downwards-directed ejection of two or more high-speed hot jets, followed by ground impingement, the formation of wall jets, the collision of these jets and, finally, the generation of upward-directed fountains. If the aircraft is, additionally, in forward flight, the combination of cross-flow and impingement gives rise to a C-shaped ground vortex 'wrapped around' the impingement zone. The intensity, structure and temperature of the jet system, in general, and the upwash, in particular, are of considerable importance to the operational stability and safety of the aircraft. Of special concern is hot-gas reingestion into the jet engines in near-ground hover, which can cause loss of power and even total engine failure.

The computation of three-dimensional jet systems, principally in the above context, has been the subject of a wide-ranging research effort at UMIST over the past 5 years, and some aspects of this work have already been reported in the previous Colloquium. Of particular interest has been the performance of second-moment closure in the highly complex flow conditions prevailing in multiple jet-injection combined with impingement and cross-flow. A wide range of jet configurations have been investigated, as shown in Fig. 1, including single jets in free cross flow; incompressible twin impinging jets without cross-flow; single, twin and triple impinging jets in cross-flow; and transonic impinging twin jets. Recent publications arising from these studies are given as refs [1-3].

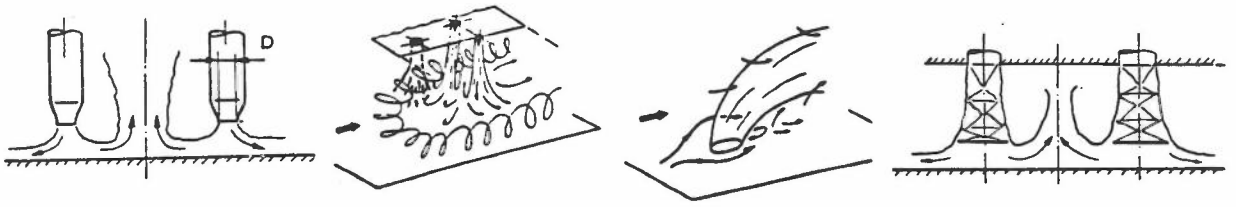

Fig. 1: Range of 3D jet flows computed with second-moment closure

Most recently, attention has focused on incompressible impinging twin- and triple-jets injected into cross-flow (Barata et al [4]) and on impinging under-expanded twin jets without cross-flow (Abbot and White [5]). This summary reports second-moment-model computations performed for the above configurations.

2. COMPUTATIONAL FRAMEWORK

Calculations with up to 370'000 nodes have been performed using a general curved-orthogonal finite-volume code, originally developed by Lin & Leschziner [7] for swirl combustors. Convection is approximated by a bounded variant of the quadratic QUICK scheme. The code incorporates the high-Re k-ε version of the eddy-viscosity model, the Reynolds-stress closure of Gibson & Launder and a variant of the latter in which the equation describing the dissipation rate of turbulence energy has been sensitised to anisotropy via its second and third anisotropy invariants. For transonic conditions, the conventional pressure-correction method used above for incompressible conditions was extended along lines suggested by McGuirk and Page [8]. This entails the use of conservation (flux) variables, which reduces discretization error in regions of high gradients and is beneficial in providing a direct linkage between mass flux and pressure gradient (so avoiding the need to linearize the mass-flux terms when deriving the pressure-correction equation). To provide stability in supersonic zones, a retarded-pressure transformation is introduced. This is a directional transformation dependent upon

local Mach number, which removes the elliptic nature of the pressure-correction equation in supersonic regions. It should be noted that the algorithm degenerates to the basic incompressible method at low Mach number, and so retains all the favourable properties of the SIMPLE algorithm.

3. RESULTS

Results are given in Fig. 2 for an impinging transonic twin jet discharged at NPR = 3.3 (NPR=Nozzle Pressure Ratio=$P_{tot,jet}/P_{ambient}$). Mach-number contours computed with the k-ε and Reynolds-stress models are compared to an abstraction of a Schlieren photograph. These highlight the typical shock-cell structure and stand-off shock wave. The comparison between computed and experimental distributions for impingement-pressure reveal only a modest sensitivity to turbulence modelling. However, predicted variations of pressure along the jet centreline show a strong model dependence, which arises from drastic differences in predicted turbulence levels: the k-ε model responds sensitively, in contrast to the stress model, to the compressive strain in the shock cells by generating inappropriately high levels of turbulence. As a consequence, there are significant differences in the impingement-shock structure.

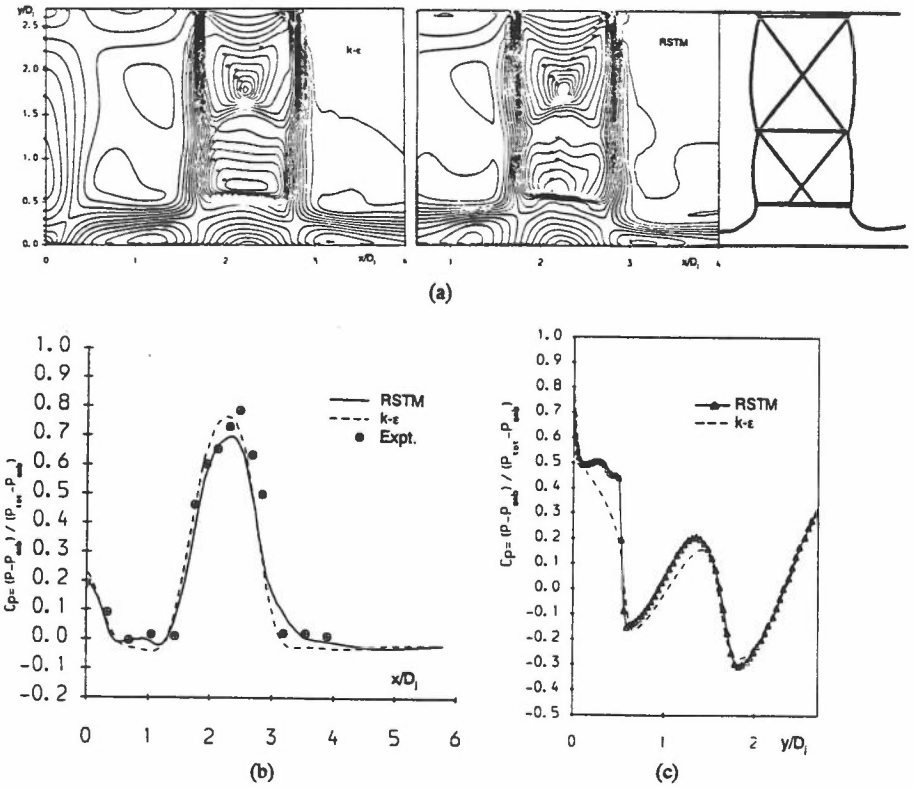

Fig. 2: Transonic twin-impinging jet at NPR=3.3 - (a)Mach contours; (b) impinging-plate pressure; (c) pressure along jet centre-line

REFERENCES

1. Ince, N.Z. and Leschziner M.A., (1993), Royal Aero Soc 1993 European Forum on Recent Developments and Applications in Aerodynamical CFD, Bristol.
2. Ince, N.Z. and Leschziner M.A., (1993), Paper 23.1, AGARD CP 123.
3. Ince, N.Z. and Leschziner M.A., (1993), Paper AIAA-93-4862-CP.
4. Barata, J.M.M., Durao, D.F.G. and Heitor, M.V. (1992), ASME J. Fluids Enggn., 114, p. 231.
5. Abbott, W.A. and White, D.R., Royal Aerospace Establishment Technical Memorandum, p.1166.
6. Lin, C.A. and Leschziner, M.A.,(1989), Proc. 6th Int. Conf. on Numerical Methods in Laminar and Turbulent Flows, Swansea, p. 1717.
7. McGuirk, J.J. and Page, G.J., (1990), AIAA J., Vol. 28, p. 1751.

CFD ANALYSIS OF UNCONVENTIONAL TRANSONIC AEROFOIL SECTIONS

Researcher : Mr F. Cantariti
Supervisor : Dr L.J. Johnston

1. BACKGROUND AND OBJECTIVES

In recent years, aerofoil profiles have been dramatically changed to improve their aerodynamic characteristics. These changes include the development of laminar flow aerofoils, supercritical aerofoils and the use of blunt trailing edges. Although trailing edge bluntness is ignored in many numerical computations, it may affect significantly the pressure distribution near the trailing edge, especially on the upper surface. Blunt base aerofoils are used for several reasons. Firstly, experiments show that increasing the trailing edge thickness results in a significant decrease in wave drag at transonic Mach numbers with no apparent penalty at subcritical Mach numbers, for trailing edge thickness up to 0.7% of chord. Secondly, trailing edge bluntness is needed from a structural point of view because supercritical aerofoil sections have nearly parallel upper and lower surfaces near the trailing edge. The aim of the present work was to modify an existing method to enable the computation of viscous transonic flows around aerofoils with blunt base.

2. COMPUTATIONAL APPROACH

An existing computational method, described by Johnston[2], which solves the Reynolds-averaged Navier-Stokes equations in conjunction with a one-equation eddy viscosity turbulence model, has been modified[1]. This involved modifications to the grid generation program and to the one-equation turbulence model in the wake region where a rather crude model was adopted: the upper and lower surface trailing-edge eddy viscosity and turbulent kinetic dissipation-rate distributions were simply imposed at all stations downstream in the wake for any points either above the trailing edge upper surface or below the trailing edge lower surface. These quantities were calculated by linear interpolation between the upper and lower surface values for any points situated directly downstream of the aerofoil base. Although this model is very simple, it is still a reasonable approximation of the near-wake region, and the discrepancies which appear in the intermediate and far wakes, where the flow relaxes away from its boundary layer formulation, are expected to have little influence on the flow development surrounding the aerofoil.

3. RESULTS

The performance of the resulting modified method was evaluated by computing the flow development around a blunt-base RAE 2822 aerofoil section at transonic conditions. Figure 1 shows the surface pressure distribution and the upper surface and wake velocity profiles. There is good agreement with experiment, apart for the velocity profile in the intermediate wake region which remains too boundary layer like. However, this expected deficiency does not affect sensibly the flow around the aerofoil. The method was then applied to the Boeing A153W Integrated Technology aerofoil, which is one of a family of transonic sections designed to have reduced detection characteristics. The inner region of the computational grid for this aerofoil is shown in Figure 2. Calculations were made over a wide range of Mach number and results were generally in good agreement with experimental data (Figures 3 and 4). The predicted variation of drag coefficient with freestream Mach number, shown in Figure 5, also agreed reasonably well with experiment, although the wave drag contribution was overpredicted at the higher Mach numbers. This behaviour was also found in the case of sharp trailing edge calculations and was attributed to an underprediction of the shock wave/boundary layer interaction by the numerical method when using the one-equation turbulence model.

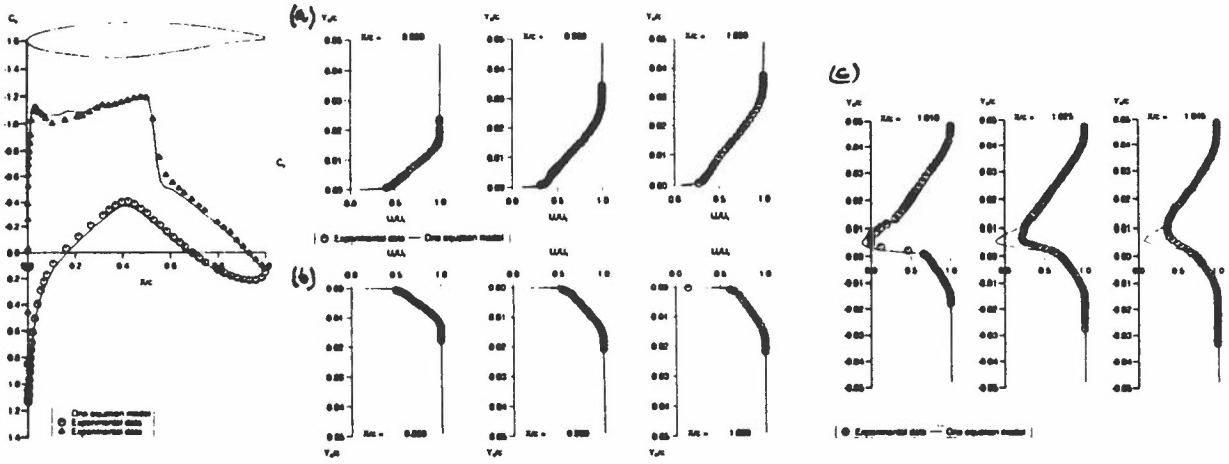

Surface pressure distributions Upper surface(a), lower surface(b) and wake(c) velocity profiles

Fig.1 RAE 2822 blunt-base aerofoil at M=0.73, α=2.98°, Re=6.1x10^6

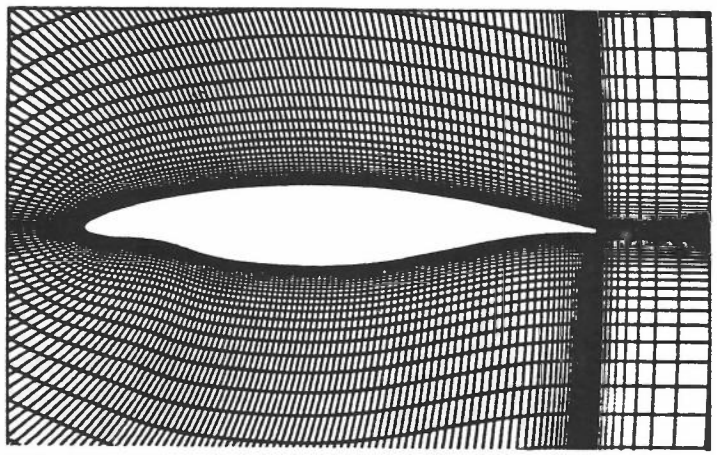

Fig.2 Inner region of the computational grid for the Boeing A153W aerofoil

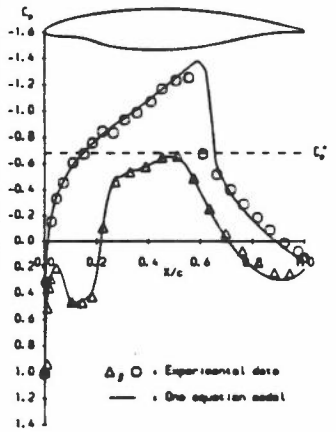

Fig.3 Surface pressure distributions M=0.731, α=1.58°

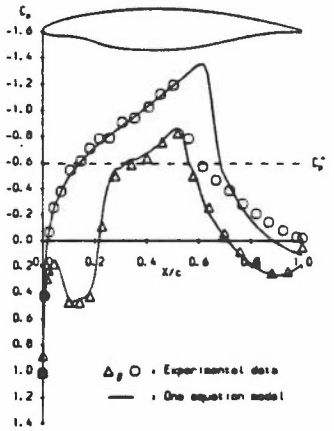

Fig.4 Surface pressure distributions M=0.753, α=1.67°

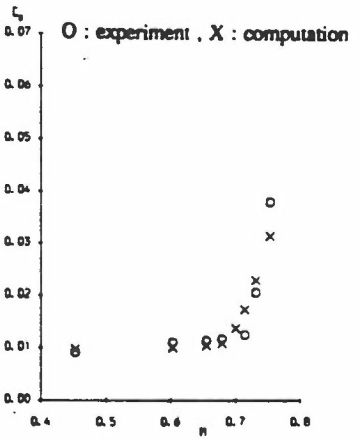

Fig.5 Drag coefficient for Mach number sweep at α=1.6°

REFERENCES

(1)CANTARITI, F. J.-J., Computation of Viscous Flow Development Around Blunt Trailing Edge Aerofoils. MSc Dissertation, Department of Mechanical Engineering, UMIST, December 1992.

(2)JOHNSTON, L.J., Solution of the Reynolds-Averaged Navier-Stokes Equations for Transonic Aerofoil Flows, The Aeronautical Journal, Vol. 95, No 948, October 1991, pp 253-273.

« Session 5 »

Combustion, Two-phase Interaction, Radiation

COMPUTER MODELLING OF FUEL SPRAYS CONTAINING ELECTROSTATIC CHARGE

Researcher : J.S. Shrimpton
Supervisors :A.P.Watkins, A.J.Yule
Sponsor : SERC

1.INTRODUCTION

The use of electric charge to promote liquid atomization and control drop deposition is common in many industrial applications such as paint and crop spraying, pollution abatement and metallic powder production. The present work seeks to model the effect of charge on drop diameter, trajectory and breakup with a view to optimising charged spray combustion. Published work is limited, being confined to one and quasi one dimensional expansion in a quiescent gas phase with no breakup.

2. THE EXISTING MODEL

The existing model [1] has previously been used to predict diesel spray breakup, dispersal and evaporation. The gas phase transport equations of mass, momentum, energy and k-ε are discretised using a finite volume grid and are solved by a non iterative implicit method. The liquid phase is represented by drop 'parcels', each containing many non-interacting spherical droplets implicitly possessing identical diameter, velocity and temperature. The Lagrangian drop equations are discretised in time, using the Euler method, to give implicit solutions for drop position, mass, velocity and temperature.

3. CHARGED SPRAY INITIAL CONDITIONS

Kelly [2] has developed a stochastic theory to predict the droplet charge, size and frequency distributions within a charged spray. The theory requires that only the physical properties of the liquid and the mean volumetric specific charge (C/m^3) of the spray need to be defined beforehand. The theory has shown to be accurate for octoil, woods metal and glycerine. Experimental work at UMIST [3] has shown that these predictions also hold for commercial grade kerosine and diesel oil. By incorporating the work of Kelly into the existing code to define the size and charge distributions the applicability of the model is extended further than the fuel oils considered in the present work to include any liquid properties that the theory can predict. Figure 1 correlates prediction and experiment for kerosine at 0.6 C/m^3. In view of the fact that the experimental result is an end state and as such includes breakup, the case for using the theory of Kelly is strongly supported.

Figure 1: Theory versus Experiment

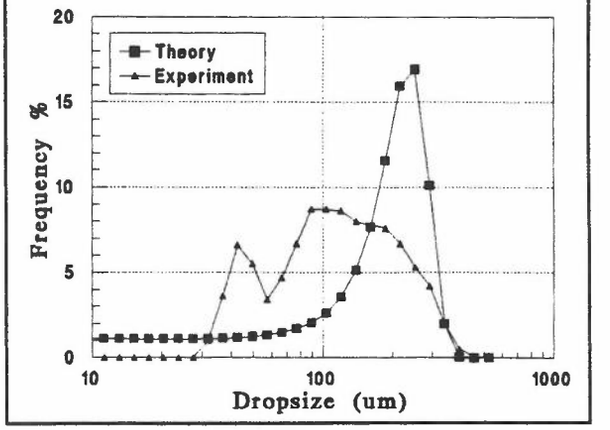

4. CHARGED DROP TRAJECTORY CALCULATION

Figure 2: Droplet Interaction

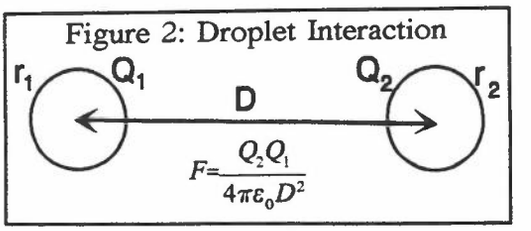

To calculate the contribution to momentum change from charged drop-drop interactions the drops are treated as point charges. Dipole interactions are thus ignored here but they are important in charged droplet deformation and breakup, below. The assumption allows the force on two droplets to be defined as shown in Fig.2. It is assumed the all the charges in the spray are of like sign, in consequence all drops are repelled from each other and the solution for n drops is highly coupled.

5. CHARGED DROP DEFORMATION, EVAPORATION AND BREAKUP.

There exists a maximum charge that a spherical drop may possess that is a function of diameter and surface tension. For $Q>Q_{max}$ the electrostatic charge repulsion exceeds the restoring force of surface tension and drop disruption occurs. In effect the charge acts to reduce the restorative effect of surface tension. This has major implications for drop breakup, as defined by a maximum deformation ratio. Also a non stationary drop will be deformed from spherical and Q_{max} is further reduced. Clearly for fast moving, highly charged drops the ratio will be significantly reduced. Previous studies have shown that there is no charge leakage from evaporating charged drops to the surrounding gas phase for drops with $Q<Q_{max}$ so for volatile or heated liquids there is an additional factor contributing to enhanced drop disruption.This behaviour has been modelled as shown by Fig.3 and is to be incorporated. The breakup of the parent charged drop is different to the uncharged case, and the non-charged bag and strip modes do not occur. Breakup is more discrete, with a number (≈20 or less) of daughter drops being produced. It has been found that the daughter drops possess a disproportionate amount of the charge with respect to their mass. This leads to end state size distributions that are at least bimodal and the spray becomes radially stratified, with a core of large lesser charged drops surrounded by a sheath of smaller, more highly charged ones.

Figure 3: Charged breakup

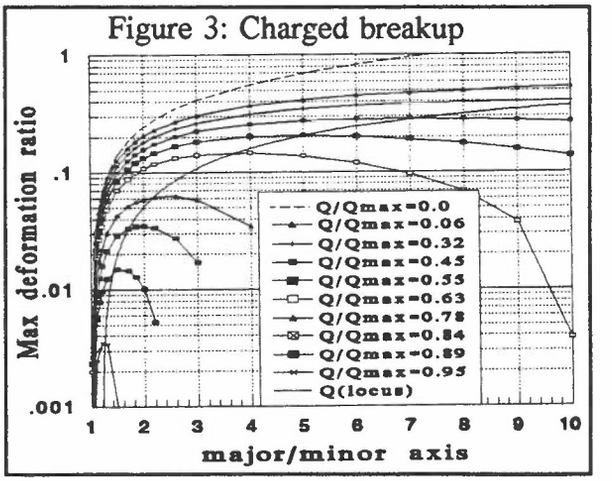

6. REFERENCES

1. Watkins, A.P.,"Three dimensional modelling of gas flow and sprays in diesel engines", Computer simulation of fluid flow, heat and mass transfer and combustion in reciprocating engines, Markatos, N.C.(ed), Hemisphere, Washington DC, 193-237, 1989.
2. Kelly, A.J.,"Low Charge Density Electrostatic Atomization",IEEE. Trans. IAS, vol 1A-20, 2, 267-273, 1984.
3. Yule, A.J.,Shrimpton, J.S., Watkins, A.P., Balachandran, W., Hu, D. "Electrostatically atomized hydrocarbon sprays.", Submitted for publication, Fuel, March 1994.

RADIATION ABSORPTION IN DENSE GAS CLOUDS BY THE DISCRETE TRANSFER METHOD

Researcher: A.I. Sayma
Supervisor: P.L. Betts
Sponsors: Palestinian Students Fund, Arab-British Chamber, ORS

1. INTRODUCTION

The Discrete Transfer Method was developed by Lockwood and Shah [1] for calculating radiative transfer in combustion chambers. This method is known to combine accuracy with economy of computer storage and CPU time. In the present study, the method is adapted for predicting radiation absorption in dense gas dispersion simulations in the finite element model FEMSET. The method was programmed and validated against standard analytic solutions. It was then used in the simulation of a dense gas dispersion scenario over flat ground and led to improvements in the predictions.

2. APPROACH

For a gas of several absorption bands, the equation of radiative transfer can be written as:

$$\frac{dI}{ds} = -kI + \int_{\nu_i}^{\nu_j} B(T)\, d\nu \qquad (1)$$

where **I** and **k** are the average intensity and absorption coefficient over a band and **B(T)** is the Planck function, which gives and monochromatic emissive power over the band (ν_i - ν_j). Scattering is neglected in equation (1).

In the Discrete Transfer Method, a number of rays of predetermined orientation are fired from each wall of the domain boundary. These rays are traced until they reach another boundary or leave the domain. For each band, the equation of transfer is integrated over each element to give the recursive relation:

$$I_{n+1} = \int_{\nu_i}^{\nu_j} B(T)\, d\nu\, (1 - e^{-kx}) + I_n e^{-kx} \qquad (2)$$

where the index **n** refers to element numbers that the ray crosses. Knowing boundary conditions at the walls, equation (2) can be solved to give the difference in the intensity of a ray crossing each element. The radiation sources are then calculated by performing an energy balance along the ray in each element. The total energy absorbed in each element is the sum over all the bands from all the rays passing through it.

3. VALIDATION TESTS

The method was validated against analytic solutions of radiative transfer between two flat plates with isothermal gas between them. Computed fluxes at the walls agreed with the analytic solution for a reasonable number of rays. The method was then compared to the analytic solution of radiative transfer between two parallel plates at steady state where the computed energy sources were used indirectly to calculate temperature distribution in the gas. Results are compared with the analytic solution of Heasalt and Warming [2] in Figure(1).

The method was then used, with two Methane absorption bands, in the simulation of the

Burro-8 [3] dense gas dispersion field trial modelled over flat ground. The maximum radial distance travelled by the lower flammability level contour at 1m height is compared in Figure (2) with the solution with no radiation modelling and with the experimental results. Improvements in the prediction are noticed. A sensitivity test of the method for gases with wide absorption bands indicated that modelling radiation is necessary in many dense gas dispersion scenarios.

REFERENCES

1. Lockwood F C and Shah N G, "A new radiation solution method for incorporation in general combustion prediction procedures", *Eighteenth Symposium (International) on Combustion*, The Combustion Institute, 1405-1413, 1981.
2. Heasalt M A and Warming R F, "Radiative transport and wall temperature slip in an absorbing planer medium", *Int. J. Heat Mass Transfer*, 8:979-994, 1965.
3. Koopman R P et al., "Burro series data report LLNL/NWC 1980 LNG spill tests", Technical Report, Lawrence Livermore National Laboratory, 1982.

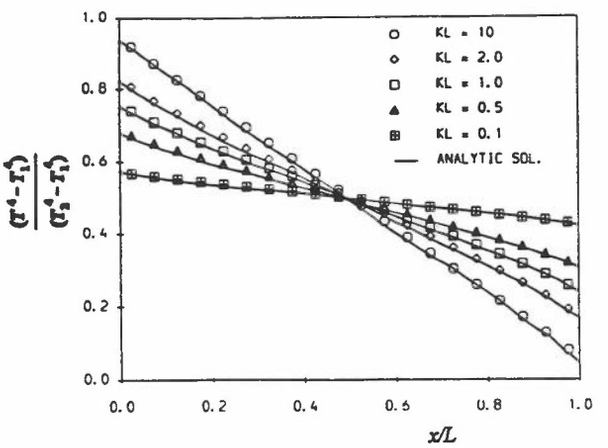

Fig 1 Temperature distributions between parallel black plates.

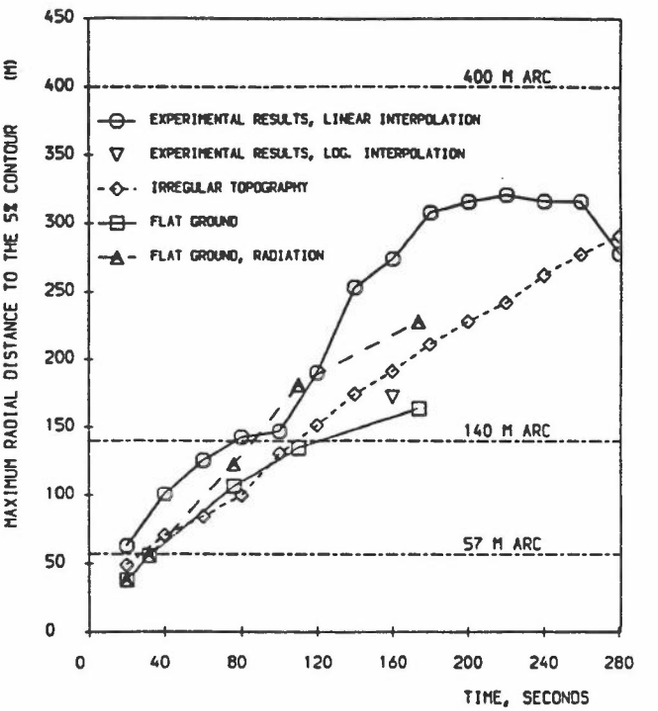

Fig 2 Comparisons of maximum distances to Lower Flammability Limit in Burro-8 Trial.

TRANSPORT AND REACTION RATE MODELLING FOR PREMIXED TURBULENT COMBUSTION

Researchers: Dr. S-P. Li, Dr. R. S. Cant
Sponsors: EPSRC, Shell Research Ltd., British Gas plc.

1. INTRODUCTION

Premixed turbulent combustion is important in many practical situations, most notably in the spark-ignition engine but also in jet-engine reheat systems, certain types of industrial burner and in accidental explosions resulting from leakage of combustible gases and vapours. For engineering design purposes it is essential to quantify the behaviour of such systems. Depending on the end in view it may be necessary to address questions of operating performance, fuel economy, hazard assessment, safety limits and/or pollutant formation. All of these require some means of modelling the properties and response of turbulent premixed flames, and this presents a difficult problem due to the strong interactions between turbulence, combustion chemistry, molecular transport and density change due to heat release.

2. LAMINAR FLAMELET MODELLING

Fortunately, for most fuels in common use the rate of reaction is sufficiently rapid that the timescale for chemical reaction is small compared to the smallest timescales associated with the turbulent flow field. This implies that the reaction zones within the flame are thin, and leads to the laminar flamelet formalism due to Bray, Moss and Libby [1]. In this approach the turbulent flame is considered as a collection of thin, highly wrinkled interfaces called laminar flamelets, which separate volumes of unburned reactants from corresponding volumes of fully-burned products. All chemical changes and molecular transport take place within the laminar flamelets, which have local structure similar to that of a laminar flame subjected to straining and curvature by the surrounding turbulence. The modelling consequences of this physical observation are twofold. First, the problem of modelling turbulent transport in the presence of variable composition and density is reduced to the much simpler problem of modelling turbulent transport in two separate constant-density streams, with occasional transitions between them as a flamelet passes by. Second, the problem of modelling the mean turbulent reaction rate is simplified by taking advantage of the sheet-like nature of the reaction zone. The reaction rate per unit surface area is known from laminar flame theory leaving only the surface area per unit volume to be modelled.

3. TURBULENT TRANSPORT MODELLING

Turbulent transport in the reacting flow is treated using a standard second-moment closure model based on Favre density-weighted averaging. A second-moment treatment is considered to be necessary due to the severe local anisotropy of the Reynolds stresses encountered in flames, and to the occurrence of counter-gradient diffusion resulting from preferential acceleration of low-density burned gas in the presence of the self-induced pressure gradient within the flame. Neither of these effects can be represented by a simple gradient- transport model. Within the flame, the flamelet assumption leads to a simple formalism for the decomposition of unknown higher moments in terms of conditional moments of lower statistical order. Closure at second-moment level is achieved by modelling the unknown conditional second moments in terms

of the known unconditional moments. A unified stress-flux closure model is formulated which reduces properly to the constant-density case at each side of the turbulent flame. Some modification is necessary in order to deal with the effects of externally-imposed compression as in the I.C. engine case [2].

4. REACTION RATE MODELLING

The chemical composition of the reacting mixture is represented by a reaction progress variable taking the value zero in unburned reactants and unity in fully-burned products. As a consequence the mean turbulent reaction rate is represented as the volumetric rate of production of the progress variable. Since the flame is locally sheet-like this volumetric rate may be expressed as the mean rate of reaction per unit surface area multiplied by the mean surface area of the flame sheet found in unit volume of space. The reaction rate per unit surface area may be computed to any desired level of accuracy given sufficient knowledge of the relevant chemistry. A major advantage of the flamelet approach is that this may be done separately from any turbulent flame calculation and the results stored in a "flamelet library" for subsequent interpolation. Modelling activity is then confined to representing the surface-averaged effect of the turbulence on the reaction rate [3], and to representing the generation and destruction of flame surface area by the mean flow, the turbulence, curvature and propagation effects [4]. The former is tackled with the help of data on surface pdfs of strain rate and flame curvature obtained by Direct Numerical Simulation [5], while the latter is based on the derivation and modelling of a balance equation for the mean flame surface area per unit volume [6].

5. IMPLEMENTATION AND RESULTS

The model has been implemented in a 2D Cartesian and axisymmetric code known as TARTAN. The datails of the numerical method employed and some of the results obtained to date are given in a companion paper.

REFERENCES

1. Bray,K.N.C., Moss,J.B., Libby,P.A. (1985) "Unified Modelling Approach for Premixed Turbulent Combustion-Part I: General Formulation", Combust.Flame, 61 , 87-102.
2. Cant,R.S., Bray,K.N.C. (1989) "A Theoretical Model of Premixed Turbulent Combustion in Closed Vessels", Combust.Flame, 76 , 243-263.
3. Cant,R.S., Kostiuk,L.W., Bray,K.N.C., Rogg,B. (1994) "Flow Divergence Effects in Strained Laminar Flamelets for Premixed Turbulent Combustion", Combust. Sci. Tech., 99 , 123-126.
4. Cant,R.S., Pope,S.B., Bray,K.N.C. (1990) "Modelling of Flamelet Surface-to-Volume Ratio in Turbulent Premixed Combustion", Proceedings of the 23rd Symposium (International) on Combustion, pp809-815, The Combustion Institute.
5. Cant,R.S. (1994) "Direct Numerical Simulation for Premixed Turbulent Combustion Modelling", Proceedings of the 74th AGARD FDP Meeting and Symposium, Chania, Crete, Greece, 1994, to appear.
6. Cant,R.S. (1993) "Turbulent Reaction Rate Modelling Using Flame Surface Area", Proceedings of the Joint Meeting of the British and German Sections of the Combustion Institute, Cambridge, 1993, pp48-51, The Combustion Institute.

PREMIXED COMBUSTION MODELLING FOR I.C. ENGINE APPLICATIONS

Researcher: Dr. S-P. Li
Supervisors: Dr A. P. Watkins, Dr. R. S. Cant
Sponsor: EPSRC

1. INTRODUCTION

A model for premixed turbulent combustion described in a companion paper has been implemented in a two-dimensional Cartesian or axisymmetric geometry for use in the further development of combustion models suitable for I.C engine applications. A code known as TARTAN has been developed and several validation tests have been carried out. The numerical method is based on a modified PISO algorithm incorporating second-order bounded spatial differencing together with second- order implicit time differencing. Results are most encouraging and further development is proceeding.

2. NUMERICAL APPROACH

The application of second-order differencing to combustion problems is complicated by the need to keep bounded scalar variables such as the reaction progress variable strictly within their physical limits. Schemes such as QUICK, while nominally third-order accurate, fail to meet this requirement in the presence of moderate gradients of the dependent variable. In the present work the bounded second-order CCCT scheme [1] is employed and is found to give entirely satisfactory results, even when gradients (in the vicinity of the flame) are very strong. For I.C. engine applications it is necessary to consider time-dependent reacting flows, and second-order time accuracy is desirable. This is achieved here using Crank-Nicholson implicit time differencing in conjunction with a modified semi-implicit PISO algorithm. Spatial solutions are obtained using a pentadiagonal line relaxation solver together with a tridiagonal conjugate-gradient pressure solver.

3. TEST CASES AND RESULTS

Validation of the code and the initial version of the model has been carried out with reference to the experimental data of Cheng and Shepherd [2] obtained in an axisymmetric impinging- jet flame. A stoichiometric ethylene-air mixture was supplied at 5m/s with 8% turbulence through a nozzle of diameter 50mm surrounded by an air coflow at the same velocity. This flow was made to impinge on a thermally insulating flat plate placed 100mm above the nozzle exit. A statistically-stationary planar turbulent flame was formed at a well-defined location between the nozzle and the plate. Two components of mean and fluctuating velocity were measured using LDA, while the scalar field was determined using Mie scattering from seed particles in the unburned gas. Comparisons between measured and computed values of velocity and progress variable are shown in Figure 1.

Further validation tests have been carried out for the time- dependent case of one-dimensional flame propagation. An analytical solution for the turbulent flame speed is available for this case using the theory of Kolmogorov, Petrovski and Piskunov (KPP) [3]. The numerical results are shown in Figure 2 and yield a flame speed within 3% of the analytical value, thus demonstrating the efficacy of the second-order time-stepping scheme.

4. CONCLUSIONS AND FUTURE WORK

Work carried out to date has verified that the TARTAN code is accurate, stable and robust. The initial version of the BML flamelet model for this study has been validated for a simple impinging-jet burner test case. Work now in progress will extend the modelling to confined and time-dependent test cases more representative of engine combustion. The end in view is a model for combustion that will be widely applicable in a range of spark-ignition engine codes.

REFERENCES

1. Gaskell,P.H., Lau,A.K.C. (1988) "Curvature-Compensated Convective Transport: SMART, A New Boundedness-Preserving Transport Algorithm", Int. J. Numer. Meth. Fluids, 8, 617-641.
2. Cheng,R.K., Shepherd,I.G. (1991) "The Influence of Burner Geometry on Premixed Turbulent Flame Propagation", Combust. Flame, 85 , 7-26.
3. Hakberg,B., Cant,R.S., Bray,K.N.C. (1993) "Prediction of the Turbulent Burning Velocity for the BML Model", Proceedings of the Joint Meeting of the British and German Sections of the Combustion Institute, Cambridge, 1993, pp84-87, The Combustion Institute.

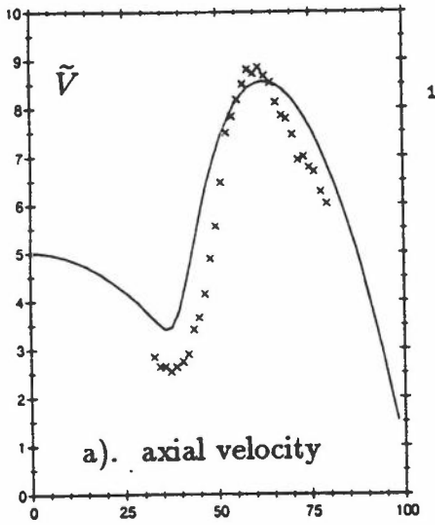

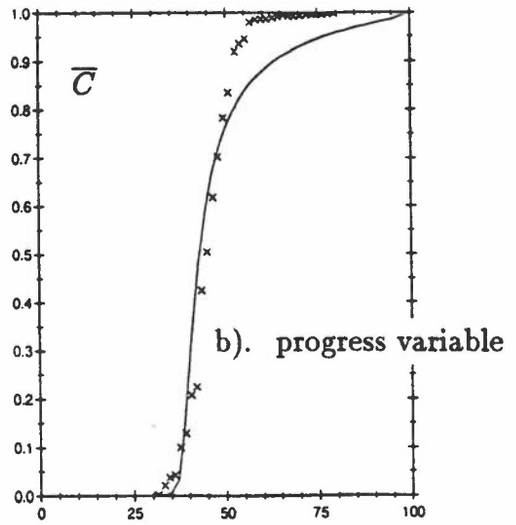

Figure 1: predictions along the centreline

× experimental data [2]

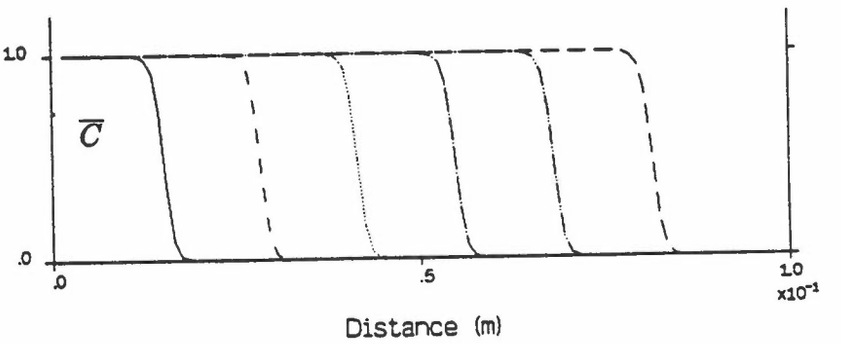

Figure 2: flame propogation

δt	U_T (m/s)		
	KPP	C-N	Euler
1.0×10^{-4}	1.12	1.15	1.33
2.5×10^{-4}	1.12	1.16	1.55
5.0×10^{-4}	1.12	1.16	1.69

Table 1: flame speed

PARTICLE DISPERSION IN A PLANE HORIZONTAL JET

Researcher: J. Rusas
Supervisor: M.A.Leschziner
Sponsor: University of Aalborg

1. INTRODUCTION

The Lagrangian description of particle motion within an Eulerian framework for the fluid carrier requires information on the carrier's instantaneous turbulent fluctuations which, when imparted to the particles, give rise to particle dispersion. Most commonly used stochastic Lagrangian method for particle dispersions (e.g. Gosman & Ionnides [1]) extract an isotropic turbulent velocity fluctuation u_f from the predicted carrier turbulence energy and a Gaussian PDF having a standard deviation of $(2/3k)^{0.5}$. The time over which u_f acts on a particle is the minimum of the eddy-life time and the eddy-transit time (here called "eddy-lifetime model"). The principal drawbacks of this methodology are, first, the ambiguity associated with the choice of time scales, and second, that no account is taken of the fact that turbulent fluctuations are correlated in time and direction.

Zhou and Leschziner [2,3] have developed a model in which time correlation and anisotropy are taken into account without any explicit time scales being prescribed. In this, the vectorial velocity fluctuation $\vec{v}_t$ at time t is correlated to the fluctuation at the previous time step by $\vec{v}_{t-\delta t}$. In addition the components of $\vec{v}_t$ are correlated so as to comply, statistically, with prescribed Reynolds-stress components. This model has been shown by Zhou and Leschziner to return considerably higher levels of spread than traditional models, in better agreement with experimental data for highly anisotropic shear layers (Lazaro & Lasheras [4], Ishima et al [5]).

This summary reports the application of the Zhou & Leschziner's anisotropic model an experiment by Perkins and Hunt [6] in which a stream of particles is falling normally through a plane jet, as shown in Fig. 1, onto a plate. Modelling is performed with an appropriately modified and extended version of the code STREAM (Lien & Leschziner [7]).

2. THE DISPERSION MODEL

Fig. 1 shows a single discrete particle at time t-δt, located at $\vec{r}_{p,t-\delta t}$ relative to an origin 'O'. At time t, a fluid (i.e. carrier) particle originating at $\vec{r}_{f,t-\delta t}=\vec{r}_{p,t-\delta t}$ will have moved to $\vec{r}_{f,t}$ while the discrete particle will, in general, be located at $\vec{r}_{p,t}$. The task is to determine the carrier fluctuation at $\vec{r}_{p,t}$. The velocity fluctuation of the carrier phase at time t at location $\vec{r}_{f,t}$ may be related to the velocity fluctuation at t-δt by:

$$\vec{v}(\vec{r}_{f,t}) = \{\beta\}\ \vec{v}(\vec{r}_{f,t-\delta t}) + \vec{d}_t \qquad (2)$$

where $\{\beta\}$ accounts for effects arising from previous time levels, while $\vec{d}_t$ represents effects arising from randomness during the time interval δt. Similarly, the carrier velocity fluctuation at location $\vec{r}_{p,t}$ can be related to the fluctuation at location $\vec{r}_{f,t}$ by:

$$\vec{v}(\vec{r}_{p,t}) = \{\gamma\}\ \vec{v}(\vec{r}_{f,t}) + \vec{e}_t \qquad (3)$$

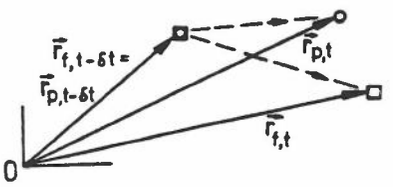

Fig. 1: Motion of particle and carrier-fluid packet in δt

For relatively small or light particles and relatively short time step δt, the departure of $\vec{r}_{p,t}$ from $\vec{r}_{f,t}$ is small, in which case, the velocity fluctuation at the particle's position at time level t is simply represented by equation (2). The task is thus reduced to determining the matrix $\{\beta\}$ and the vector $\vec{d}_t$. An analogous path may be adopted if correlation (3) is to be included.

A sampling process may be constructed which 'retrieves' $\vec{v}_f$ in such a way that a sufficiently

large set of sampling events satisfies the statistical constraints imposed by the available time-averaged correlations of the velocity fluctuations $\overline{u_i u_j}$. Furthermore, given time-correlation functions of the form $R_{ij}(\delta t) = (\overline{u_{i,t-\delta t}\, u_{j,t}})/\sqrt{\overline{u_{i,t-\delta t}^2}\,\overline{u_{j,t}^2}}$, temporal correlation may be accounted for without the use of time scales. The derivation process is too involved for it to be included herein, and the reader is referred to references [2,3] for details.

3. APPLICATION

The experimental arrangement, shown in Fig. 2 consists of a horizontal nozzle of 150 mm width and 10 mm in height placed 235 mm above the floor. Air is blown into a otherwise unconfined space. Particles are released from a vibrating hopper, 289 mm above the jet, and collected in trays on the floor. The experiment consisted of several test combinations, and the test run chosen here was for a jet exit velocity of 25 m/s, a particle diameter of 244 μm and a hopper downstream position of 200 mm. This configuration was also investigated by others and presented at the 6th Workshop on Two-phase Flow Predictions at the University of Erlangen [8].

In Fig. 2, the experimental particle-concentration distribution is compared with computed solutions arising from the eddy-lifetime model and the present anisotropic particle dispersion model. Both numerical distributions are shifted downstream, apparently as a result a somewhat excessive level entrainment in the aerodynamic calculation and hence excessive forward motion between the jet and the confining walls. Significantly, the widths of the predicted distributions differ drastically, with the eddy-lifetime model returning a much too narrow profile - a general weakness of solutions arising from isotropic eddy-lifetime models and contributed to the 6th Workshop on Two Phase Flow Predictions [8]. Qualitatively similar differences in predicted concentration distributions have also been observed by Zhou & Leschziner for other shear flows transporting particles *along* the flow with dispersion occurring *across* the flow.

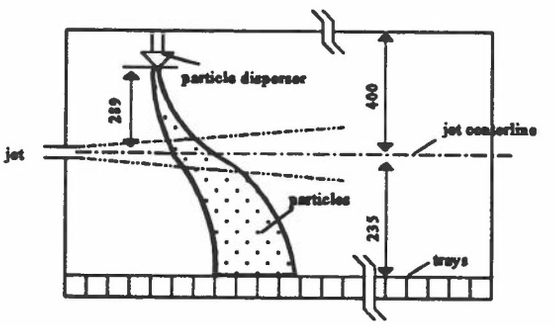

Fig.1. Horizontal jet test facility

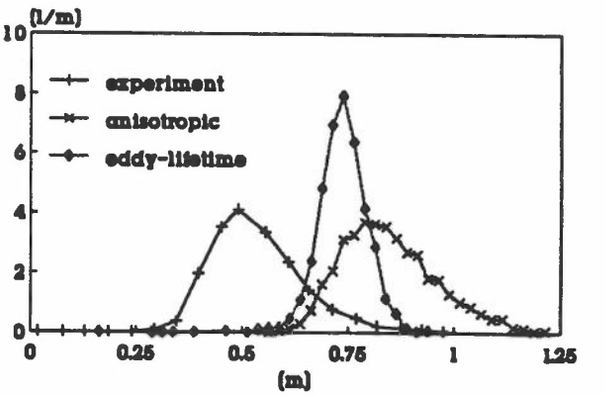

Fig.2. Normalized particle mass collected on the floor

REFERENCES

1. Gosman, A.D. & Ionnides, E. (1981) AIAA Paper 81-0323.
2. Zhou, Q. and Leschziner, M.A. (1991), Gas Solid Flow, ASME FED-Vol 117, p. 1.
3. Zhou, Q. and Leschziner, M.A. (1992), Proc. 8th Symp. on Turbulent Shear Flows, p. 10.3.1.
4. Lazaro, B.J. and Lasheras, J.C. (1989), Proc. 7th Symp. on Turbulent Shear Flows, p. 15.3.1.
5. Ishima, T., Hishida, K. and Maeda, M., 1991, Proc. Int. Conf. on Multiphase Flows, Tsukuba.
6. Perkins,R.J. & Hunt,J.C.R., 1990, Report to Warren Spring Laboratory.
7. Lien F.S. and Leschziner, M.A., Turbulent Shear Flows 8, Springer, p. 205.
8. Sommerfeld, M. (Ed) (1992), Two-Phase Flow Predictions, Proc. 6th Workshop.

DEVELOPMENT OF A 3D NON-ORTHOGONAL GRID COMPUTER CODE FOR D.I. DIESEL ENGINE APPLICATIONS

Researcher: K. Park
Supervisor: Dr. A.P. Watkins
Sponsor: ORSA and ODF

1. OBJECTIVE

Engine codes for Diesel engine applications have mainly used curvilinear orthogonal grids for the simple piston bowl boundary shapes; cylindrical or omega shaped.

However a number of combustion systems have been developed recently with a much more complicated boundary shape in order to use spray wall impaction as a means of breaking up the fuel spray and/or directing it in a desired direction[1]. This project is considering the use of a number of cut off pips to achieve these objectives. Some early results have been published[2].

In case of a complicated boundary with cut-off pips, it is difficult or impossible to generate an orthogonal grid. Thus a non-orthogonal grid computer code has been developed.

2. APPROACH

The mathematical model by Watkins[3] is used. The gas phase is described by Eulerian conservation equations and the liquid phase by Lagrangian equations for position and momentum. Also the effects between the phases, e.g. mass and momentum transfers, are given as sources or sinks.

The equations are transformed into general non-orthogonal curvilinear coordinates, and discretised. The discretised formulation is solved with the spray non-iterative implicit solution algorithm Spray EPISO.

3. ASSESSMENT

A number of different non-orthogonal grids numerically generated and the results are compared with that from an orthogonal grid. As shown in Fig. 1, the spray shapes do not show any significant differences, only the wall spray developments are reduced slightly, but this seems to be due to the effect of grid spacing rather than grid distortion.

The code is also tested for a wide range of conditions and its results are compared with experiments (Fig. 2). The variation of the wall spray radius and height match well with these experiments.

4. APPLICATION

The code is applied in order to optimise the shape of diesel engine piston bowl with fuel impingement, and the results are compared with these for the conventional shape.

As shown in Fig. 3, the droplet distribution in the impingement shape show good mixing with the gas, whereas for the conventional shape the spray does not reach to the centre area, without squish effects the airflow.

5. CONCLUSION

The simulation results using the non-orthogonal grid computer code are in good agreement with a wide range of experiments, and it has the major benefit that it can be applied for a complicated boundary shape, even though a small loss of accuracy for high velocity regions with high distorted grids is expected.

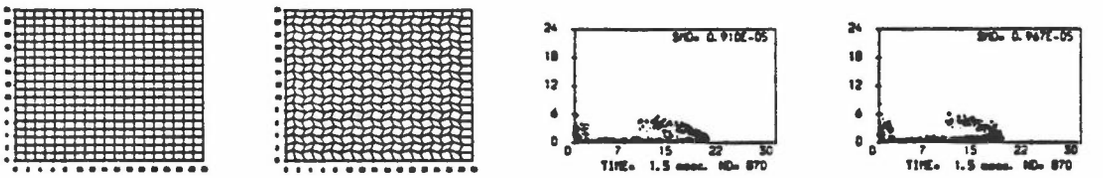

Fig. 1. Non-orthogonal grid test

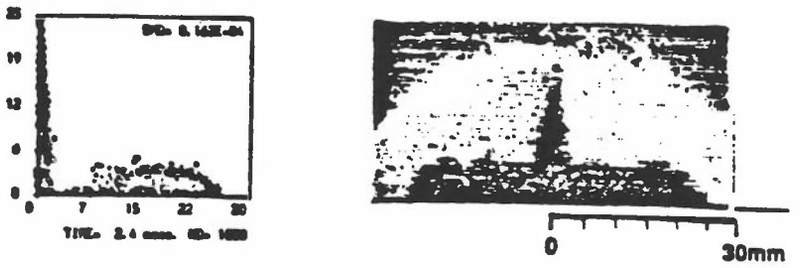

Fig. 2. Wall impaction test

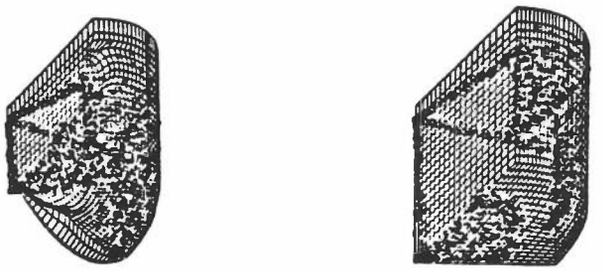

Fig. 3. Application to the impingement shape of piston bowl

REFERENCE

1. Park, K. and Wang, D.M. and Watkins, A.P. "A contribution to the design of a novel direct-injection diesel engine combustion system-analysis of pip size" Appl. Math. Modelling, vol. 17, pp 114-124, 1993.

2. Kato, S. and Onishi, S. "New type of diesel engine by impingement of fuel jet (OSKA-D)" SAE paper 901618, 1990.

3. Watkins, A.P. "Three-dimensional modelling of gas flow and sprays in diesel engines, computer simulation for fluid flow, heat and mass transfer and combustion in reciprocating engine" Hemisphere, Washington, pp 193-237, 1989.

COMPUTER MODELLING OF METERED-DOSE INHALERS

Researcher: Craig A. Dunbar
Supervisors: A.P. Watkins (UMIST), and P. Burt (GRD)
Sponsors: EPSRC (formerly SERC) and Glaxo Research and Development (GRD)

1. BACKGROUND

The metered-dose inhaler (MDI), shown in Fig.1, is a compact pressurised spray dispenser designed for oral inhalation of multiple doses of finely dispersed drug in the treatment of various pulmonary diseases, the most common being asthma. The spray is generated by flash evaporation of CFC-based propellants which disperse the formulation issued from the metering valve. However, since the introduction of the Montreal Protocol [1], which aims to eliminate the production of all chlorine based chemicals by the year 1995, there has been an urgent need to find "ozone-friendly" replacements to CFC propellants.

The introduction of a CFD code to model the spray characteristics of an MDI offers a new and relatively inexpensive addition to the costly and extensive development of non-CFC based MDI formulations. The code will be able to yield valuable information on the physical processes of the spray formation which could lead to practical design improvements of the MDI.

2. APPROACH

The MDI spray code is being developed from an existing 2-D axisymmetric diesel spray code. The spray issued from an MDI is an unsteady, transient, multi-phase flow and is described in terms of Eulerian continuum conservation equations for the continuous gas phase and Lagrangian transport equations for the dispersed liquid phase. The finite-volume technique, along with the hybrid differencing scheme, is used to transform the non-linear, partial differential gas phase transport equations for spatial discretization and the Euler implicit method is used for temporal discretization. The turbulence transport is represented by the k-ϵ turbulence model and the coupled equations for pressure and velocity are calculated using the predictor-corrector method. The discrete droplet model (DDM) is used to describe the droplet histories with the addition of droplet collision and breakup models.

3. PRELIMINARY RESULTS

The spray produced from an MDI must contain particles with sizes less than 5μm for the drug to reach the target area for treatment, i.e., bronchioles. Therefore, drop size information, as shown in Fig. 2, is central in the characterisation of the MDI spray. Figs. 3-4 show gas field properties which influence the spray history via momentum transfer. The gas field contours of vapour mass fraction and temperature, which are influential in the evaporation history of the spray, are shown in Fig. 5, and is an example of the codes ability to provide information which is very difficult to obtain experimentally.

4. FUTURE WORK

Experimental work is currently being undertaken at GRD to characterise the MDI spray using phase-Doppler anemometry (PDA). The preliminary results of this work have shown the spray to be considerably asymmetric and it will therefore be necessary to extend the code to three dimensions.

REFERENCES

1. Council Regulation (EEC) No 3952/92, OJ No L 405, 31.12.92

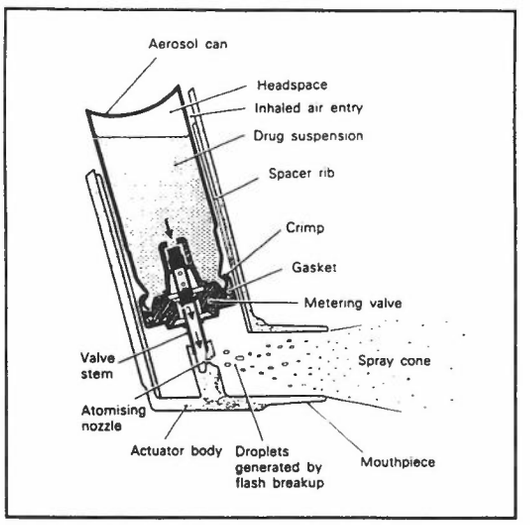

Fig. 1: Metered-dose inhaler

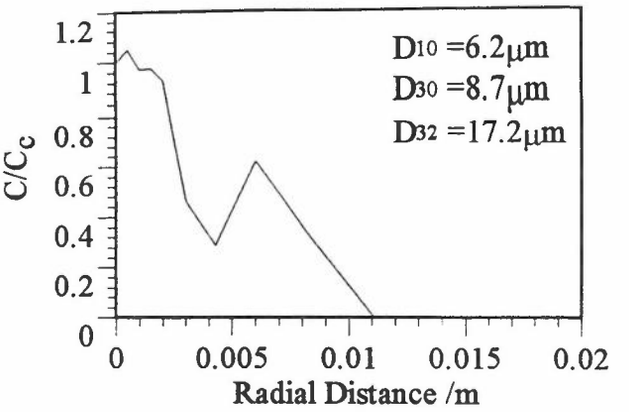

Fig. 2: Drop mass concentration radial profile (x=0.04m)

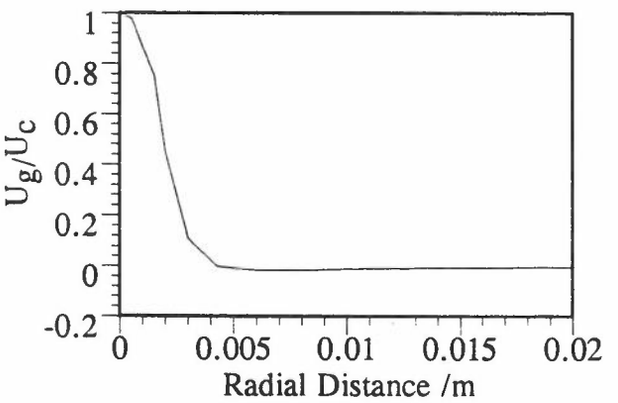

Fig. 3: Dimensionless axial gas velocity radial profile (x=0.04m)

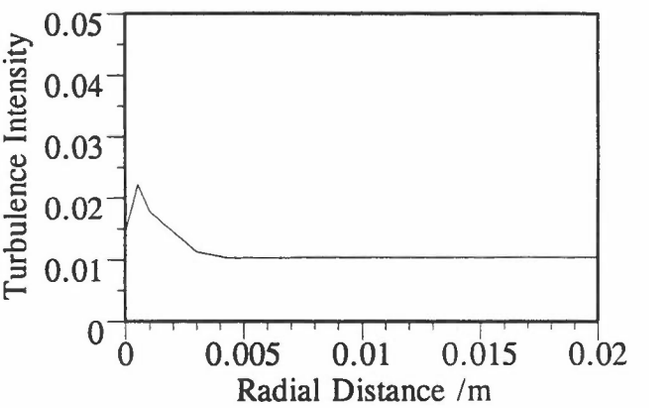

Fig. 4: Gas turbulence intensity radial profile (x=0.04m)

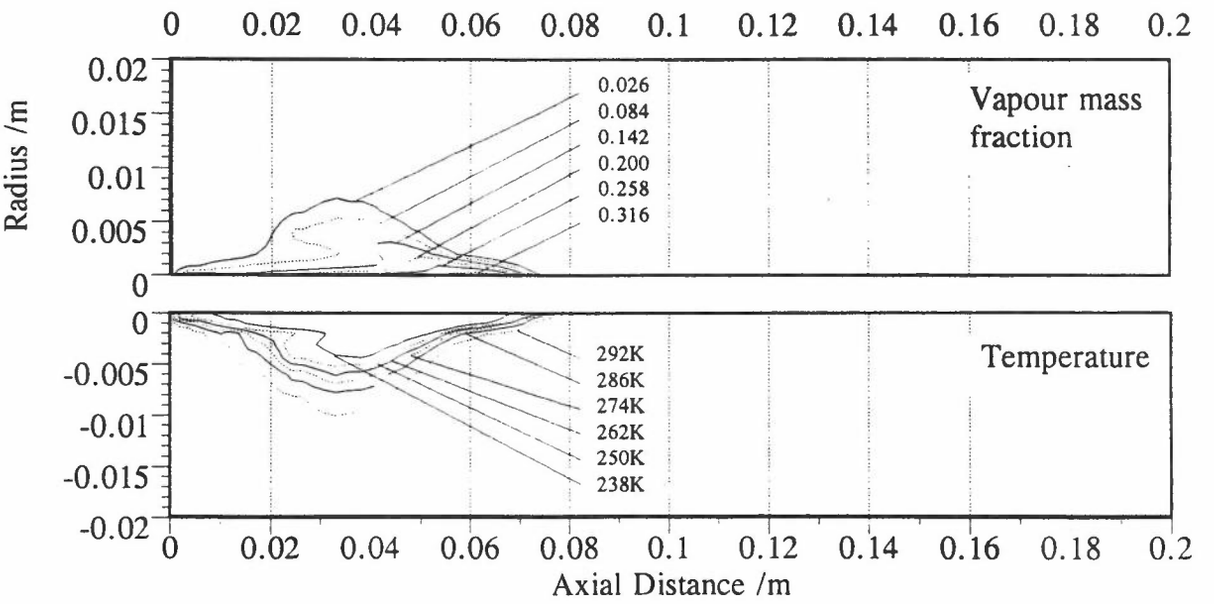

Fig. 5 : Gas field profiles of vapour mass fraction (above) and temperature (below)

« Session 6 »

Internal Flows

COMPUTATION OF FLOW AND HEAT TRANSFER THROUGH STATIONARY AND ROTATING U-BENDS

Researcher: Ms H-Y Li
Supervisors: Dr H Iacovides and Prof B E Launder

1 OBJECTIVES

The high operating temperatures of modern gas-turbines necessitate the development of cooling systems, in which relatively cool air is circulated inside the turbine blades through internal cooling passages. The cooling flow within these passages is greatly influenced by the presence of U-bends of strong curvature and also by the rotation of the blades. The objective of this study is the assessment of the effectiveness of eddy-viscosity and also of relatively simple second-moment models when used for the computation of such flows.

2 APPROACH

The computations presented concern flow and heat transfer through a U-bend of square cross-section which has a curvature ratio $R_c/D = 0.65$ and which, as shown in Figure 1, can rotate about an axis parallel to the axis of curvature. A three-dimensional finite volume solver was employed and following our earlier work in this field [1] a bounded version of the QUICK scheme, LODA, was used for the convective discretization of all transport equations. Four different turbulence modelling arrangements have been tested: (a) A high-Re k-ε model with a one-equation k transport model in the near-wall regions, (b) A high-Re ASM model with the one-equation model in the near-wall regions, (c) A low-Re ASM model in which the near-wall dissipation rate is obtained from a prescribed length scale [2], ASM1, (d) A low-Re ASM model in which the dissipation rate equation is solved across the wall sub-layer [3] ASM2.

3 RESULTS

For the stationary case, the velocity profile comparisons of Figure 2 indicate that as the turbulence model is successively refined, the onset of flow separation along the inner wall of the U-bend is more realistically predicted. Even when the full low-Re ASM model is employed there is still however further room for improvement. For the rotating cases, the vector plot comparisons of Figure 3 show that the low-Re ASM computations are more successful for the case of positive rotation, where the Coriolis force reinforces the curvature force. The heat transfer comparisons, however, that the low-Re ASM models employed are unable to return realistic heat transfer predictions over the outer wall of the stationary U-bend.

4 CONCLUSIONS

In computations of flow through U-bends of strong curvature it becomes necessary to employ a second-moment closure in order to correctly reproduce the flow separation within the U-bend. The low-Re second-moment models employed are however in need for further improvement.

5 REFERENCES

1 Bo T, Iacovides H and Launder B E, to appear Int J for Num Meth in Heat and Fluid Flow.

2 Iacovides H and Li H-Y, IAHR, 5th Int Symp on Refined Flow Modelling and Turbulent Measurement, Paris, France, 1993.

3 Iacovides H and Launder B E, ICHMT Int Conf on Heat Tr in Turbomachinery, Athens, Greece, August 1992.

4 Cheah S C, Iacovides H, Jackson D C and Launder B E, ASME Paper 94-ST-226, Int Gas-Turbine Congress, The Hague, 1994.

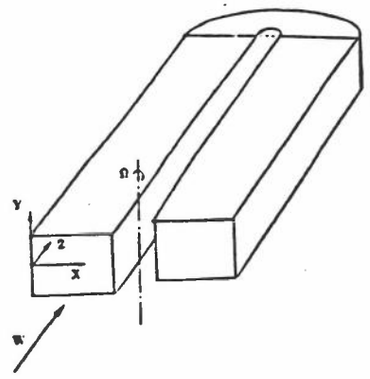

Figure 1 Flow Geometry

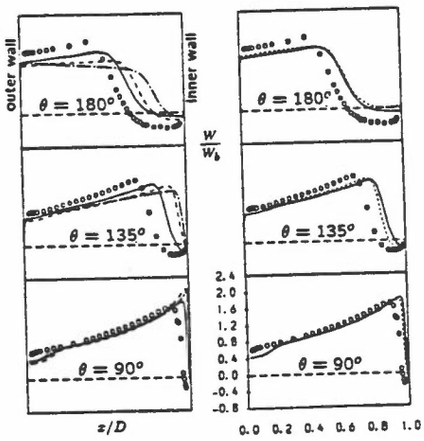

Figure 2

Streamwise velocity profiles along the duct symmetry plane

— · — k-ε/1-eqn

- - - ASM/1-eqn

—— Low-Re ASM1

----- Low-Re ASM2

o o o Data [4]

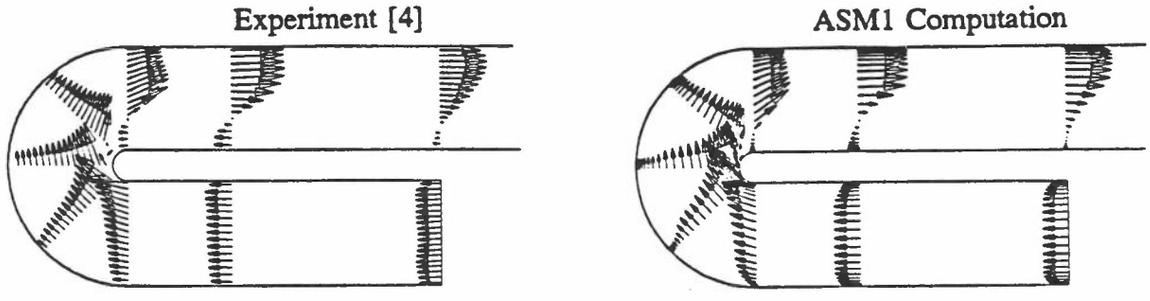

(a) Positive Rotation, Ro = 0.2

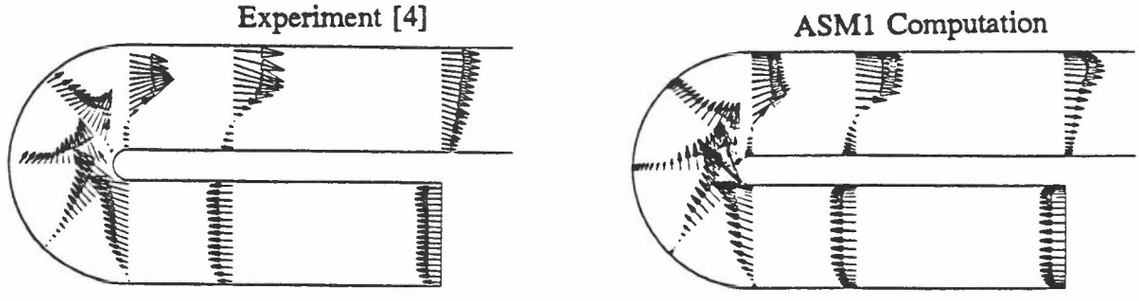

(b) Negative Rotation, Ro = 0.2

Figure 3 Vector Plot comparisons along symmetry plane

COMPUTATION OF FLOW AND HEAT TRANSFER THROUGH RIBBED PASSAGES

Researcher: Mr M Raisee
Supervisor: Dr H Iacovides

1 OBJECTIVES

In blade cooling passages and also in other cooling applications, heat transfer enhancing ribs are often employed. In the case of blade cooling passages, due to the effects of rotation and curvature, secondary motion is also present. In such circumstances, the use of low-Re turbulence models becomes necessary. The overall objective of this investigation is to determine low-Re models that are suitable for the prediction of three-dimensional flow and heat transfer through rib-roughened passages. In this initial stage only two-dimensional cases are considered.

2 APPROACH

For the initial part of this investigation a two-dimensional axisymmetric code is employed, based on the finite volume methodology and which uses a semi-staggered grid arrangement. Three different turbulence models have been tested; a high-Re k-ε model with a one equation model within the near-wall regions, the Launder and Sharma low-Re k-ε model and a low-Re differential stress model. The first case investigated concerns flow and heat transfer through a rib-roughened pipe for which measurements of the local Nusselt number are available [1]. Only one interval between successive ribs is computed and repeating boundary conditions are applied.

3 RESULTS

Figure 1 shows the predicted flow fields using the k-ε/1-eqn model and the low-Re k-ε model. The flow behaviour returned by the two models appears to be similar. The corresponding Nusselt number comparisons are shown in Figure 2. While the k-ε/1-equation model predicts a thermal behaviour that is very close to the measured one, the low-Re k-ε, even with the Yap term computes Nusselt number levels that are unrealistically high.

4 CONCLUSIONS

Initial tests indicate that in flows through stationary ribbed tubes the k-ε/1-eqn model produces reliable heat transfer predictions while the Launder and Sharma low-Re k-ε over predicts wall heat transfer. A low-Re differential stress model is now being tested.

5 REFERENCES

1 Baughn J W and Roby J L, HTD-Vol 202, 28th National Heat Transfer Conf & Exhibition, San Diego, California, 1992

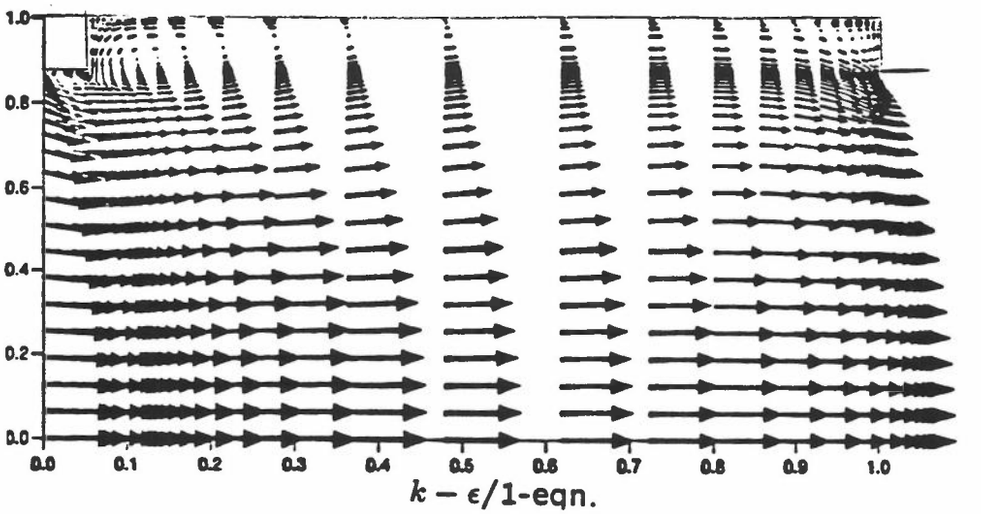

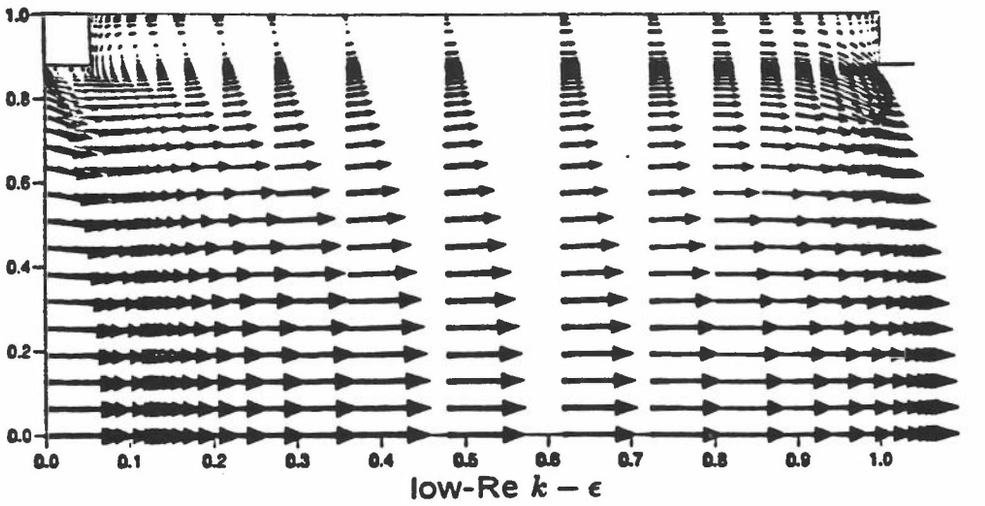

Figure 1 Predicted flowfield for flow within a ribbed tube

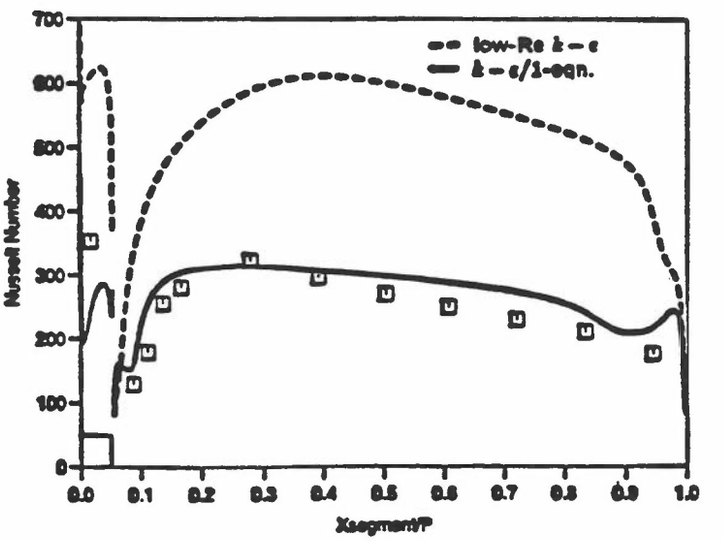

Figure 2 Nusselt Number comparisons

MODELLING OF FLOW IN ROTOR-STATOR CAVITIES

Researchers: Mr P Toumpanakis and Mr M Te-Braak
Supervisor: Dr H Iacovides

1 OBJECTIVES

Flow in axisymmetric cavities formed between discs, one or both of which may be rotating occur in cooling systems of gas-turbines. As shown in Figure 1, in such systems fluid is pumped radially outwards along the rotating disc and returns to the cavity centre along the stationary disc. Flow in the centre of rotor stator cavities is usually laminar and due to the convective effects of radial motion the rotor boundary layer can remain laminar over a significant proportion of the rotor surface. The objective here is to employ low-Reynolds number models of turbulence transport in the computation of these flows.

2 APPROACH

Four turbulence models have been tested: (a) A high-Re k-ε with the 1-equation model in the near-wall regions, (b) The Launder and Sharma low-Re k-ε model, (c) A low-Re differential stress model and (d) The High-Re version of the Wilcox k-ω model. Three rotor-stator cases have been computed for which measurements are available ([1] and [2]). The first case involves a cavity of aspect ratio of 0.08 for a rotational Reynolds number (Re = $\Omega b^2/\nu$) of 10^6. The other two cases concern a cavity of aspect ratio of 0.127 at Re_θ values of 1.6×10^6 and 0.3×10^6.

3 RESULTS

The k-ε/1-eqn and the k-ω model failed to predict the laminar flow region at the cavity centre. As shown in Figure 2, with the inclusion of the Yap term, both low-Re models predict the correct behaviour at the outer region of the cavity but also predict unrealistically large laminar regions along the rotor. In order to overcome these predictive deficiencies a modification related to solid body rotation is introduced to the ε transport equation. The constant $c_{\varepsilon 1}$ is divided by $(1 + 5\Lambda)$, where

$$\Lambda = \left((\omega - s)^2\, \omega \right)^{1/3} \quad ,\omega = \frac{k}{\varepsilon}\left[\frac{1}{2}\left(\frac{\partial U_i}{\partial x_j} - \frac{\partial U_j}{\partial x_i}\right)^2\right]^{1/2}$$

$$\text{and} \quad s = \frac{k}{\varepsilon}\left[\frac{1}{2}\left(\frac{\partial U_i}{\partial x_j} + \frac{\partial U_j}{\partial x_i}\right)^2\right]^{1/2}$$

As shown in Figures 3 and 4, by making the dissipation rate sensitive to the presence of solid body rotation flow predictions are greatly improved over a range of rotational speeds.

4 CONCLUSIONS

In the prediction of rotor-stator flows it is necessary to use low-Re models of turbulence transport. Use of the Yap term improves flow predictions near the outer shroud while transition is better predicted when ε is made sensitive to the effects of solid body rotation.

5 REFERENCES

1 Cheah S C, Iacovides, H Jackson D C and Launder B E, To appear Int J of Expt Thermal and Fluid Science

2 Itoh M, Yamada Y, Imao S and Gouda M, Proc 1st Symp on Engrg Turb Modelling & Measurement, pp 569-668, Elsevier, 1990.

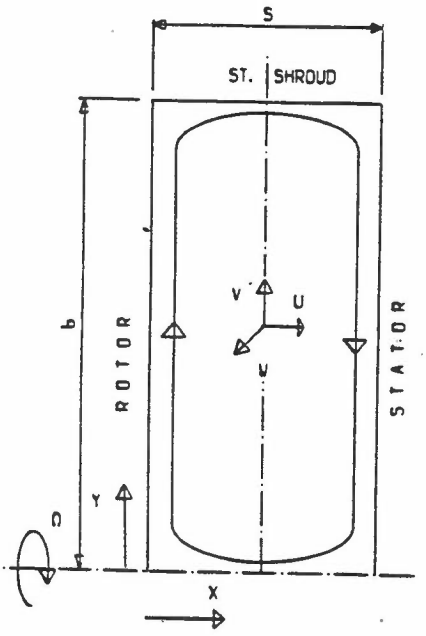

Figure 1 Rotor-stator system

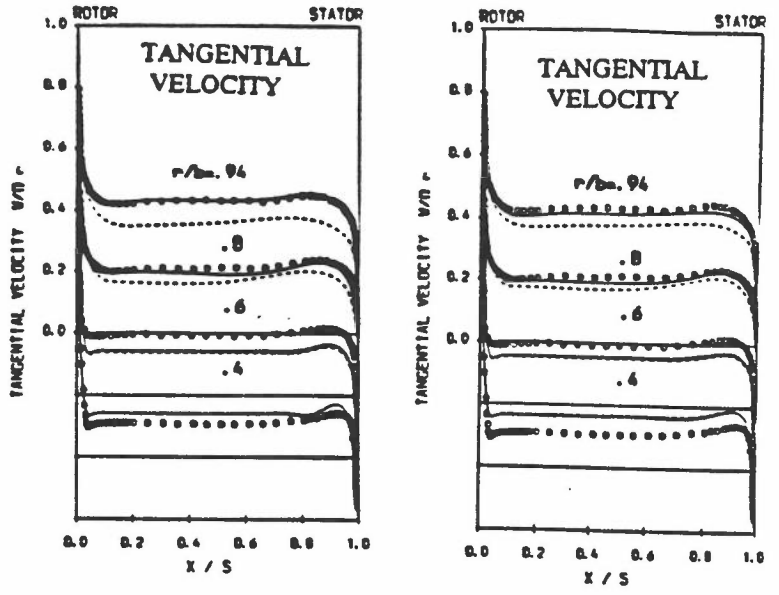

Figure 2 Low-Re computations for s/b = 0.8 and $Re_\theta = 10^6$

- - - Without Yap term ___ With Yap term

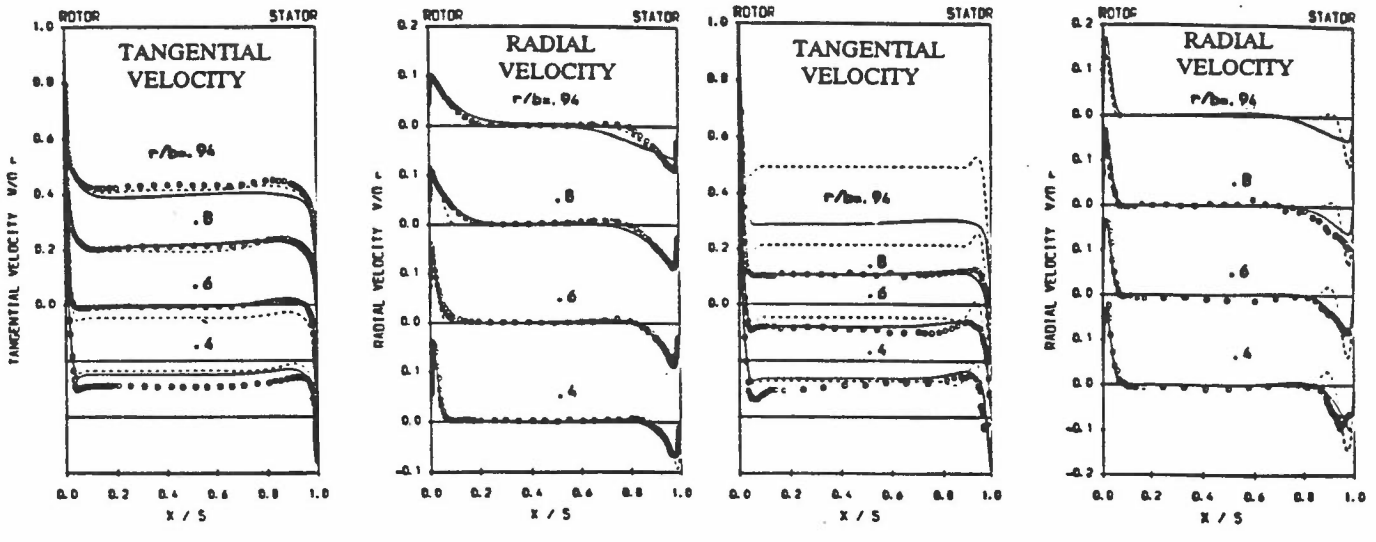

Figure 3 Comparisons for s/b = 0.08 & $Re_\theta = 10^6$ DSM Model with Yap correction term

- - - Without ε modification

___ With ε modification

Figure 4 Comparisons for s/b = 0.127 and $Re_\theta = 0.3 \times 10^6$ DSM with Yap term

- - - Without ε modification

___ With ε modification

MODELLING THE FLOW IN A TRANSITION DUCT

Researchers: F.S. Lien and M.A. Leschziner

1. INTRODUCTION

Transition ducts - so called because they consist of stretches having different cross-sectional shapes connected by a gradually changing 'transition' portion - are encountered in a variety of engineering applications, include rectangular-to-circular air-intake ducts preceding aero-engine intakes, hydraulic shaft tubes used to diffuse water exiting from vertically-oriented turbines at hydro-electric power plants, and channels for cooling fluid embedded in turbine blades. In an industrial environment, major issues of interest include the minimisation of losses, the provision of the shortest possible duct for given cross-sectional shapes at inlet and outlet, the avoidance of separation and the minimisation of flow distortion at the duct exit.

From a fundamental, fluid mechanic point of view, the process of primary significance is the generation of transverse motion by lateral pressure differences arising from cross-sectional changes. The mechanism may be explained by reference to the geometry in Fig. 1. A dimensional reduction in one lateral direction combined with an increase in another provokes a pressure gradient which 'squeezes' boundary layer fluid from the reducing axis towards the elongating one, a process which renders the boundary layer highly three-dimensional. The lateral redistribution of boundary-layer vorticity and the distortion of the vortex lines that goes with it give rise to pairs of counter-rotating vortices which transport low-momentum boundary-layer fluids into inner duct regions, creating strong distortions in the streamwise velocity field. The severity of this distortion is crucially affected by the rate of decay of the vortical motion beyond transition. If this field is subject to an adverse streamwise pressure gradient, due to increase in area or curvature, separation can easily ensue, resulting in a dramatic increase in losses and very severe flow non-uniformities.

This summary reports a computational study of the flow in a round-to-rectangular transition duct examined experimentally by Davis & Gessner [1]. The emphasis of the study is on the performance of different turbulence models, in particular their ability to resolve correctly the streamwise vortices which, through transverse convective transport, provoke large flow distortions downstream of the transition section.

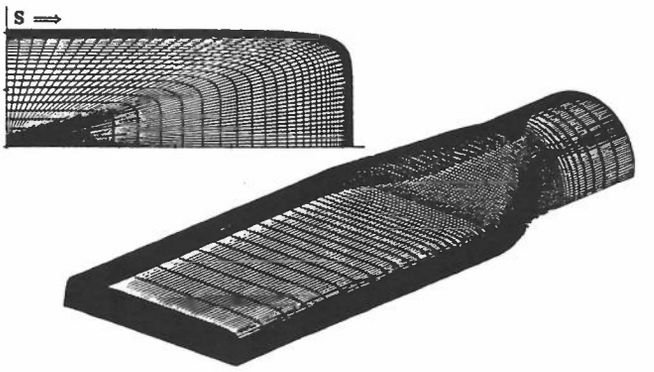

Fig. 1: CR duct and grid

2. COMPUTATIONAL APPROACH

Computational solutions have been derived from a non-orthogonal, co-located finite-volume algorithm incorporating third-order QUICK and second-order TVD/MUSCL discretisation for convection. A total of five turbulence models have been investigated:

- o the low-Re model of Lam & Bremhorst [2];
- o the low-Re model of Lien & Leschziner [3];
- o a zonal model combining Wolfshtein's [4] low-Re k-l model with the high-Re k-ε model of Jones & Launder [5];
- o the above zonal approach, but with Yakhot et al's "RNG" k-ε model [6] replacing Jones & Launder's form.

These models are applied over a single grid of 80x50x45 nodes covering one quarter of the duct (Fig. 1). Multiblock solutions have also been obtained to investigate sensitivity to grid disposition.

At the time of writing, preliminary second-moment-closure calculations have been obtained, and these are superior to the eddy-viscosity results, although it is the accurate resolution of the near-wall flow which is the decisive issue.

3. RESULTS

The flow feature displaying the highest sensitivity to turbulence modelling is the transverse circulation downstream of the transition section. As seen from Fig. 5, the low-Re models return a transverse circulation which agrees well, in terms of both location and intensity, with the experimental variations. In contrast, the high-Re variant gives rise to a high level of diffusive transport in inner duct regions which then rapidly erodes the vortex. Associated with the differences in transverse motion are strong variations in near-wall turbulence energy and distortions of streamwise momentum. A complete set of results, including turbulence energy and shear-stress fields, may be found in ref. [3]. All results suggest that the resolution of the near-wall region is of crucial importance.

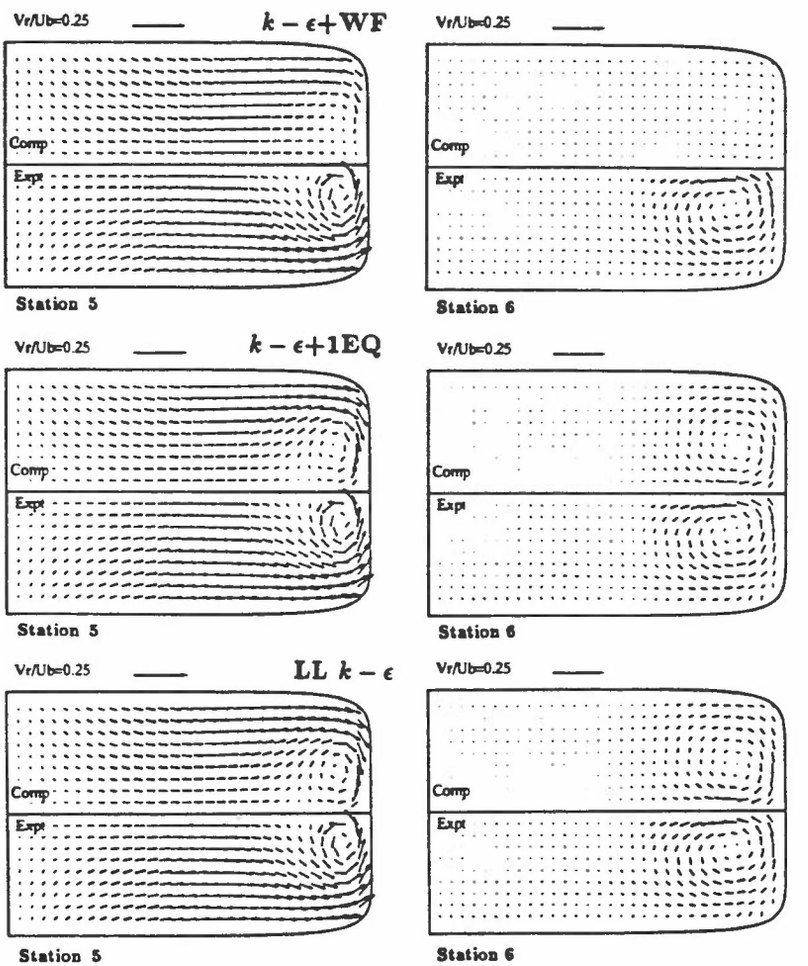

Fig. 2: Fields of transverse motion at two duct cross-sections downstream of transition

REFERENCES

1. Davis, D.O. and Gessner, F. (1990), AIAA paper 90-1505.
2. Lam, C.K.G. and Bremhorst, K (1981), ASME J. Fluids Engineering, 103, p. 456.
3. Lien, F.S. and Leschziner, M.A. (1994), Proc. ASME Symposium on Advances in CMFD.
4. Wolfshtein, M.W. (1969), Int. J. Heat Mass Transfer, 12, p. 301
5. Jones, W.P. and Launder, B.E. (1972), Int. J. Heat Mass Transfer, 15, p. 301
6. Yakhot, V., Orszag, S.A, Thangam, S., Gatski, T.B. and Speziale, C.G. (1992), Phys. Fluids A, 7, p. 1510

COMPUTATION OF 3D FLOW IN LINEAR TURBINE CASCADE

Researchers: F.S. Lien and M.A. Leschziner
Sponsor: Rolls Royce plc

1. INTRODUCTION

The flow in turbomachine passages, especially in high-load conditions, is among the most complex encountered in fluids engineering, principally because of the range of physical mechanisms contributing to important operational parameters and loss characteristics. In the case of a 'linear' turbine cascade, which is the main focus of present summary, the boundary layer originating at the stagnation line is initially laminar. On the suction side, close to the leading edge, a favourable pressure gradient tends to delay the onset of transition. The exact location of transition and its streamwise establishment length depend strongly on the values of the turbulence intensity and dissipation length scale in the main passage stream outside the boundary layer. Towards the trailing edge, the adverse pressure gradient associated with pressure recovery in the passage may lead to separation. On the pressure side, on which surface curvature is concave, Taylor-Gortler vortices are generated, enhancing turbulence and favouring the onset of transition. Further downstream the favourable pressure gradient accelerates the flow and re-laminarisation may occur. Inside the passage, strong transverse motions are induced by horse-shoe vortices convected into the passage and by the interaction between pressure gradients and the boundary layers developing on the spanwise walls. This transverse circulation convects high levels of turbulence energy from the end walls to the mid-span, giving rise to a complex transitional pattern on the blade surfaces. Behind the trailing edge, the passage vortices have profound effects on the wake structure and associated losses.

The above processes pose serious challenges to any turbulence modelling strategy, yet the majority of turbomachine computations are still being undertaken with algebraic formulations or none at all. In this study, undertaken as a contribution towards a recent ERCOFTAC workshop on turbomachine CFD, a low-Re k-ε model has been used to compute a 3D turbine cascade.

2. TURBULENCE MODELS

The most serious difficulty encountered in the turbomachinery calculations is the accurate prediction of transition. Even for a two-dimensional flat-plate boundary layer this is no mean task. When using a low-Re k-ε model, the near-wall turbulence level in the initial portion of the developing boundary layer is increased through diffusion from the free stream. As the boundary layer becomes thicker, C_μ, k and μ_t start rising, and this initiates and feeds the turbulence generation process leading rapidly to fully established turbulence. Recent LES results by Voke and Yang [1] suggests, however, that transition is provoked by pressure fluctuations in the free stream, i.e. by a mechanism entirely unrelated to that predicted by traditional low-Re models. Whether this can be captured within the framework of a Reynolds-averaged approach remains to be seen.

Here, the traditional route has been explored by using the low-Re k-ε model of Lien & Leschziner [2] (denoted by LL). This particular variant has been constructed subject to the constraint that it should return, as the wall is approached, the turbulent length scale prescribed either in Wolfshtein's or Norris & Reynolds' one-equation models [3,4]. This approach has been motivated by the wish to counteract the inherent tendency of the ε-equation to return excessive length-scale values in adverse pressure gradient, to improve computational stability and to reduce the grid-density required to support a grid-independent solution. The predictive capability of this model for a transitional flat-plate boundary layer at Tu=3 %, with computation starting ahead the leading edge, is indicated in Fig. 1. The same figure also shows the sensitivity of free-stream dissipation length scale to the onset of transition.

The above flat-plate computation and those presented below for the cascade have been performed with the general non-orthogonal co-located finite-volume code STREAM of Lien & Leschziner [5] in which convection is approximated by the QUICK scheme or a TVD variant thereof.

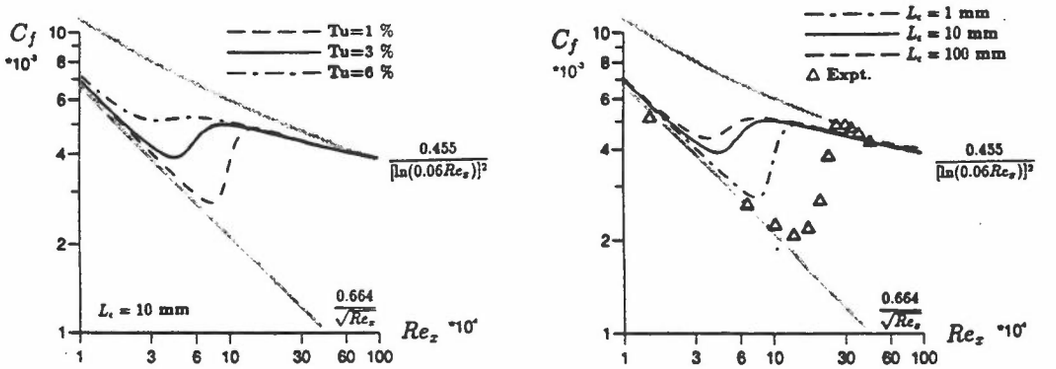

Fig. 1: Response of LL low-Re k-ε model to free-stream turbulence and length scale for a flat-plate boundary layer

3. APPLICATION TO CASCADE

Calculations have been performed in the passage shown in Fig. 2, experimental data for which have been obtained by Cleak & Gregory-Smith [6]. Fig. 3 show mass-averaged distributions of loss, secondary kinetic energy and turbulence energy along the passage. While these results appear encouraging, it is evident from Table 1 that, far downstream, the losses are far too high and the secondary kinetic energy too, due to much too early transition on the blade suction side following leading-edge impingement. In reality, major portions of the suction side flow appear to be transitional.

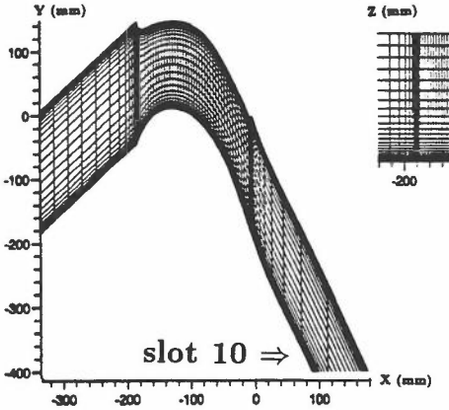

Fig. 2: Passage geometry and mesh

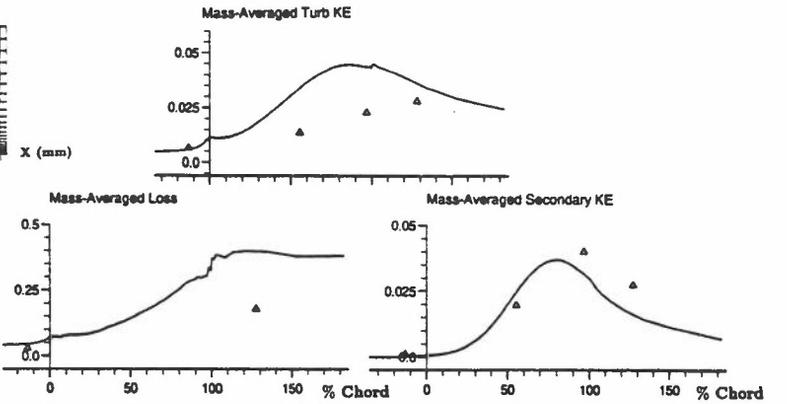

Fig. 3 Mass-averaged loss and energy characteristics

	Mass-Averaged Values at Slot 10			Mixed-Out Values at Slot 10	
	Experiment	Calculation		Experiment	Calculation
Total Loss	0.179	0.400	Total Loss	0.208	0.422
Midspan Loss	0.095	0.324	Midspan Loss	0.098	0.328
Secondary Kinetic energy	0.026	0.016	Yaw Angle	−66.7°	−66.3°

Table 1: Mass-averaged losses and secondary kinetic energy at slot 10

REFERENCES

1. Voke, P.R. and Yang, Z.Y., (1993), Paper 21-2, Proc. TSF9, Kyoto.
2. Lien, F.S. and Leschziner, M.A., (1993), Engineering Turbulence Modelling and Experiments 2 (W. Rodi & F. Martelli, eds.), p. 217.
3. Wolfshtein, M.W., (1969), Int. J. Heat Mass Transfer, 12, p. 301.
4. Norris, L.H. and Reynolds, W.C., (1975), Rep. FM-10, Dept. Mech. Eng., Stanford Univ..
5. Lien, F.S. and Leschziner, M.A., (1994), Comp. Meth. Appl. Mech. Eng., 114, p. 123.
6. Cleak, J.G.E. and Gregory-Smith, D.G., (1991), ASME Paper 91-GT-57.